Development of an Ankle De-loading Device Based on Stewart Platform

Hengyang Ding

2019

Development of an Ankle De-loading Device Based on Stewart Platform

Hengyang Ding

A thesis submitted to Auckland University of Technology in fulfilment of the requirements for the degree of Master of Engineering

2019

Mentor Supervisor: Dr. David White

Primary Supervisor: Dr. Lorenzo Garcia

Secondary Supervisor: Dr. Mark Beckerleg

Attestation of Authorship

I hereby declare that this submission is my own work and that, to the best of my knowledge and belief, it contains no material previously published or written by another person nor material which to a substantial extent has been accepted for the qualification of any other degree or diploma of a university or other institution of higher learning.

Signature_____

Acknowledgements

Abstract

This paper presents an ankle de-loading device based on a Stewart platform for ankle pain caused by Osteoarthritis (OA)/Rheumatoid Arthritis (RA) or ankle fracture surgery. The developed device aims to relieve the ankle pain by lifting the posterior section of the foot and distributing the ankle pressure to other parts of the body. The thesis elaborates on design and development process of the device. The developing process of the system follows strictly the engineering design process. The final design of system was selected among three different concepts. The structural calculations of the system were conducted, and the developed system was built for further experiments. Validation experiments for ankle de-loading performance were conducted by comparing the force condition with and without the device using force sensors placed on foot sole. The result indicated that the reaction force at the posterior section of the foot was decreasing significantly. Therefore, we can assume that the developed device can de-load the ankle joint force by leaning the foot heel toward the toe section.

Table of Contents

List of Figures

List of Tables

Chapter 1

Introduction

A report published by the United Nations (2019) predicts that, by 2020, 727 million people or 9,3% of the total world population will be elderly as they will be aged sixty-five or older. According to the United Nations (UN) report (2019), the elderly population will reach up to 15.9% by 2050, or approximately 1.5 billion people. Thomas, Peat, Harris, Ros and Peter's (2004) investigation of self-reported pain among the elderly shows that pain is mainly experienced in the lower limb, particularly in the hip, knee and foot. Dunn et al (2004) found that nearly 14.9% of the reported pain is happening in the ankle joint and the prevalence of the rheumatoid arthritis (RA) in joint among the adults around the world is about 1% (Alarcon, 1995). The likelihood of arthritis increases with age and can cause mobility, and balance impairment, disability, falls, and fractures, which could also cause the ankle pain. (Menz & Lord, 2001; Keegan, Kelsey, Sidney, & Quesenberry, 2002; Tinetti, Speechley, & Ginter, 1988).

In addition to age causing lower limb pain, ankle juries are also common among athletes (Fong, Hong, Chan, Yung, & Chan, 2007), representing about 45% of all athletic injuries (Ferran & Maffulli, 2006). Both elderly and sports related ankle injury problems could lead to chronic ankle instability. In fact, Adal, Pourkazemi, Mackey, and Hiller (2019) propose that 50% to 79% of ankle pain might be the result of instability. Continuous ankle pain is likely to affect people's ability to engage in everyday activities and might even cause

emotional distress (Smith, Avis, & Assmann, 1999). The reason why this is happening is because of osteoproliferation, which refers to an extra growth of bone tissue, after the bone's healing as well as RA of the ankle (Dieppe & Lohmander, 2005).

1.1 Research Objective

Ankle problems caused by osteoarthritis (OA) and external factors, such as ankle fractures, may affect the range of motion (ROM) and weakness and stiffness of the ankle joint. After an ankle fracture surgery, the bones in the joint might recover to the shape they used to be, but the damage to the cartilage in the ankle joint may not be able to recover and as a result might increase the friction between the joint bones (Pritzker, 2003), thereby causing joint pain. Ankle problems and their effects can severely impact on a patient's engagement with day-to-day activities, for instance walking up stair, and the severity of the pain is likely to increase with age (Glazebrook, et al., 2008; Reyes-Gibby, Aday, & Cleeland, 2002). In other words, the quality of the patients' life might significantly decrease, which might negatively impact their emotional wellbeing. Smith, Avis, and Assmann (1999) found that a continuous engagement with their normal pre-pain activities helps patients maintain their emotional wellbeing, which in turn aides them in their rehabilitation process.

Usually, the rehabilitation training of the ankle joint is devised by physical therapists and involves basic rehabilitation equipment, such as walking sticks, walking boots or an ankle brace. However, different types of rehabilitation devices are in development for better treatment and more effective training to help with the rehabilitation process (Jamwal, Hussain, & Xie, 2015; Nomura,

Yonezawa, Ogitsu, Mizoguchi, & Takemura, 2015; Saglia, Tsagarakis, Dai, & Caldwell, 2009; Wheeler, Krebs, & Hogan, 2004). Devices like ankle-foot orthosis (AFO) are getting more and more prominent in modern medical training and rehabilitation of the lower limbs (Taiar, et al., 2019). Although many of these devices have been developed and tested in clinic trials, most of them have no sufficient degrees of freedom (DOF) to simulate the complete motion of the human ankle joint (Hassan, et al., 2019; Yoshizawa, 2010). Consequently, when wearing such AFO devices, the ankle joint movement remains restricted when engaging in normal activities, which means the musculoskeletal system of the lower limb will not be trained thoroughly.

According to a study by Dieppe and Lohmander (2005), overload and other human body systemic factors such as obesity are part of the causalities of OA related ankle pain. However, most devices do not focus on relieving the force from the ankle joint area, which is a central cause of pain in the joint section. Solving this issue is the main motivator of the current research study.

1.2 Research Question

With the problem described above, the following research question is considered in this thesis.

- Could a system be able to de-load the ankle and solve the pain problem caused by severe ankle fracture or OA/RA?

1.3 Research Contribution

In this project, we developed an AFO device with sufficient DOFs for ankle joint movement. The main purpose of the developed device is to de-load the pressure in the ankle joint by distracting the force from the joint to other parts

of the body so that the ankle pain might be relieved. Fixing the problem of the cartilage's lack of recovery is rarely possible (Newman, 1998). In this project, the author is working with the hypothesis of a certain designed structure with dynamic system is able to guide the reaction force bypassing the ankle joint to the other parts of the body in order to alleviate the pain. If successful, this solution could increase rehabilitation success rates and thereby reduce the need of follow up ankle recovery surgery. The developed device is aiming to help the patient with the rehabilitation process and help the physical therapists monitor the ankle joint pain level with the data from inbuilt sensors. The developed device will not impede patients to engage in their normal activities and could offer them relief from the pain. Finally, the device was constructed to ensure it would be easy to wear in and take off.

1.4 Thesis Organization

This thesis is organized in seven chapters.

Chapter 1 introduces the background of the ankle pain problem, objective and outcome of the research.

Chapter 2 gives a comprehensive review of the ankle structure, the reasons of ankle pain, and the motion of the ankle for later device design. Similar devices research will also be included for concept inspiration and generation of our device.

Chapter 3 describes the different concepts of the device and evaluation. The systems included in the final selected concept will be discussed, and the draft model of our device will be formed.

Chapter 4 presents the detail design of different systems in the developed device. Including material selection, dimension calculation, failure simulation, and program description.

Chapter 5 gives the test design of the developed device. The scenario of the experiments and material used will be shown.

Chapter 6 shows the results from the validation experiments. The results will be evaluated to describe the developed device's performance.

Chapter 7 discusses the performance and improvements of the device. Further research possibilities will be recommended, and conclude the whole research.

Chapter 2

Literature Review

The development of a de-loading system necessarily draws on knowledge from different fields, including anatomy, physiology, mechanical engineering and etc. Keeping the ankle's flexibility in motion is the prerequisite in developing the device. Thus, the study draws on the principles of biomechanics, meaning the movement and the structure of the ankle need to be taken into consideration, especially the postural control of the ankle. These features of the ankle provide a basic rudiment of the system; all subsequent designing processes are based on this. The anatomy of the ankle is described in order to explain why OA/RA and after-ankle-surgery rehabilitation are an issue not only for the patients themselves but for the physical therapists and the doctors around the world (Alarcon, 1995; Dunn, et al., 2004).

During walking gait, force is inevitably applied on the ankle joint. The purpose of our device is to distract the force from the ankle to other parts of the lower limb. In other words, most of the force will bypass the ankle joint and disperse to other parts of the body. The amount of force distracted from the ankle joint will be taken into consideration to quantify the maximum loading. The system is designed to be a wearable device, like an exoskeleton. Therefore, a consideration of human's gait cycle study, as a modern ergonomic topic, is required. The study of the gait cycle explores how the foot interacts with the ground and the lower limb motion in a complete gait cycle. Different steps in a gait cycle mean that the force applied on the joint will be

different in each motion during the whole cycle (Dąbroś, Iwaniec, Patyk, & Wesół, 2018). The developed device is designed to accommodate for the maximum load condition, and take the users' wearing experience into consideration when using the device. Since the ankle joint problem is a worldwide issue, there are already a substantial number of ankle devices on the market and under development (Irby, Kaufman, Mathewson, & Sutherland, 1999; Nomura, Yonezawa, Ogitsu, Mizoguchi, & Takemura, 2015). These existing devices are examined in detail as a detailed consideration might inspire ideas for the conceptual design.

2.1 Ankle Structure

The working principles of the ankle is the key in designing the de-loading system since the device is not only supposed to fit the ankle but support the postural control on the ankle. The ankle joint complex is comprised of the lower leg and the foot and enables the motion that allows the lower limb to interact with the ground, which is a key requirement for gait and other activities of daily living (Brockett & Chapman, 2016). The foot and ankle are made up of the twenty-six individual bones of the foot plus the long-bones of the lower limb and together they form a total of thirty-three joints (Gary, 2010). In a healthy foot, those bones enable the joint to have triplanar movements with 3 DOFs, which are dorsiflexion (true flexion) and plantarflexion (extension) in sagittal plane, inversion and eversion in frontal plane, adduction and abduction in transverse plane. In those movements, the ROM in the sagittal plane is between 65° to 75° in total (Grimston, Nigg, Hanley, & Engsberg, 1993), where dorsiflexion has a range from 10° to 20°, and plantarflexion ranges between 40° and 55°. The range for the movement in

frontal plane is approximately 35° (23° for inversion and 12° in eversion) (Stauffer, Chao, & Brewstec, 1977), in transverse plane the range is about 5° for adduction and abduction each (Arndt, Westblad, Winson, Hashimoto, & Lundberg, 2004). In other words, the foot is a rather complex structure, which proved challenging for the design process as it was near impossible to consider all bones and their specific characteristics. As a result, we focused our design efforts on the main bones which comprise the ankle joint: Fibula, Tibia, Talus and Calcaneus, the positions of which are given in *Fig. 1* below.

As it is shown in *Figure 2-1*, the ankle joint complex is made up of the talocalcaneal (subtalar), tibiotalar (talocrural), and transverse-tarsal (talocalcaneonavicular) joint (Gary, 2010). Each joint has different functions in the movement of the ankle.
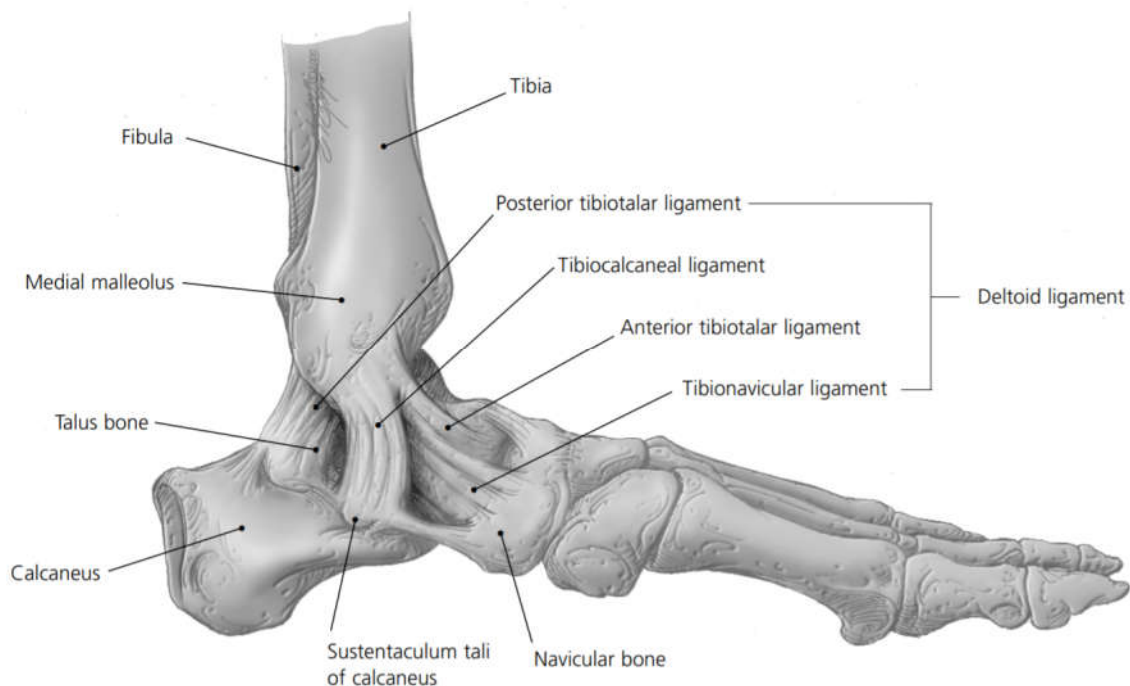
Figure 2-1 Lateral view of the human ankle (Wolfe, 2001)

The subtalar joint is made up by calcaneus and talus, and the calcaneus is the strongest, largest and most posterior bone of the foot. It is located inferiorly to the talus, and forms a triplanar, uniaxial joint with the talus (Ren'e, 1997). This geometry allows inversion and eversion of the ankle, and whilst other motion is permitted at this joint, most of the eversion and inversion of the foot is provided here (Michael, Golshani, Gargac, & Goswami, 2008). This main part of the joint is located in the heel section of the human foot.

The talocrural joint, also known as tibiotalar joint or true ankle joint, is the most important joint that our device will focus on, consists of three bones: talus, fibula and tibia. They form a bracket shaped socket to fix the position of those three bones (Brockett & Chapman, 2016). This part of the ankle joint works with three groups of ligaments which maintain the stability, resist eversion and inversion motion, and limit valgus and varus stresses within in the joint (Wolfe, 2001). Most ankle fractures happen because of inversion, for the stress applied in the joint is beyond the maximum pressure strength of ankle joint bones (Tejwani, 2017). A severe ankle fracture usually involves the breaking of two bones: fibula and tibia (Tejwani, 2017). The tibiotalar joint connects the end of tibia and fibula, the bracket shape of this joint makes these two bones form a functional junction in the human ankle (Brockett & Chapman, 2016). With its special shaped joint, the talocrural joint participates in almost all the motions of the foot, which results in a higher risk of cartilage abrasion and causes OA/RA problem (Huch, Kuettner, & Dieppe, 1997). The detailed reason for this will be discussed in the following section for better understanding.

The transverse tarsal joint is at the junction of the talus and navicular. It is considered to be part of the same functional unit as the subtalar joint because

they share a common axis of motion and both joints contribute to eversion-inversion motion of the foot (Brockett & Chapman, 2016).

The design process described in this thesis is based on this outline of the ankle structure. Fractures in the foot can result in stiffness and cause pain after surgery. The following section further explores and explains the causes of ongoing foot problems such as stiffness and pain in greater detail.

2.2 Ankle Pain

Normally, ankle pain will be caused by two conditions: OA/RA and ankle joint recovery after fracture surgery. Both circumstances can cause ankle stiffness and weakness of the joint, resulting in a restriction of movement. Understanding the causality of these conditions will inform the developed system's design focus point, improving the applicability and usability of the device.

2.2.1 Osteoarthritis (OA)

OA is a common disorder of synovial joints. Pathologically, it is characterized by focal areas of damage to the articular cartilage centered on load-bearing areas, new bone formation at the joint margins (osteophytosis), changes in the subchondral bone, variable degrees of mild synovitis, and thickening of the joint capsule (Pritzker, 2003). Such disorder in synovial may cause deformation in the subchondral bone (Watt & Doherty, 2003), which will increase the friction between the bones. The bone in the joint with damaged cartilage can progressively destruct the joint because bone has a greater ability to repair itself than cartilage, and this deformation of the bone can change the shape of the joint and cause osteoporosis (Dieppe, Cushnaghan, Young, &

Kirwan, 1993; Mazzuca, et al., 2004). McCrae, Shouls, Dieppe and Watt (1992) suggest that the pain correlates with both synovitis and subchondral bone changes, and Simkin (2004) supports the theory that intraosseous hypertension has been implicated as an important factor in osteoarthritic pain due to the weight pressure applied to those two joint tissues.

Due to the causes of the pain described above, the loss of the cartilages increases the friction of the contacted bones in the joint, in our case, the ankle joint. Furthermore, according to Burdett (1982), the ankle joint may suffer pressure of approximately five times the body weight in normal walking status, and up to thirteen times of the body weight while in intense exercise (Burdett, 1982). Such pressure will cause sustained injury to the subchondral bone if the joint is affected by OA. This condition is more likely to affects the elderly as the slow regeneration of the bone structure and osteoporosis can make the ankle pain problem worse day by day if there is no efficient treatment. According to Felson and Schaible (2009), the sustained and pressure-induced trabecular tension due to the continuous force being applied on the damaged joint tissue is at the core when trying to relieve pain from the OA problem in a mechanical way. In other words, reducing the pressure in the OA joint may relieve the pain.

2.2.2 Ankle Recovery After Surgery

Approximately one in every 10,000 people worldwide suffers an ankle sprain every day (Soboroff, Pappius, & Komaroff, 1984). These injuries include severe conditions which require an operation. Usually, ankle injuries happen in the talocrural joint due to its specific location and shape in the ankle, and the most common outcome of ankle injuries are malleolar fractures. The ankle

fracture can be classified into three types (Kennedy, et al., 1998), with illustrations provided in *Figure 2-2*:

1) Type A - describes a fracture of the lateral malleolus distal to the syndesmosis (the connection between the distal ends of the tibia and fibula). Usually stable, but sometimes it needs an open reduction and internal fixation (ORIF) especially if the medial malleolus is fractured;

2) Type B - describes a fracture at the level of the tibial plafond (syndesmosis);

3) Type C - describes a fracture proximal to the level of the tibial plafond and often have an associated syndesmotic injury. Unstable requiring ORIF.

(a) Locked plating system (Tejwani, 2017)

(b) Total ankle replacement (Roukis, et al., 2016)

Figure 2-2 Examples of the two ankle fracture fixation methods in modern medical

After a severe ankle fracture, the doctor determines the type of the fracture based on an X-ray film and makes a diagnosis. If this kind of situation cannot be treated by closed means, early surgical intervention must be carried out (Schepers, De Vries, Van Lieshout, & Van der Elst, 2013). Operative treatment options for an ankle fracture are ORIF or external fixation. External

fixator is often used as a temporary fixation before a more permanent ORIF, but in certain circumstances it can be used as a definitive treatment modality or in combination with ORIF in complicated fractures requiring additional stability (Ovaska, 2015).

 As one of the fixation methods, locked plating systems are very common in ankle fracture surgery (see in *Figure 2-2(a)*) (Tejwani, 2017). This system can be very useful in treating patients with poor bone quality or in patients with complex fractures. In ankle fracture surgery, angular stable implants have been emphasized, especially for geriatric patients (Ovaska, 2015). However, with this kind of treatment, the ankle joint loses its motion, as the implant system on the bones impedes the original movement of the structure. This obstruction affects the nervous system around the ankle, which causes pain. In addition to the locked plating system used in ankle fracture fixation surgery, there is another medical method called total ankle arthroplasty (TAA) which is increasingly used as a solution of RA problem (see in *Figure 2-2(b)*) (Pugely, et al., 2014; Raikin, Rasouli, Espandar, & Maltenfort, 2014). Unfortunately, the debate on whether it is a good idea to replace or fuse the ankle still remains. There are still many patients who feel uncomfortable with the total replacement of their own body tissue and worry about its failure (Raikin, Rasouli, Espandar, & Maltenfort, 2014). However, Marx and Mizel (2008) believe that TAA is a good choice for RA patients based on its presumed improvement for the gait cycle due to a decrease of unnecessary movement in the ankle joint. And Su, Kahn and Figgie (2004) indicate that TAA helps decreasing the stress on the midfoot and subtalar joints. Nonetheless, the problem of the TAA is still obvious, the patients need to treat the system carefully for the significant risk factor of developing an underlying

inflammatory arthritis with a high ratio needing reoperation (Raikin, Kane, & Ciminiello, Risk Factors for Incision-Healing Complications Following Total Ankle Arthroplasty, 2010). In this study's case, the author is focusing on relieving the remained pain after removing the implant system. This poses a problem for the bones' recovery process. When a facture happened in the ankle joint, it is not only the bone fracture, but the soft tissue like cartilage in the bracket shaped socket of the ankle joint and subtalar joint might be damaged as well. As it was mentioned previously, the bone may be healing faster than the cartilage, and the loss of the cartilage is irreversible and permanent, which can then result in ongoing pain for the patient (Newman, 1998). According to a follow-up survey to patients with an OA/RA problem who had the TAA surgery in the United States, Buechel, Buechel and Papas. (2003) found that 14% of the patients suffer from pain which limits their daily activities. This suggests that both of the most common internal ankle fixation methods cannot reliably solve the ankle pain problem.

2.3 Gait Cycle

Bipedal walking is an important characteristic of humans. The movement of the foot in an one step cycle involves the following six phases: heel strike, foot flat, mid-stance, heel-off, toe-off, and mid-swing (Loudon, Swift, & Bell, 2008; Shultz, Houglum, & Perrin, 2015) (*Figure 2-3*).
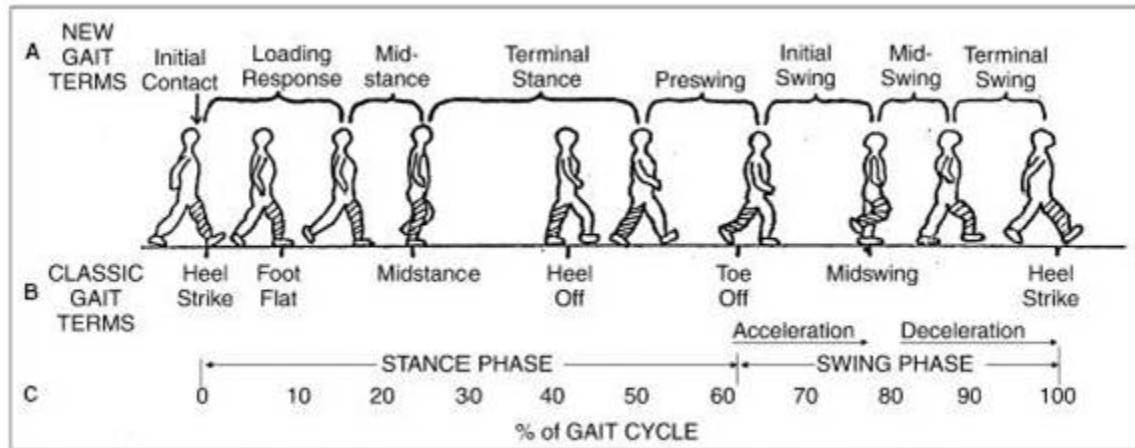
Figure 2-3 Human gait cycle (Unstal & Baerga, 2004)

During the first phase, also known as initial contact, there is a plantar flexor moment as the ankle's dorsiflexors contract eccentrically to allow forward progression of the shank over the foot (Shultz, Houglum, & Perrin, 2015). In the toe-off phase, the plantarflexion moment continues with the plantar flexors contracting concentrically towards toe-off. However, the movement in those phases differs depending on walking speed (Burdett, 1982). As a person walks faster, the ankle's kinetic patterns remain similar in profile but are executed with greater magnitude. There is also substantial individual variation in the gait movement.

The whole foot makes contact with the ground starting from the foot flat to the mid-stance phase. During these phases, the body is supported by one single leg (Unstal & Baerga, 2004). The ankle problem, such as ankle dorsiflexion weakness that is due to OA/RA or severe ankle fracture, may lead to a lack of heel strike and decreased floor clearance. The consequences of such a problem are an increased step height and prolonged swing phase (University of Washington, 2015), which increases the time of the stance phase of the other leg and thereby causes an imbalance in both feet which might pose a threat to

patients as it increases the chances of falling and tripping. The type of ankle pain problem this study is focused on occurs in the heel section, where the toe is more likely to bear weight (Malanga & Delisa, 2010). Since the device developed in this study deals with the pain problem in the ankle joint complex, the design needs to focus on the joint force distraction, using forefoot as a fixed point of the device without paying too much attention to the connection between the ankle pain and forefoot pressure.

Based on movement and ankle power analysis (Brockett & Chapman, 2016), both the movement and the ankle power increase enormously when in the second and third phase of a gait cycle, which is foot flat to mid-stance. Because the whole body's weight is added on one ankle (the other foot is usually in the last phase of a step), the value of ankle power is about five times than the other four phases (Burdett, 1982). Experimental studies indicate that approximately 83% of the load is transmitted through the tibiotalar joint, and the remaining 17% is transmitted through the fibula (Calhoun, Li, Ledbetter, & Viegas, 1994). In one gait cycle of human walking, the amount of load transferred through the fibula varies, with increased loading occurring during dorsiflexion. This indicates that the device will mainly focus on distracting the force on the ankle joint during in the second phase of a gait cycle. As mentioned above, our device is aiming to distract the force in the stance phase, when the whole-body weight is applying pressure on the system. In other words, the device should be able to support the entire body weight, and in the design process, the maximum body weight should be taken into consideration in order to meet different users' conditions.

2.4 Related Devices

There are already several kinds of devices, such as knee braces, which can distract the force from the knee, and rehabilitation braces for the ankle, which do not have a force distraction function. However, according to our best knowledge, there is no device that serves to de-load the ankle. By learning the principle of both force distracting and non-force distracting devices may inspire new ideas for the design of the external de-loading system.

2.4.1 Knee Braces

OA of the knee is a common problem in modern society. Pain in the knee joint of patients affected by OA typically occurs when the knee is loaded during the stance phase of gait, which begins at heel strike and ends with toe-off (Self, Greenwald, & Pflaste, 2000). Knee braces that were designed to relieve the pain in the knee joint create a valgus movement which tends to force the leg into a "bow-legged" position, reducing the exposure time of the subchondral bone and the cartilage in knee joint with OA/RA problem. The recorded data shows a huge relief in pain among those who wear a leg brace compared with to those who do not.

The above study suggests that, if an external force is added to the joint section, the level of pain will be relieved. Adding an external force to the joint to change the load applying point results in pain relief for the patient. This finding suggests the hypothesis that adding certain external forces on the joint via an ankle de-loading device, would lead to pain relief for the joint. The external force applied on the knee joint by the knee brace reduces the contact time of the pain area in a gait cycle. The reasons of pain in the ankle joint are

linked to the movement of the knee joint. The external force will be applied to relieve the ankle from the force during the stance phase, as most ankle pain problems are caused by the pressure in the ankle joint (Simkin, 2004). The applied force from our device aims to distract part of the reaction force from the ground to the other part of the lower limb instead of letting the force wholly concentrate on the ankle joint. Furthermore, since the de-loading device seeks to distribute the force to other parts of the body, we believe the knee to be a good option to act as a transfer station to affix the device to considering its anatomical characteristic of being at the junction of thigh and crus. The knee joint is a rather good fixing platform for de-loading devices, knee braces, or similar rehabilitation apparatuses.

2.4.2 Ankle Brace

There are two main categories of ankle braces: non-rigid stabilizers and semi-rigid orthoses (Kaminski, 1998). Neither of these two kinds of ankle braces is able to distract the force from the ankle joint, their ability is to limit the extremes of subtalar joint inversion and eversion while permitting talocrural joint dorsiflexion and plantar flexion (Miller & Hergenroeder, 1990). In other words, these kinds of ankle braces are able to prevent the ankle from the danger of sprain or fracture by fixing the subtalar joint in a certain position. And most of these braces work only in sagittal plane with only 1 DOF, which are dorsiflexion and plantarflexion (Hassan, et al., 2019; Yoshizawa, 2010). However, the movement of the ankle joint in a complete gait cycle includes at least 3 DOFs in three different rotation directions (Loudon, Swift, & Bell, 2008; Shultz, Houglum, & Perrin, 2015), not to mention that once the knee brace is fitted, the movement of the lower limb on three planes in 3D space need to be taken into consideration. This means that the study needs to develop

a de-loading system with at least 3 DOFs in three different rotation directions that is compatible with a knee brace design. Above kinds of the brace designs are used as references for the mechanical structure design described in detail in Chapter 4. These established designs are modified with a dynamic system for force distribution and motion improvement.

2.4.3 Similar Devices

As the ankle pain problem and its rehabilitation is a huge problem, research groups all over the world are working on a better and more functional AFO. We have been looking for different AFO devices to consider for inspiration; however, the majority of them have only 1 or 2 DOFs (Carberry, et al., 2011; Chinh, Tan, Long, & Tien, 2017), which is insufficient for foot motion. In spite of the insufficient DOF, the design of those devices' that include a lot of dynamic system and mechanical structure provide inspiration for the development of the de-loading system. The ankle de-loading device developed for this study combines certain mechanical structures with their dynamic system featuring 6 DOFs.

A group in Japan has developed a device with a DOF of 6 (Nomura, Yonezawa, Ogitsu, Mizoguchi, & Takemura, 2015; Onodera, Ding, Takemura, & Mizoguchi, Posture Control Using New Ankle-Foot Assist Device with Stewart Platform Type Parallel Link Mechanisms, 2012). Their system is based on a Stewart platform, also known as a hexapod (Stewart, 1965). Such a mechanism provides the developed system with 6 DOFS; however, in their case, the device is used for preventing and decreasing the chance of tripping while walking. Thus, their design is using pneumatic cylinders as linkages, and those cylinders were found to be able to support the 3D motion of the

ankle joint. Due to the working principle of the pneumatic system, the device cannot apply enough force to de-load the pressure in ankle joint and relieve the ankle pain. We need to find a better solution for platform linkage to meet the requirement of the device. The conceptual design of the device, which will be presented in Chapter 3, combines all the information in the literature review section.

Chapter 3

Conceptual Design

We formed our general concept for the de-loading device on our examination of the ankle structure, gait motion, and similar devices. As it was mentioned previously, the human ankle joint got 3DOFs in three rotation directions, and with the help of crus the joint is able to move in three planes, which means the joint has 6DOFs in 3D space with respect to the knee joint. The traditional design of AFO is mainly used for ankle rehabilitation and to prevent the joint from further injuries. However, AFO designs with ankle joint motion restriction also limit patients' engagement in daily activities, which can negatively impact on their mental health. The idea of the device developed in this study is to distract the force in the ankle joint and to provide at least 3DOFs in three rotation directions for its movement.

The conceptual design mainly follows two steps, concept generation followed by concept evaluation and selection. The main point of the concept generation phase is to generate different design ideas for concept and to come up with different concepts for solving the ankle pain problem. Then in concept evaluation and selection phase, the different design concepts are discussed and evaluated before the final design is presented. The result of the conceptual design is a draft prototype of our device that can be developed further the future during the embodiment design phase.

3.1 Main Mechanical Structure Conceptual Design Strategy

The device developed in this study is specially designed for human ankle joint complex. There are several features the developed system's mechanical structure should have:

- The device should be able to simulate human ankle motion and move with the foot;

- The device should be able to distract the force from the ankle joint by using the designed structure to make the reaction force bypass the joint;

- The device needs to be user friendly and fit securely, which means that patients can put it on and take it off with ease and that it attaches to the lower limb tightly.

There are a lot of similar systems under development or already available on the market (Girone, Burdea, & Bouzit, 1999; Nomura, Yonezawa, Ogitsu, Mizoguchi, & Takemura, 2015); however, most of them are used for ankle rehabilitation by limiting the motion of the ankle joint.

As mentioned previously, the injuries that cause the ankle pain problem tend to be located in the talocrural joint, which is the joint where most of the motions come from, among which inversion and eversion are the motions happen most in fracture. Tibia, fibula, and talus are included in those two motions and injury to these bones can lead to malleolar fractures. After ORIF or external fixation surgery, the recovery process can be full of pain and the patients may suffer ankle instability. AFOs that were designed for rehabilitation limit the motions of inversion and eversion and prevent the risk

of sprain and secondary damage on the recovery area. The support from those AFOs comes mostly from plastic or steel plates that have only one axis rotation that allows for the motion of dorsiflexion and plantarflexion, which covers the function of the talocrural joint as a hinge connection that is mainly used for one axis rotation motion. However, during normal walking, the ankle joint will have a supinated 5° position (abduction), and the restrictions of the movement from those AFOs might cause sore muscles and ankle ligament stiffness (Loudon, Swift, & Bell, 2008; Shultz, Houglum, & Perrin, 2015). The loss and restrain of ankle motions can lead to an imbalance in walking and affect the patients' daily life. The developed device aims to relief the patients from the ankle pain as well as decrease the restriction of the ankle joint, thereby allowing patients to engage in daily activities will greater ease compared to other AFOs.

3.1.1 Concept Generation

This study is inspired by the research of Nomura, Yonezawa, Ogitsu, Mizoguchi and Takemura (2015), who faced the same problem of improving AFO's insufficient DOF in motion of the ankle joint. They developed a system to prevent tripping, which is a common side-effect of AFOs' restriction of movement. They had the same concern regarding the lack of DOFs in existing AFOs on the market, and they aimed to develop a device that supports patients in engaging in day-to-day activities by providing support to the users' foot in every direction of the ankle joint. They discovered a parallel-link mechanism with 6DOFs (*Figure 3-1*) that was designed decades earlier by Stewart (1965), and built their system based on this platform. The Stewart platform was originally designed for simulating flight conditions for pilot training; however,

the research team found that the system could also be transferred to AFOs. The Stewart platform seems to be a perfect solution for the movement of the ankle.

Nomura's team is not the first research team to integrate the Stewart platform into an AFO. Previously, Girone, Burdea and Bouzit (2002) have also used the Stewart platform for their design of an ankle rehabilitation system called Rutgers Ankle. However, Rutgera Ankle is only used to detect the patients' ankle motion and not wearable. Thus, it is a fixed platform on which patients put their ankle so that the system can collect data on patients' ankle movement.

Yonezawa et al. (2014) also developed an AFO system based on Stewart platform which can be also wore around the crus. This system is used to measure the ankle angle accurately and reproduce the force with linkages made by pneumatic cylinders to help the ankle's movement. However, their developed system is only wearable when the user is in a fixed position, such as sitting in a chair, but does not allow patients to walk or engage in other outdoor activities.
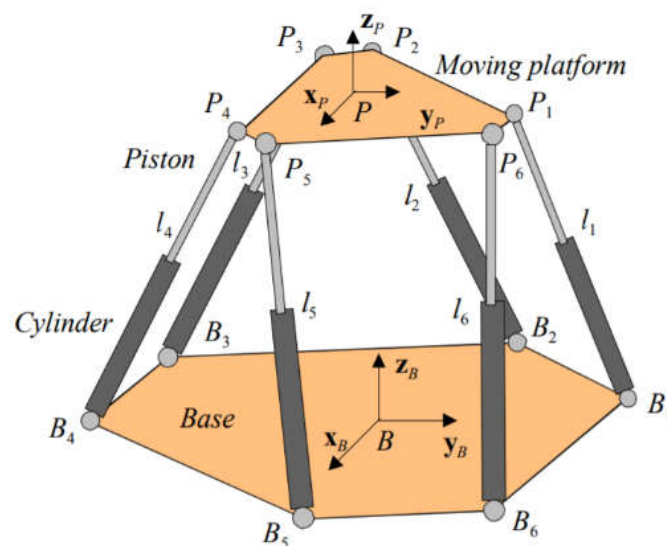
Figure 3-1 Stewart platform kinematic structure (Lopes, 2010)

Those two similar devices demonstrate the possibility of combining AFOs with the Stewart platform to create 6 DOFs. Nomura's team also developed a wearable device based on Stewart platform, using the same pneumatic cylinders for the linkage used for the Rutgers Ankle. Their portable device is much lighter and more convenient for wearing than the previous two system; however, their device has a problem. Because their device uses pneumatic cylinders, an air pump is needed to control the system and this air pump needs a power supply. As far as the air pump itself is concerned, it is not conducive to being carried around due to its weight, and neither is the power supply needed for the air pump to work. And as discussed above (see Chapter 2), this system is just for preventing tripping, which means that the force generated by the pneumatic cylinders is not enough to support the body and relieve the ankle pain. Based on this identification of weaknesses in existing device, the device developed in this study focuses on creating a wearable and force distracting device for the ankle joint.

We decided to base the main mechanical frame of our developed device on the Stewart platform as previously discussed. It was explained in the literature review section why ankle fracture and OA/RA patients suffer from ankle joint pain problem. In a complete human gait cycle, the leg in stance phase will support the whole body's weight. If the cartilage in the talocrural joint has been damaged, regardless of whether that is due to an ankle fracture injuries or daily walking abrasion, the friction in the talocrural joint will increase without intervention (McCrae, Shouls, Dieppe, & Watt, 1992). This can then stimulate the joint nerve, which causes pain in the ankle joint. The description of the main cause factors of ankle joint pain suggests that the main issue is the pressure applied on the ankle. Those forces will come either from the body

weight transfers through the lower limb to the joint or from the ground's reaction force in the gait cycle. We believe the method to relieve the patients for the ankle pain problem is to decrease or distract the forces mentioned above to other parts of the body. The main design point is to let the force bypass the ankle joint and the Stewart platform structure will act as a transfer station to replicate the function of the ankle joint, which will support the body in stance and daily motion.
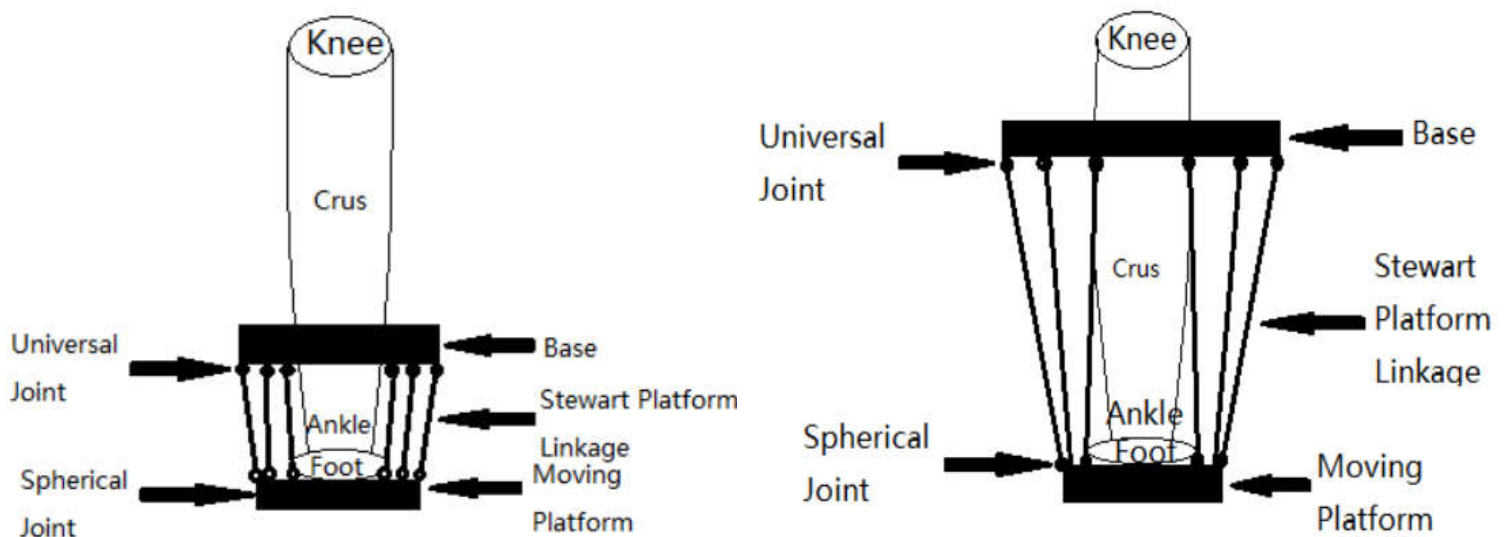
(a) Concept of fixing around the lower crus

(b) Concept of fixing around the upper crus
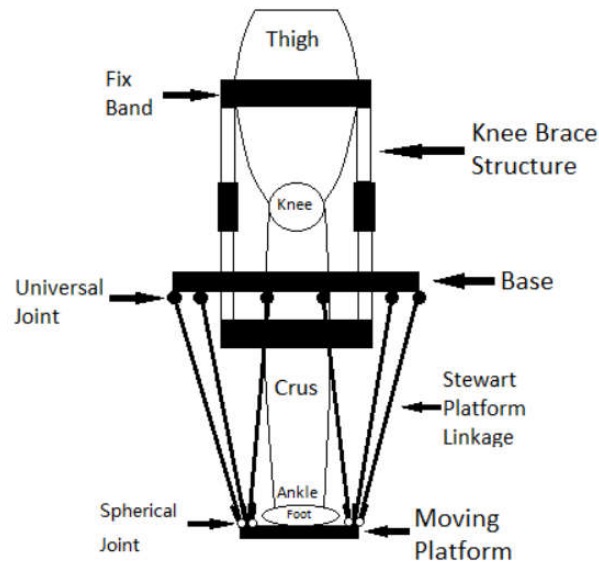
(c) Concept of fixing around the knee joint

Figure 3-2 Three concepts of the device

As mentioned above, the developed device aims to decrease the force applied on the ankle joint. We believe the best way to secure the device is by placing it around the ankle joint and fixing it on human lower limb. *Figure 3-2 (a), (b)* and *(c)* illustrates three proposed concepts for the device based on Stewart platform, each of them has a different fixing position on the lower limb. *Figure 3-2(a)* shows the option of fixing the device around the lower crus, meaning the ankle joint. The concept presented in *Figure 3-2(b)* illustrated the option of attaching the device around the upper crus but below the knee joint. The last of the three concepts is a design that involves the device being fixed around the knee joint shown as shown in *Figure 3-2(c)*. The following section presents a discussion of the advantages and disadvantages of the three concepts, which forms the bases on which the final design is chosen.

3.1.2 Concept Evaluation and Selection

A research team in Japan used the same Stewart platform and attached the device on the shin of the lower limb (Onodera, Ding, Takemura, & Mizoguchi, Performance Evaluation of Novel Ankle-Foot Assist Device for Ankle-Foot Rehabilitation, 2014). However, their fixation method features some issues. Firstly, using a fixation point on the shin is not secure as the device can easily slip down from lower limb if the device's weight is too heavy. This would also apply to the concepts shown in *Figure 3-2(a)* and *(b)*. We believe the best solution for to this problem is to add another fixation point on the thigh, as the human thigh's perimeter dimension is larger than the crus' dimension because more muscles are attached to the thigh (Platzer, 2008). The two fixation points on the shin and thigh should prevent the device from slipping down or riding up. Based on these considerations, the concept shown in *Figure 3-2(c)* has been chosen as the final conceptual design for the system.

Since there will be two different fixation points on the lower limb, and their positions will be located around the femur above the knee joint and the tibia below the knee joint, it is necessary to design a knee brace structure that connects the two fixation points and another one that connects the Stewart platform structure to the brace. This will ensure that the distracted force is applied to the knee joint and thigh in order to relieve the ankle pressure.

The design of the knee brace structure including the whole knee joint needs to consider the hinge for simulating the knee movement. The knee joint includes three bones (Burgener, Meyers, Tan, & Zaunbauer, 2002), and in this design the structure will mainly simulate the function of the tibiofemoral joint. The tibiofemoral joint allows for the movement of femur and tibia with joint capsule, which can be considered as a lubricant of the joint. The design of the knee joint structure is based on the features of these two bones. The knee joint is a hinge joint, the contact section of femur and tibia is the moving center of the joint. But with the help of anterior and posterior cruciate ligaments in knee joint, the extension of the ligaments needs be considered for the knee brace structure design. As for the Stewart platform structure, unlike the usual construction, the device developed in this study places the base and the moving platform (also as known as end effector) upside down as shown in *Figure 3-3*. The base is placed around the crus and the moving platform is placed under foot sole, so that the moving platform can replace the foot and replicate its motion in stance phase. Several studies have indicated that the ankle joint movement is related to the reaction force applied from the ground to the sole of the foot (Duncan, Kowalk, & Vaughan, 1997; Wervey, Harris, & Wertsch, 1997); therefore, reducing the force applied to the foot sole is a

central part of the solution for decreasing the ankle pressure, and thus relieve the patients from ankle pain problem.
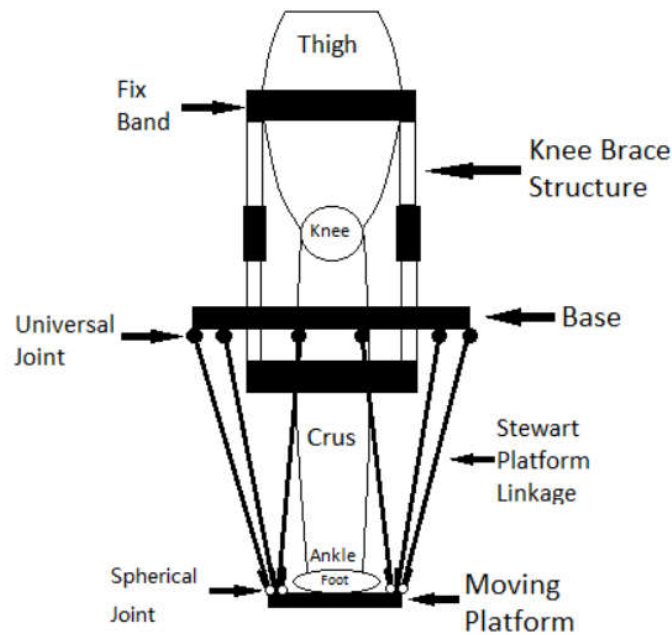
Figure 3-3 Final mechanical structure concept design of the device

The main working principle of the device is now becoming clear; the linkage of the main frame lifts the foot up and make gaps between foot sole and moving platform. The moving platform contacts the ground instead of the original foot sole, and the force is transferred through the six linkages of the main frame to other parts of the body, decreasing the force applied on the foot sole. The idea of the mechanical frame structure is that when the patient is wearing the device, the leg is lifted, creating a gap between the foot sole and the moving platform. When the patient is walking or engaging in other movements which would normally apply pressure on the ankle joint, the moving platform bears the force instead of the foot and transfers the force to the other parts of the body. Meanwhile, the moving platform allows the motion of foot in 6 DOFs due to the special structure of the Stewart platform.

Thus, the ankle joint pain cause by the pressure is relieved thanks to the force distraction of the mechanical structure, and the motion of the ankle joint is not affected because of sufficient DOFs and ROM provided by the hexapod structure.

The structure of the system has been discussed in this section and the rough sketch of the conceptual design of the main mechanical frame has emerged. As mentioned above, the knee brace structure is supposed to be attached around the knee joint in order to fix the Stewart platform structure and transfer station of the force. However, a solution is still needed for the connection between the Stewart platform structure and the knee brace structure. Modern knee brace designs that are currently available usually contain two sets of support structures to act as femur and tibia. Since the support structure of the knee brace is used to bear the load, the strength of those two structures should be good enough to bear the force transferred from the ankle joint. And at the same time, the shear force applied on the connection point also bears the same force as the knee brace structure does. The design and materials used for the connection part need to be carefully calculated to account for their tensile failure since they need to be able to meet the load of the worst or the heaviest situation.

Another main design point is the linkage between the platform and the base. The developed system should be able to support the whole-body weight in stance phase, and the actuators used as Stewart platform linkages should be able to exhibit characteristics which are similar to human skeletal muscles. An examination of the different actuators that are currently on the market revealed several common features. The advantages and disadvantages of each of these actual actuators are presented in *Table 1* below.

Table 1 Advantages and disadvantages of different actuator types

Actuator Type	Advantages	Disadvantages
Mechanical	- Cheap - Repeatable - No power source required - Self-contained - Identical behavior extending or retracting	- Manual operation only - No automation
Electro-mechanical	- Cheap - Repeatable - Operation can be automated - Self-contained - Identical behavior extending or retracting - DC or stepping motors position feedback possible	Many moving parts prone to wear
Linear motor	- Simple design - Minimum of moving parts - High speeds of possible - Self-contained - Identical behavior extending or retracting	Low to medium force
Piezoelectric	- Very small motions possible at high speeds - Consumes barely any power	- Short travel unless amplified mechanically - High voltages required, typically 24V or more - Expensive and fragile - Good in compression only not in tension - Typically used for Fuel Injectors
Hydraulic	- Very high forces possible - Relatively high power to size ration (or power density)	- Can leak - Requires position feedback for repeatability - External hydraulic pump required - Some designs good in compression only
Pneumatic	- Strong - Light - Simple - Fast	Precise position control impossible except at full stops
Twisted and coiled polymer (TCP)	- Light - Simple	- Low efficiency - High temperature - Contraction only

There are several types of actuators we believe are suitable for our device. Each actuator type has its own set of features; however the system needs an easy-to-control type of actuator, and some of the actuators on the market are only good in compression or extension. The device should be able to extend and retract when used in day-to-day activities. A weigh chart of several actuator types we believe would be suitable for our device is presented in *Table 2*. Each actuator type will be weighed in five aspects which we considered to be essential features for developing the system, using a score 1-5 criteria, with five as the highest score for each aspect, the score will be given by comparisons among chosen actuator types. Based on these comparisons, the electro-mechanical actuator emerged as the most suitable choice. The data presented suggests that the electro-mechanical actuator can not only provide enough load for supporting the body weight, but that it is also easy to control with an appropriate controlling unit.

One big advantage the electro-mechanical actuator has over the pneumatic one is that the electro-mechanical actuator only needs a suitable power supply, while the pneumatic actuator needs an air pump to drive the rod, which is inconvenient for patients to carry. The assembly of the pneumatic system includes two pipes for the air inlet and air vent on the cylinder, which requires more space than the electro-mechanical actuator, which only needs two wires for its power supply.

The last design feature that needs to be discussed before finalizing the design is the control segment concept design. This is discussed in section 3.2. All design choices are combined into the final draft design shown in *Figure 3-3*, which served as the guidelines for the construction of the prototype. The prototype will be shown in following result and test section (Chapter 5).

Table 2 Weigh chart for actuator selecting

	Power	Dimensions	Control	Cost	Assembly	Total
	5	5	5	5	5	25
Electromechanical	5	5	5	4	5	24
Linear motor	5	3	5	4	3	20
Piezoelectric	2	1	1	4	1	9
Pneumatic	2	4	5	5	3	19

3.2 Electronic System Conceptual Design Strategy

This section is separated into two parts: the electronic components conceptual design and the control conceptual design. Electronic components are used to measure the forces occurring in the device, while the control protocol is used to control all the mechanical electronical systems of the device and process all the detected data.

3.2.1 Electronic Components Selection Strategy

The linkage actuator that has been chosen for the system is the electro-mechanical actuator. The actuator is controlled by changing the current and current direction by the use of an H-bridge. Under normal circumstances, the electro-mechanical actuator uses a DC motor to extend or retract the rod; however, an H bridge is a popular option to change the rotation direction. An H bridge is an electronic circuit that switches the polarity of a voltage applied to a load. These circuits are often used in robotics and other applications to allow DC motors to run forwards or backwards (Williams, 2002). H bridges are available as integrated circuit boards or can be built from discrete components. There are quite a number of different types of H bridge integrated circuit boards available on the market, and different types of circuit boards are designed for different power situations. The specific choice of the H bridge circuit board discussed later below after the specific actuator has been chosen.

To see if the developed system's performance achieves this, we needed to find a way to measure and record the force applied on the foot sole. As mentioned above, the applied force on the foot sole is related to the pressure in the ankle

joint. Thus, if several force sensors were placed on the foot sole, then the detected data from the sensors could be used to estimate the validation of the developed device.

The concept behind the device allows it to be in different states during the various stages of a complete gait cycle. The data of force distraction needs to be linked with the data of the gait cycle to determine if the device is properly de-loading the ankle joint throughout the different phases. The method of using force sensors placed on the foot sole to detect the gait cycle was suggested by Dąbroś, Iwaniec, Patyk, and Wesół (2018). However, for the current study it is not sufficient to use force sensors since the force is transferred to other parts of the body by the developed device. Thus, the data coming from the force sensors while the device is activated cannot prove the phases in a gait cycle.

Another gait cycle detecting method proposed by several research teams is the use of gyroscopes that detect the leg motion. The development of such sensors is proven to be reliable (Boutaayamou, et al., 2015; Sanchez-Guzman, Guerrero-Castellanos, Mino-Aguilar, Ambrosio-Lazaro, & Linares-Flores, 2017). In the device developed for this study, several gyroscopes ware used to detect the gait cycle and to correlate the data with the force sensors' data. The performance of the developed device will be assessed based on these two sets of data.

Based on the discussion above, it was decided to fit the device with six actuators, several force sensors, and several gyroscopes. Furthermore, it also necessary to include a platform to control all parts, integrate and process data from different sensors, and give feedback to researchers and users. The Arduino development board is used in a wide range of device development

and data processing. Since there are quite a number of sensors are used, the Arduino board used in this study should have more ports for collecting different data. The processed data is transferred from the Arduino board to a computer for evaluation. For the current study, since the device is movable and wearable, allowing the users to walk around with the device fixed on their legs, the connection between the board and the computer with a data line would limit the patients' movements and thereby affect the activity range of the device. To solve this problem, a Bluetooth module supported by Arduino is used. With the Bluetooth module, the user is be able to walk freely while the researcher collects the data and does not have to follow the user.

Those components make up the whole electronic system of the device. The following section describes the control strategy of the developed device and how to process the data.

3.2.2 Control Strategy

Since the system uses a variety of electronic components, a strategy should be applied to control all selected electronic components. The control strategy needs to consist of two programs: a data process program and a device control program. The workflow description is shown in *Figure 3-4*. As mentioned above, several sensors are used to collect data of gait cycle and force applied on the foot sole. The device's interaction with users will determine their satisfaction with the system, which is why it is important to consider how to address any safety issues related to the device (see in Chapter 4) and the patient while the system is running. The control of the entire system does not only focus on data collection and processing but aims to remain user-friendly as well.
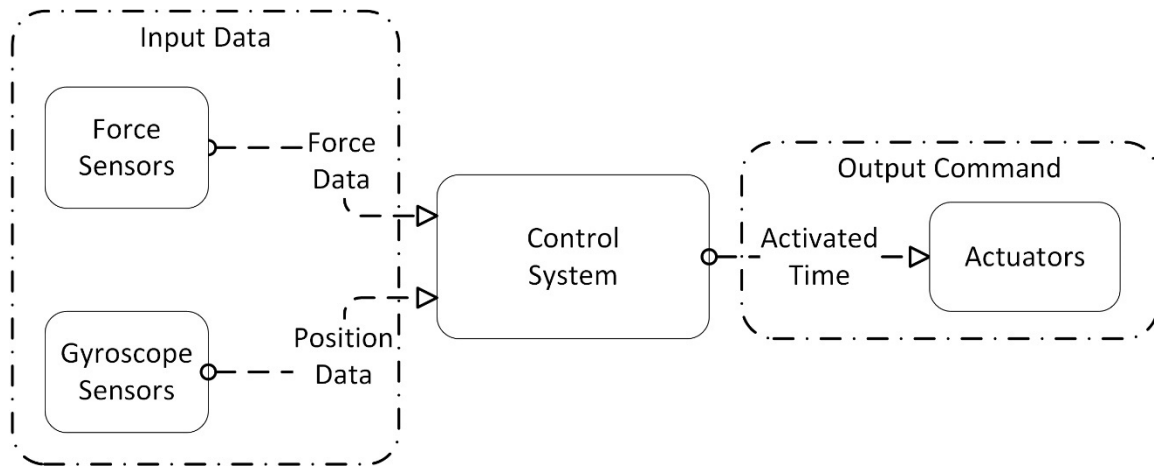
Figure 3-4 Control system workflow description

The data collected from the sensors can then be used to analyze the motion of the user. The input signal is recorded to see if the device is working properly; however, the raw data from the sensors is difficult for the researchers to understand. It is common for such data to be distorted by interferences from other places. For instance, different noises can decrease the accuracy of the detected data collected by both force sensors and gyroscopes. Therefore, filters need to be applied in the control system to avoid such interferences. There are different types of filtering algorithms for different situations. Moreover, the force sensor might face problems such as a sudden jump in detected data from the force sensor. To reduce those noises of a sudden jump, a low-pass filter (LPF) is added to the program. The LPF is a filter that passes signals with a frequency lower than a selected cutoff frequency and attenuates signals with frequencies higher than the cutoff frequency. While no filter can eliminate unwanted noise from the sensor completely, the LPF will decrease the effect of the noises from the force sensor to a minimum level, by cutting off most of the sudden jump noises. The LPF provides a smoother signal from

the force sensor, removing the short-term fluctuations and leaving the longer-term trend, which provides clearer output and facilitates data analysis.

LPF is only applicable to the force sensors of the system, but the other sensor, the gyroscope, requires different adjustments to assure clean data output. Modern gyroscope sensors are a motion tracking device with a 3-axis gyroscope and a 3-axis accelerometer embedded in one silicon chip. The gyroscope detects the motion around its axis. Data from the gyroscope alone cannot provide accurate information when calculating the velocity of the object, which is why most of the algorithms usually combine the data of both gyroscope and accelerometer. The velocity of the object can be determined by its acceleration and integration over time, allowing the position of the object to be determined. The working principle of the acceleration is a weight that is free to move horizontally, which is attached to a spring and a device to measure the tension in the spring. The device reacts to the force generated by the weight when it is accelerated by integrating that force to produce a velocity (Feynman, Gottlieb, & Leighton, 2013). This allows for higher accuracy data provided by the gyroscope, especially with regards to the measurements of the sensors observed over time. Kalman filtering, also known as linear quadratic estimation (LQE), is used in this situation. This filtering method produces estimates of unknown variables that tend to be more accurate than those based on a single measurement alone, by estimating a joint probability distribution over the variables for each timeframe. The detailed algorithm in the program will be described in the following section.

While developing a device which is intended to be put on the human body, safety issues are an inevitable problem. User's safety is always the most important aspect that needs to be considered. Electro-mechanical actuators are

used in the system for the device developed in the current study. Those kinds of actuators have a rather high torque, thus, should any malfunctions occur, they could potentially seriously hurt the wearer of the device. To prevent such situation from happening, a security control program has to be included in the system program. The security protocol needs to be able to stop the actuators before the device is out of control. Seeing that the actuator is controlled through its activated time, a timer subprogram needs to be added to the main program. The time subprogram ensures that, when the timer reaches its maximum number, the system stops the actuators immediately. Nevertheless, there are always the possibilities of a bug in the program or a circuit problem, such as short out, interfering with the proper working of the system. It is not possible to avoid such problems by an embedded program in control chip, which means that a physical stopper is needed instead. When the control of the actuators somehow malfunctions, the users themselves can manually stop the system by cutting off the power supply to the device. The physical emergency stop button will give the user more confidence in the device as they can independently touch and control the working status of the system.

This chapter has provided a detailed description of the concept of the control program of the device, providing in-depth discussions and justifications for the choices made for the different parts the device. In the following chapter, the detailed design will be presented, which combines all aspects mentioned so far. Particularly, the detailed dimensions and control codes will be described. The conceptual design of the system establishes a clear insight into how the system works and is controlled. The following chapter will focus on building on the integrated concept idea and testing its performance. The

conceptual design is just the first step of the device development, more issues of the developed device will be discussed later.

Chapter 4

Main Mechanical Structure Design

The previous chapter has introduced the system's concept design, including the conception of the structure and control system of the device. The following chapter presents the considerations that pertain to the detail design phase. It follows a similar structure to the discussion of the concept design phase and ends with the presentation of the final device design draft, which is illustrated in *Figure 3-3*. The current chapter on the detail design phase discusses every aspect of the design features, starting with the dimensions of the mechanical main frame structure, followed by the selected electronic components, and finally the programming method for the system.

Based on the information gathered during the conceptual design phase, it was decided that the main mechanical frame of the device should consist of a Stewart platform structure and a knee brace structure. This means that the design combines two different structures that are very different from each other. The design of the Stewart platform requires a focus on the connection of each platform and the ROM for each linkage. The cylinder selected for the system is an electro-mechanical actuator, which can load great pressure. The motor of the actuator should be able to hold the actuator's rod and support the pressure created by human body. In other words, the self-locking feature, which is the primary difference to the pneumatic actuators, is the reason why the electro-mechanical actuator is more suitable for the system. In this section, the design process is presented in two parts, and all the calculations provided

assume that the device is under the maximum load, which is 1500N (approximately 150kg). All the connections used are grade 8.8 standard bolts and nuts, and the material used in the device is stainless steel (ferritic) with a thickness of 2mm provided by the school's workshop. The Stewart platform and knee brace structures and their simulation results based on the mechanical property of stainless steel (ferritic) are explained separately in following section.

4.1 Knee Brace Structure Design

A knee brace structure is used for fixing the base of the Stewart platform to the lower limb around the knee. The dimension difference between the thigh and the crus makes it possible to maintain the device around the knee while the system is activated. Like it was described above, the principle of the device's de-loading function is that the foot will be lifted by the device and create a gap between the foot sole and the moving platform, which will take the place of the original function of the foot. If the fixation point of the device is attached to a part of the human body other than the lower limb, we believe that it is likely that such a fixation method would not be stable. The human thigh has more muscles than the crus does (Platzer, 2008), meaning that the human thigh is thicker. While the device is being placed on a user's lower limb, the Stewart platform will be placed around the crus. Attaching the device around the crus would not be enough to securely fix the structure to its position due to the musculoskeletal system of the crus (Schuenke, Schulte, & Schumacher, 2006). There is a dimension reduction from the crus to the connection with the knee joint, and this smaller circumference of the leg at the junction of the crus and the knee means that the fixation is likely become

loose while the user puts the developed device on. The device may loosen, causing the fixation to slide up, because of the reduction in circumference. The consequences of such an unintended change in position would be that the developed device would not be able to lift the foot up and create a gap under the foot sole, and as a result the device would not be able to work properly and therefore cannot be validated. In order to solve that problem, the fixation of the device should be expanded to the thigh. With a second fixation point the device is attached tighter to the user's leg and therefore is less likely to change position. Thus, two fixation points are needed to improve the performance of the device and in order to obtain validation of the design.

Since the knee brace structure will include the crus and the thigh, the entire knee joint will be included. The knee joint is the largest joint in the human body (Kulowski, 2007), and as mentioned above, the knee joint is a modified high joint, a type of synovial joint. However, the inner structure of the knee joint is not like a simple hinge joint; instead, the anterior cruciate ligament (ACL) and the posterior cruciate ligament (PCL) provide the knee joint's motion with extension and retraction. The knee joint moves with the help of these ligaments and the slides of patellar groove on the front femur mean that the rotation of the knee will not be on one axis only. As a result, the designed structure for simulating the motion of the knee cannot be a single pinned hinge. Several products in the existing market, like the knee braces from Donjoy Orthopaedics Inc., Bauerfeind USA Inc., and other research teams working on improving the function knee brace designs (Greenfield, Hwang, Davies, & McDaid, 2017; Irby, Kaufman, Mathewson, & Sutherland, 1999), are using the duo pin hinge to simulate the function of the knee joint ligaments. In the

current design case, a duo pin hinge will be designed for the knee brace structure.
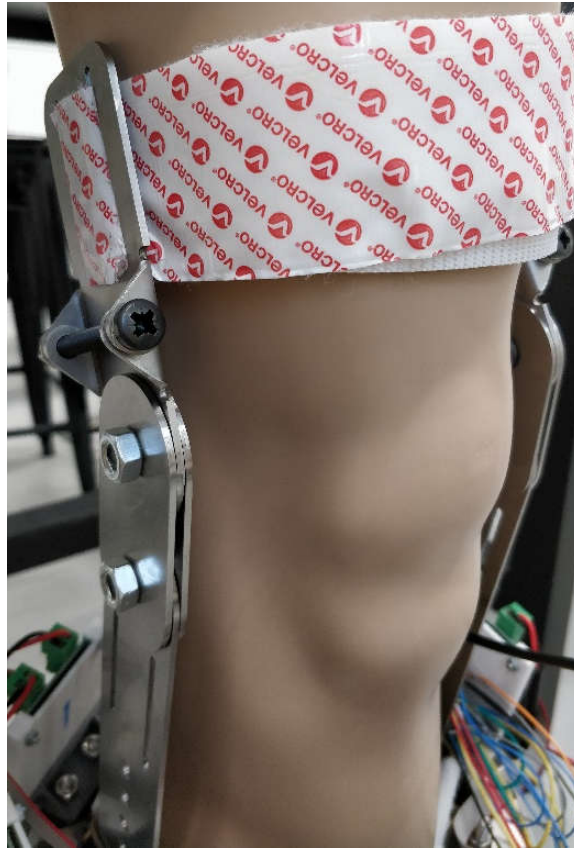
Figure 4-1 Knee brace hinge of the device

Since the dimensions of the lower limb are bound to be smaller than thigh, the design of the knee brace structure needs to be able to account for varying circumferences. According to Moreland, Basset and Hanker (1987), the angle between the femoral mechanical axis and the tibial mechanical axis is close to 180 degrees. Certain specific situations notwithstanding, the knee brace structure will be designed as a straight-line shape in hinge position as shown in *Figure 4-1*.

As for the fixation method, two high tension Velcro are used to fix the device to the lower limb. The two Velcro bandages are wrapped around thigh and

crus respectively. The thigh end of the device contains two parts, namely the thigh knee brace plate and the thigh knee brace joint plate, which are used to hold the Velcro and allow it to wrap around the thigh.

When considering the dimension differences between different users, it was decided to connect the thigh knee brace plate to the thigh knee brace joint plate with a bolt hinge. Such a hinge design allows the user to wrap the Velcro tightly around the thigh. As for the crus end of the knee brace structure, which is called the crus knee brace plate, in addition to its function of facilitating the fixation of the device with Velcro it is also used to connect the thigh structure to the base part of the Stewart platform structure.

In order to account for different height and length differences of the crus of different users, ten holes are added to the metal connection under the Velcro slot, with each hole being located 15mm away from the next hole. The force transferred by the actuators will be applied to this plate, through the holes that provide the connection to the Stewart platform. The maximum force that may be applied on these holes will be 750N for each knee brace plate. Since there are two plates on the right and left side of the leg, each plate will share approximately half of the maximum force. The connection with the Stewart platform structure is established through two 10mm M6 bolts, and for a better assembly experience, the holes are designed with a diameter of 6.5mm, through which a M6 bolt can be easily inserted. The maximum shear stress applied on the bolt is calculated in *Equation 1* (Budynas & Nisbett, 2011).

$$\tau_{bolt} = F_{max}/A_{bolt} = \frac{750N}{(\pi \cdot (6/2)^2)mm^2} = 26.526 \, Mpa \qquad (1)$$

(a) Connection on top two holes   (b) Connection on bottom two holes
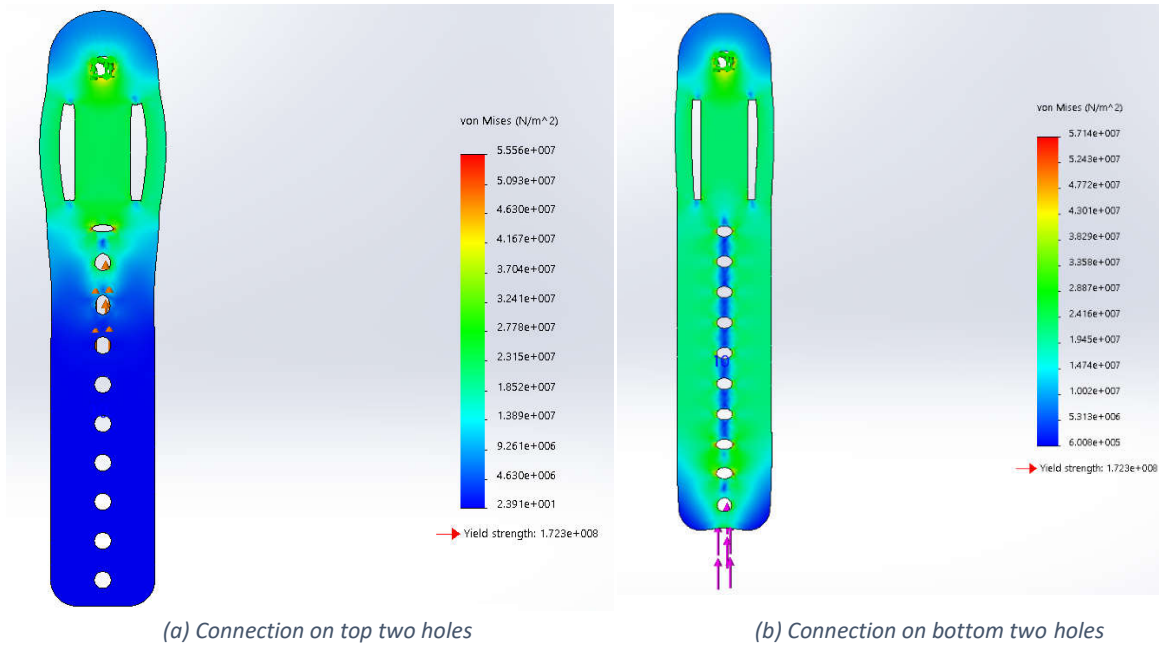
Figure 4-2 Simulation results of crus knee brace plate in different connection situations

Based on the calculation presented above, the maximum shear force applied on the M6 bolt of the knee brace plate is around 6.631Mpa, and according to the international standard of a grade 8.8 bolt, the yield strength is 640Mpa. This means that the M6 bolt can be safely used in knee brace structure. At the same time, the plate will also be able to bear a force of 750N while the device is in use and needs to support the maximum body weight of the user. The static simulation results for of the plate are shown in *Figure 4-2*.

Depending on the situation, the Stewart platform base can be connected to any two holes of the knee brace plate. *Figure 4-2(a)* shows the situation where the connection is on the top two holes while *Figure 4-2(b)* shows a situation where the connection is on the bottom two holes. The fixation place in both simulations is a M8 pin hole for the knee brace joint connection on top of the plate. As shown in both *Figure 4-2(a)* and *4-2(b)*, every result's maximum stress turns out far smaller than the yield strength of the selected material,

which means that the design is safe and stable in simulation. *Figure 4-3(a)* and *(b)* show the structure and the method how the knee brace is attached to the thigh and crus, and there are two knee brace joint covers used to connect the crus and thigh knee brace parts.
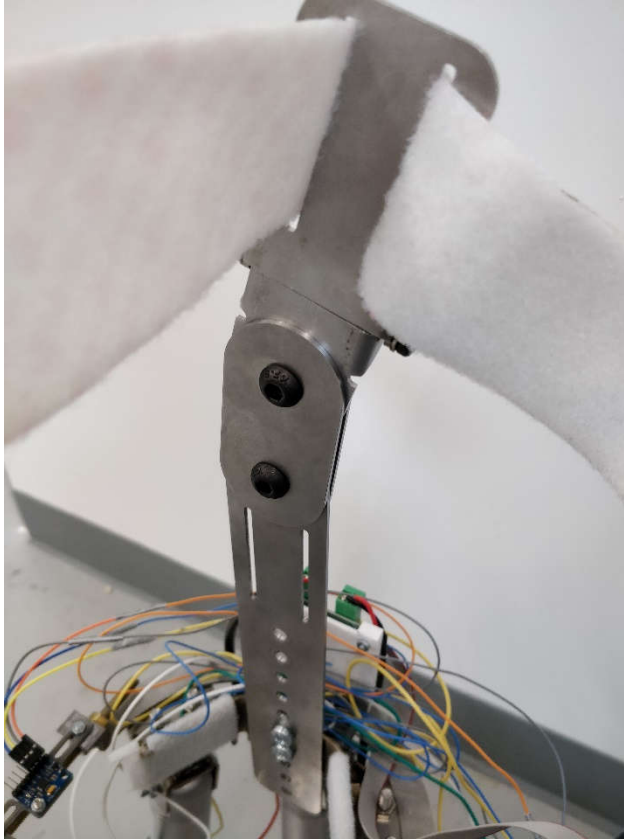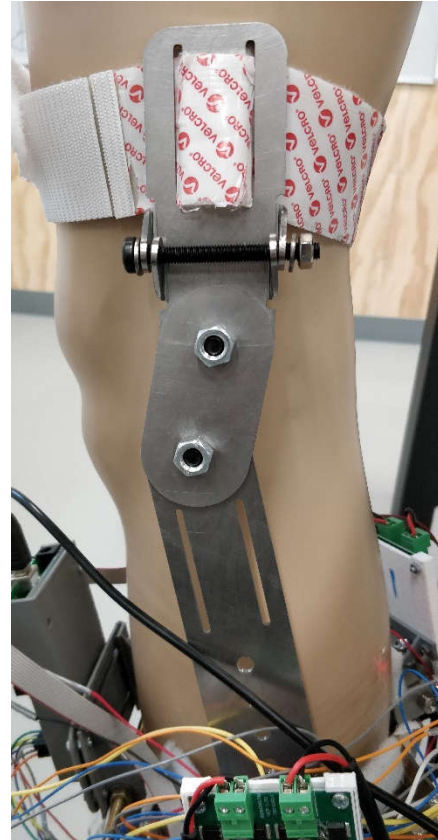
(a) Structure of the knee brace   *(b) Knee brace attached on the dummy's leg*

Figure 4-3 Knee brace of the device

4.2 Stewart Platform Structure Design

The most important thing in a Stewart platform structure design is the connection of the actuator with the base and the moving platform. In the design process, there is one important aspect that should be mentioned with regard to the electro-mechanical actuator, which has been chosen as the linkage of the system. The working principle of the actuator is when it is on,

the motor inside the actuator starts to rotate and push or pull the rod to the desired displacement and fix the rod's position with the motor's static torque. The torque is too high so that normal person cannot change the displacement of the rod. However, after the device is activated and the rod is fixed in a certain position, it still needs to replicate the motion of the foot, meaning that small changes to the rod's displacement may still be needed. Thus, a damping system is needed for the actuator, as the damping system can be moved easily to allow small changes to the positioning to be made by the foot motion in gait cycle. Such design will solve the problem of fixed rod.

As for the connections to the base and the moving platform, since the moving platform is the part that needs to be able to move in the system, the rod head of the actuator is connected to the moving platform. The Stewart platform was chosen because of its DOF and ROM, and to ensure these movements can be fully realised, the connection between the linkage and the two platforms should be the universal joint. This kind of joint can provide rotations on three axes, and it the universal joint in the Stewart platform that are responsible for the platform's 6 DOFs. As mentioned, the rod will be driven by the DC motor, and rotated with it because the universal joint is not suitable in such rotation condition due to its characteristic of not a constant-velocity joint (Budynas & Nisbett, 2011). With the high-speed rotation, the universal joint might break down, however, there is another joint that can provide 3 DOFs on three rotation axes and that will not be broken in a high-speed rotation, namely the spherical joint. The dimension of the connection joints will be explained later.
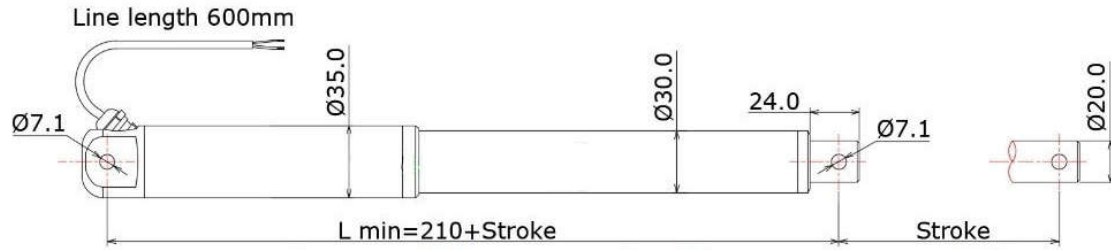
Line length 600mm

Ø35.0 Ø30.0 24.0 Ø20.0
Ø7.1 Ø7.1

L min=210+Stroke   Stroke

Figure 4-4 Detail dimension of the selected actuator

The electro-mechanical actuator is a better choice for the device; however, there are already various types of this kind of actuators on the market. To determine the exact actuator the device should use, a research on high-duty electro-mechanical actuators has been done. When selecting the right actuators, several aspects should be taken into consideration: dimension, working power, support load, weight, and price. The device is a wearable device, like an exoskeleton, for patients with an ankle problem, thus the volume of the device should be controlled in an acceptable range. The Stewart platform structure's design is based on the dimension of the actuator, especially for the dimension of the universal joint and the spherical joint. While selecting the actuator, users' safety issue is an aspect that needs to be considered. As a wearable device, and powered by electricity, the working voltage should be much lower than the human body safety voltage level, in case the device short circuits or other causes situation which might cause unexpected injuries on users by electricity. Luckily, most of the electro-mechanical actuators' working voltage in the market is 12V or 24V (Cadick, Capelli-Schellpfeffer, & Neitzel, 2005). This voltage level is the safety level for human body. As mentioned above, the maximum load of the device is 1500N, and every actuator needs to be able to support a load of 250N on average under the maximum load. However, 250N is only the straight up force each actuator will be exposed to; in practical use, due to the tilt angle of the

actuator in 3D space, the situation is much more complicated compared to the straight up force situation. This requires a moving range restriction design for universal and spherical joints. The maximum moving tilt angle is decided by the support load of the selected actuator. The calculations are based on the relationship between support load of the actuator and the maximum load applied on the device, and this is the main reason why the actuator should be selected before beginning the design of the Stewart platform. As there is a budget on the project, the price of the actuator should be controlled in a minimum number under the conditions all above. The selection of the actuator was made is by researching the existing market on electro-mechanical actuators. The final selection of the features for the actuator is shown in *Table 3* and the picture of the actuator is shown in *Figure 4-6*. The selected actuator's specific dimension from the manufacturer is presented in *Figure 4-4*.

Table 3 Specification of the actuator

Type	Tubular Motor	Continuous Current(A)	1.5A
Model Number	LA35T	Protect Feature	Waterproof
Commutation	Brush	Construction	Permanent Magnet
Output Power	36W	Efficiency	IE 4
Torque	350N	Stroke	50mm
Max Load	350N	Input	24V DC
Max speed	45mm/sec	Working duty	25%

Figure 4-6 Selected actuator
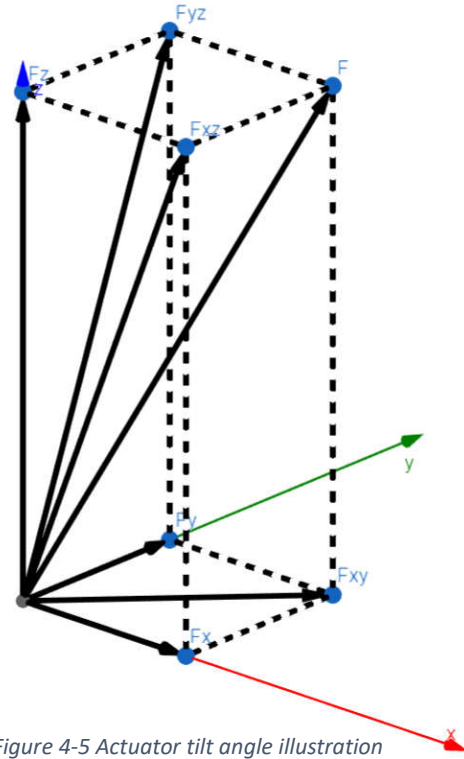
Figure 4-5 Actuator tilt angle illustration

Since the specification of the actuator are settled, the dimensions of both actuator's heads have also become clear. The first thing that needs to be determined is the actuator's maximum tilt angle. As shown in *Figure 4-5*, F_{Zmax} is the straight up force applied on the actuator, which has been specified as 250N for the maximum load. The force F_{max} is the maximum support load the actuator is be able to bear, which is 350N. With the number of F_{Zmaz} and F_{max} being given, the maximum tilt angle θ_{max} between the vertical axis Z and the support force is given in *Equation 2*,

$$\theta_{max} = \arccos\left(\frac{F_{Zmax}}{F_{max}}\right) = \arccos\left(\frac{250N}{350N}\right) \approx 44.42deg \quad (2)$$

With the result of θ_{max}, and bearing in mind safety factors, the tilt angle of the actuator must be smaller than 44.42 degrees to prevent overload. It was decided to ensure that, for the device developed in this study, 40 degrees is the maximum tilt angle θ_{max} of the actuator with the vertical axis. All

following dimension calculations of universal and spherical joints will be based on this maximum tilt angle.

Following the basic maximum tilt angle, the next feature that needs to be considered in design process is the joint design. There are two types of joints included in the system, the universal and spherical joints. Spherical joints will be used to connect the actuator's rod head to the moving platform, while universal joints are used to connect the other head to the base of the Stewart platform. Both types of joints are designed so that their rotation angle is equal to or less than 40 degrees as calculated above. Except for the dimension calculation, strength calculation and simulation in SolidWorks based on the material mentioned before will also be conducted. Since the device is designed to be used in daily life, it is crucial that we can guarantee the safety and stability of the device, which hinges to a large extent on the structure strength of the device. The following section describes the designing process of the structure strength in detail.

4.2.1 Spherical Joint Design

The spherical joint mainly consists of two parts, a socket base and a ball joint with actuator rod connection slot. The design point described in this section is to ensure that the tilt angle provided by the joint cannot be over 40 degrees, and at the same time that the joint is able to roll in the socket base smoothly to reduce friction from the device and establish a smooth foot motion. The point of this device is to de-load the force applied on the ankle joint, but the friction of the device will apply the force to it; therefore the less the friction from the joints, the better it is for the performance of the device. Since the

socket base's dimension of the ball joint is determined by the size of the ball joint, the spherical structure needs to be designed first.
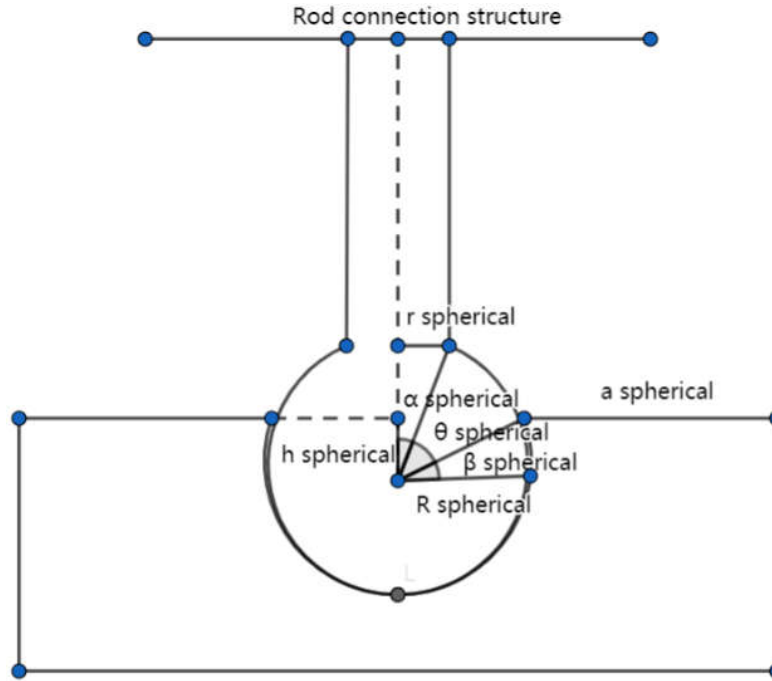
Figure 4-7 Detail design of the spherical joint

As the draft design of the spherical joint presented in *Figure 4-7* shows, the ball joint needs to be inserted into the socket base where it is fixed. To determine the radius of the beam that connects the ball and the rod connection structure, which in *Figure 4-7* is labelled $r_{sphrical}$, the relationship between $r_{sphrical}$ and other parameters needs to be found. Among all the other parameters, $\theta_{sphrical}$ represents the angle the spherical joint can rotate, which in our case is 40 degrees. In other words, the spherical joint should be stopped by the beam when the tilt angle reaches 40 degrees. The relationship of the $r_{sphrical}$ with other parameters is represented by *Equation 3*,

$$r_{sphrical} = R_{sphrical} \cdot \cos\left(\theta_{sphrical} + \arcsin\left(h_{sphrical} / R_{sphrical} \right) \right) \quad (3)$$

In the equation, $R_{sphrical}$ is the radius of the ball joint and $h_{sphrical}$ represents the height from the upper surface of the socket base to the center of the joint. Because the ball joint has to be fixed so that it will not fall out of the socket, the ball joint's center has to be under the surface of the socket base. The research has decided that the radius of the ball joint $R_{sphrical}$ needs to be 10mm and $h_{sphrical}$ is half of $R_{sphrical}$. Along with the maximum $\theta_{sphrical}$, 40 degrees, the result of $r_{sphrical}$ by calculation is rounded down to 3mm.

Figure 4-8 Connection of actuator's rod with ball joint

In addition to the radius of the beam, there is another factor which could affect the tilt angle of the ball joint, which is the length of the beam. The length of the beam is directly connected to the rod connection structure which is used to fit the actuator's rod, and which plays an important role as a damping system for the device. As mentioned above, the actuator's rod needs to be fixed after it is extended or retracted to the desire place, and human force is unlikely to interfere with the fixation torque provided by the DC motor in the actuator. However, when in practical use, the device needs to replicate a lot

of small movements from foot motion, which would enable the device to more accurately restore the foot's natural movements and also be more comfortable for the users.

The main design focus of damping system is that when the actuator is fixed, the damping system should be able to connect the moving platform to the actuator while making the moving platform move like a foot in gait cycle. A damping system functions like ligaments in an ankle joint. While the actuators play the roles of tibia and fibula, the damping system is able to extend easily in the stance phase and allows the moving platform to replicate the angle of the foot after the actuators are all fixed. This is similar to the mechanical property of the ligament (Buschmann & Bürgisser, 2017), since ligaments and tendons in the ankle joint are composed of fibers that have an elastic feature which allow them to extend and retract. The damping system of the device is fitted with rubber bands, which enables it to play the role of the ligaments in the system. The connection between the actuator's rod and the spherical joint is achieved by the bolt which is positioned in a hole with a 7.1mm diameter that is located on the head of the rod (see in *Figure 4-4*). An M6 bolt is used for the connection, so there are two slots with a width of 6.5mm symmetrically placed on both side of the spherical joint structure as shown in *Figure 4-8*. A sleeve is attached at both ends of the bolt for the rubber band in order to decrease the danger of the rubber band getting stuck in the slot and to reduce the friction of the band with the components. This completes the design of the damping system. The next issue related to the spherical joint design is concerned with dimension of rod sleeve.
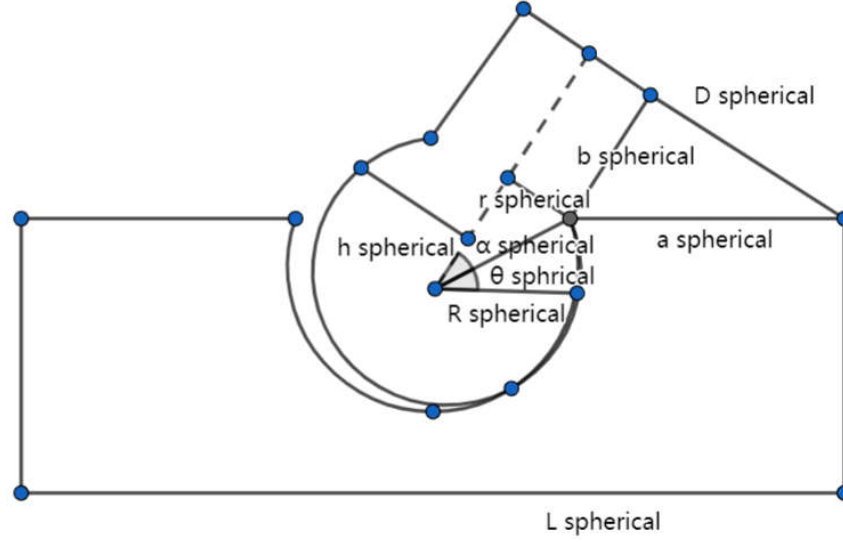
Figure 4-9 Detail design of the spherical joint (with maximum tilt angle)

To fit the actuator's rod, the inner diameter of the sleeve on the spherical joint shown in *Figure 4-8* is 21mm, which is compatible with the actuator's rod diameter shown in *Figure 4-4*. The material provided by the workshop is 2mm, thus the outer diameter of the sleeve is 25mm in total. As shown in *Figure 4-9*, $D_{spherical}$ represents the radius of the sleeve structure, which is 12.5mm. The parameter related to the tilt angle is the length of the beam, $b_{spherical}$, that runs from the upper surface of the socket base to the sleeve structure. The length of the beam should be long enough to prevent contact between the sleeve structure and the base and avoid interference with the tilt angle of the joint. Based on our design where the sleeve structure contacts with the base as shown in *Figure 4-9*, the result of $b_{spherical}$ will be the minimum length of the beam, so that the designed length should be longer than the calculated result. The calculation of $b_{spherical}$ is presented in *Equation 4*,

$$b_{spherical} = \left(L_{spherical} - R_{spherical} \cdot \cos\left(\arcsin\left(\frac{h_{spherical}}{R_{spherical}} \right) \right) \right) \cdot \sin(\theta_{spherical}) \ (4)$$

As shown in *Equation 4*, the length of the beam $b_{spherical}$ is related to the radius of the base $L_{spherical}$, the maximum tilt angle $\theta_{spherical}$, the ball joint radius $R_{spherical}$, and the height of ball joint center in relation to the upper surface of the base $h_{spherical}$. The radius of the base is 15mm, and the ratio between $h_{spherical}$ and $R_{spherical}$ is still the same as presented in *Equation 3*, which is 0.5. The result of the equation with a maximum $\theta_{spherical}$ of 40 degrees is around 4.075mm. This number marks the shortest length the beam is can have. If the height of the ball joint is subtracted from the entire length of the ball joint, which is 30mm in total, then we can say that the beam length is around 10.46mm. This beam length is longer than the minimum 4.075mm, which means that the designed length is acceptable.

There are another two parameters that need to be determined, namely the radius of the fixation plate under the base and the height of the socket base. As previously described, the ratio between $h_{spherical}$ and $R_{spherical}$ is 0.5, but any number over 15mm will be acceptable to the design and suitable for the ball joint. Thus, in the final prototype, the height of the base is 16.75mm, and the thickness of the base plate is not included. With regard to the base plate, it is used to fix the base on the moving platform with several M3 bolts and nuts. The dimension of a M3 nut is a hexagon with a diagonal of 6.3mm. In order to have a better experience in assembly and disassembly, the design includes an assembly space of 10mm for the nuts as illustrated in *Figure 4-10*.

Figure 4-10 Spherical joint's socket base with fixation plate

If the socket base of the joint is directly manufactured as a whole, the ball joint would not be able to be placed inside the base because the diameter of base's front opening is smaller than the ball joint's diameter to prevent the ball joint from falling out of the base. As a result, the base is cut into two halves, and each half has three 3.5mm diameter holes for fixation as shown in *Figure 4-10*. In order to check if the spherical joint is suitable for the system and if the material is able to bear the maximum load, a static simulation in SolidWorks is run. The results of the simulation on the base and ball joint are shown in *Figure 4-11(a)* and *(b)*. A straight downward force of 250N is applied on the base The fixation place is on the bottom surface of the base, for the base will be connected to the moving platform through six M6 bolts. Due to the rotation of the ball joint, the simulation applied the maximum force at the maximum angle of 40 degrees, which is the angle between the central axis of the ball joint and vertical line. The fixation place is located on the inner side of the ball joint, which is connected t0 the rod of the selected actuator. Both simulation results show that the designed structure of the spherical joint are safe under the maximum load. All six actuators are fitted with this

spherical joint on their rod head and connected to the moving platform of the Stewart platform.
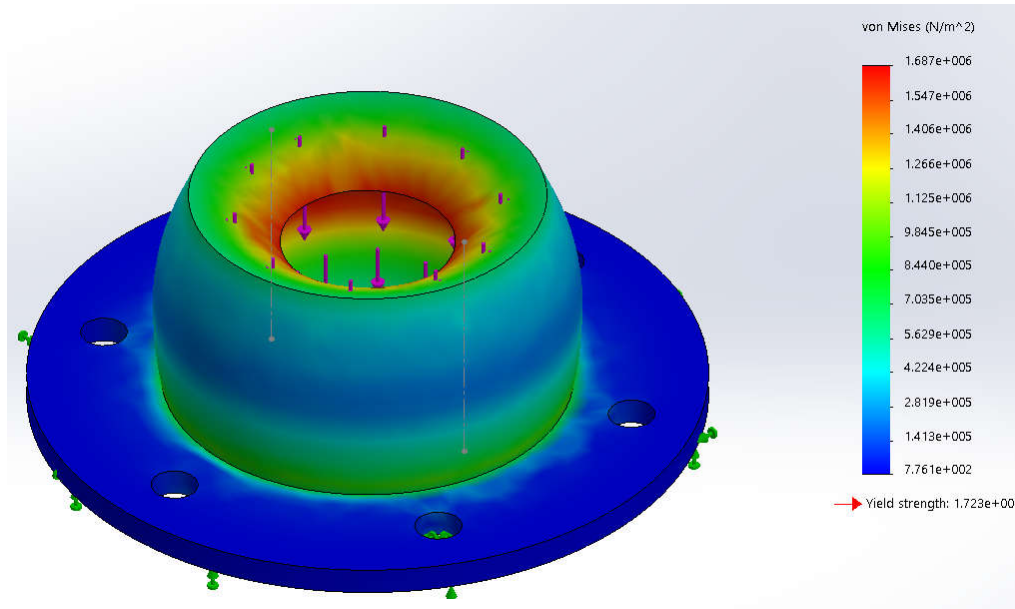
(a) Ball joint base simulation
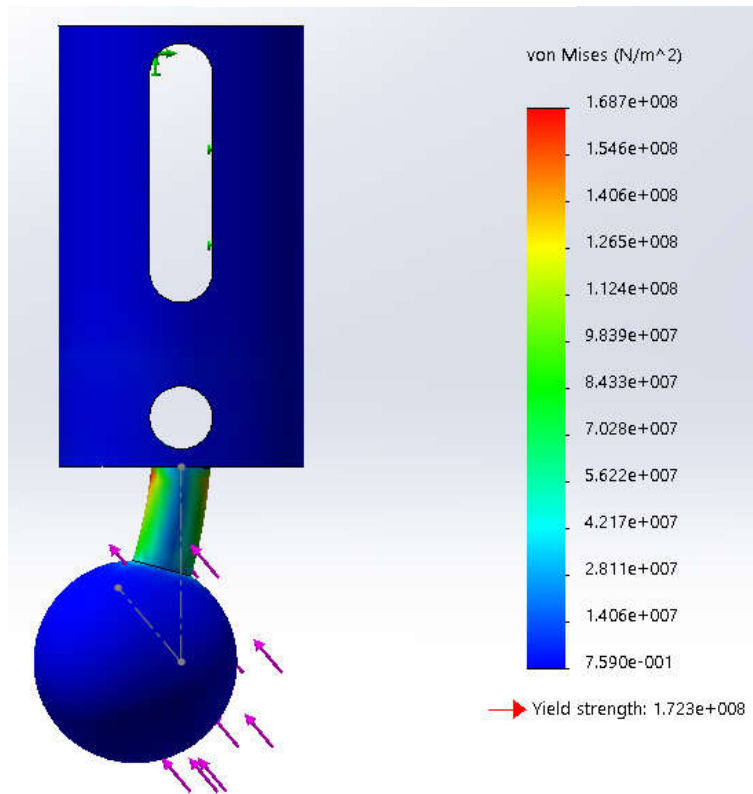
(b) Ball joint simulation

Figure 4-11 Simulation results of spherical joint

4.2.2 Universal Joint Design

The universal joint in the device is quite important and complex to design; unlike the design of the spherical joint, universal joint consists of many parts and requires more dimension calculations to ensure that the demands of the system are fulfilled. Traditionally, an universal joint is a joint or coupling connecting rigid rods whose axes are inclined to each other. They are commonly used in shafts that transmit rotary motion. Universal joints consist of a pair of hinges that are located close together, oriented at 90 degrees to each other, and connected by a cross shaft (Budynas & Nisbett, 2011). In the current study, the design is kept as simple as possible in order to facilitate material maintenance and component changes after material failure. The design uses standard grade 8.8 M6 bolts for the rotation rods in the system. According to the standard chart of a grade 8.8 bolt, its tensile strength is 800MPa, and its yield strength is 640MPa. The following calculation of the rigid rod's strength is based on this data.

Universal joints mainly consist of three parts: actuator cap, sleeve for bolts, and base ring connection. The actuator cap is placed on the actuator's non rod head, the dimension of which are given in *Figure 4-4*, and there are two parallel flat faces on two sides of the actuator. This feature of the actuator is used to place the actuator cap of the universal joint. The flat faces make it easier for the design and manufacture process because the cap does not need to be designed in a special curve. The 7.1mm diameter hole on actuator head can be used as a fixation point for the cap with a M6 bolt. The bolts used for the rigid rod of the universal joint are not directly used because the rotation of the rod cannot be achieved with just bolts and nuts. A sleeve structure needs to be designed to fit both bolts used in one universal joint. In this case, the

sleeve acts like the rotary shaft in the joint. The bolts are able to bear the full load due to their proven strength. The base ring connection is located at the upper part of the joint and used to connect the joint to the base ring. All six actuators are connected to the base ring, which is placed around the user's crus.

In addition to the fixation structure that is attached the actuator's head, actuator cap also needs two ears to connect it to the rotary rod. In the beginning of the design process, initial parameters need to be established which will inform subsequent design decisions. The dimension of the ear is assumed to be like the picture shown in *Figure 4-12*. The initial width of the ear is 20mm, the diameter of the hole for the bolt is 6.5mm. In order to determine if the initial parameters are acceptable for the design, several calculations need to be made. Since the initial width of the ear has been given, the strength of the ear should be checked to see if the dimensions are acceptable in relation to the characteristics of the material.
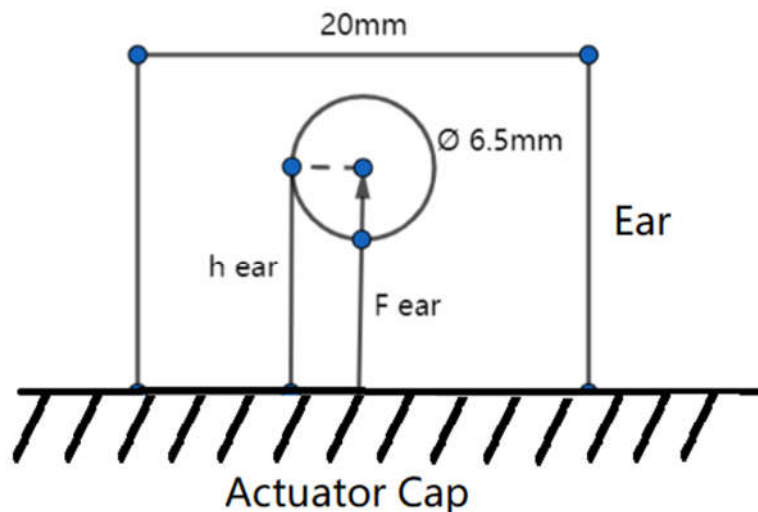

Figure 4-12 Initial actuator cap ear diameter

The first calculation given in *Equation 5* presents the calculation of failure of the ear when under tension,

$$\sigma_{tear} = \frac{F_{ear}}{A_{ear}} \qquad (5)$$

Here, σ_{tear} represents the pressure the ear needs to be able to bear, F_{ear} is the maximum force applied on the ear, and A_{ear} is the area that bears the load. F_{ear}, which in this case is 350N, the same maximum load of the mechanical property of the selected actuator. The joint needs to be strong enough to guarantee safety and stability, therefore the maximum force that it needs to be able to withstand should be the same as the maximum force that the actuator can withstand. The area of the ear is based on the thickness of 2mm mentioned previously. The area bearing the load A_{ear} is calculated in *Equation 6*.

$$A_{ear} = 20 \times 10^{-3}m \times 2 \times 10^{-3}m - 6.5 \times 10^{-3}m \times 2 \times 10^{-3}m = 27 \times 10^{-6}m^2 \, (6)$$

Using the values of the area A_{ear} and the maximum F_{ear} that have been provided above and the tension pressure that was calculated using *Eq. 5*, the result of *Equation 6* is 12.96MPa. The result from the tension calculation should be compared to the result from the bearing calculation, to see if both calculation results are suitable for the current material, which is stainless steel (ferritic). The result of failure of ear by bearing is based on *Equation 7* (Budynas & Nisbett, 2011).

$$\sigma_{bear} = \frac{F_{ear}}{d_{ear} \cdot T_{ear}} \qquad (7)$$

Here, d_{ear} refers to the ear hole's diameter and T_{ear} is the thickness of the ear, which is 2mm. With data given above for F_{ear} and d_{ear}, the result of *Equation 7* is 26.92MPa. Both calculation results of the maximum pressure the ear

needs to be able to bear is far lower than the chosen material's yield strength, which is 172.34MPa. After the tension and bearing calculation, the shear stress of the initial design is calculated to check if the design is safe. The failure of the ear by shear is given by *Equation 8* (Budynas & Nisbett, 2011).

$$\tau_{ear} = \frac{F_{ear}/2}{h_{ear} \cdot T_{ear}} \tag{8}$$

In the equation above, h_{ear} is the height from the surface of the actuator cap to the center of the ear hole, which in this initial design is set to 5mm. The result of the shear pressure based on the given data is 17.5MPa. In addition to the pressure applied on the cap, the bolt connecting the cap with the universal joint sleeve is also under pressure. To assure its safety from breaking down under such pressure, the shear pressure of the bolt should be calculated as well. The calculation of failure of the bolt by shear is presented in *Equation 9* (Budynas & Nisbett, 2011).

$$\tau_{ebolt} = \frac{F_{ear}}{A_{bolt}} \tag{9}$$

The area of a standard M6 bolt A_{bolt} is around $2.827 \times 10^{-5} mm^2$. This area bears the shear pressure applied on the bolt, which means 12.379MPa. According to the above calculations of the different pressures applied on the actuator cap, the initial design proves to be appropriate while in practically use. The ear bears the reaction force from the bolt of the rotary rod, and the direction of the force received is directed downward from the center of the hole to the bolt. The weight of the actuator is far lighter than the force applied on the actuator cap. All the pressure calculations given above only apply to be the situation of received downward reaction force, the applied force by actuators will be neglected. The design of the universal joint requires further

calculations in later discussion, and the initial dimension of the actuator could be changed based on the results for different scenarios.
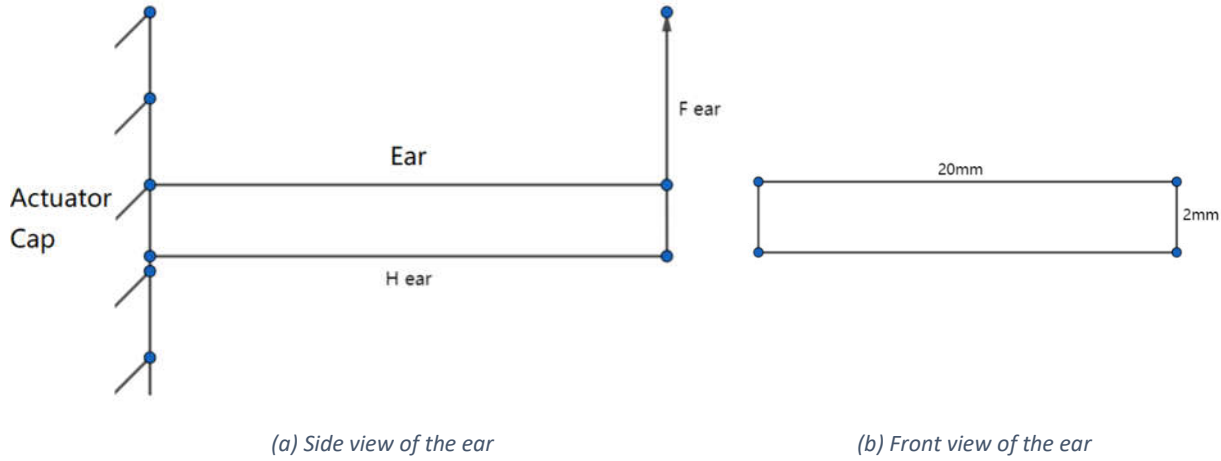

(a) Side view of the ear   (b) Front view of the ear

Figure 4-13 Actuator cap ear height calculation illustration

Figure 4-13 (a) and *(b)* show the side and top views of the actuator cap's ear (further illustration in *Figure 4-15* and *Figure 4-16*). Several initial dimensions of the ear, such as the thickness and the width, have be confirmed to be safe based on the calculations presented above. There is another important parameter that needs to be decided to continue with the design process, namely the height of the ear H_{ear}. The calculation assumes that the force applied on the head of the ear F_{ear} is the same maximum support force of the selected actuator, 350N. The highest bending stress σ_{ear} is calculated using *Equation 10* (Budynas & Nisbett, 2011).

$$\sigma_{ear} = \frac{M_{ear} \cdot y_{ear}}{I_{ear}} \tag{10}$$

Here, M_{ear} is the moment F_{ear} is applied on the ear, y_{ear} is the neutral axis of the ear, and I_{ear} is second-area moment of the ear. The moment M_{ear} is applied by F_{ear} is calculated using *Equation 11*.

$$M_{ear} = F_{ear} \cdot H_{ear} \tag{11}$$

In *Eq. 11*, the height of the ear H_{ear} is an unknown value which need to be determined, so that further calculations related to the base ring connection can be done. By calculating the maximum length of the ear, the height H_{ear} designed for the ear will have a range to determine, and there is no need to be concerned about the failure problem. The value of the second-area moment of the ear I_{ear} is determined using *Equation 12* (Budynas & Nisbett, 2011).

$$I_{ear} = \frac{2 \times 10^{-3}m \times (20 \times 10^{-3}m)^3}{12} \approx 1.333 \times 10^{-9}m^4 \tag{12}$$

The value of I_{ear} is shown in *Eq. 12*, and the value of the neutral axis y_{ear} is $1 \times 10^{-3}m$. The maximum bending stress σ_{ear} is the yield stress of the selected material, which is 172.34MPa. Thus, when applying these values to the given equation, the result shows that the maximum length of H_{ear} is around 0.6564m. The range of the ear's height is 0mm to 656.4mm, any value in this range will be guaranteed safe from failure.

The only calculation left to be done is the distance between the two ears. Since there are two ears on the actuator cap, the length between them is related to the length of the sleeve of the rotary rod. The sleeve should be able to fit inside the gap between the two ears as well as be able to bear the load applied on it. *Figure 4-14(a)* illustrates how force is applied on the sleeve. The sleeve is used to fit the bolt and functions as a rotary rod. The bolt inside the sleeve will distribute the force continuously over the inner side of the sleeve. For the calculations it is assumed that the applied force F_{sleeve} is the maximum force of the support force of the actuator, which is 350N. The force situation applied on the sleeve is a uniformed load of $\frac{175}{l_{sleeve}} N \cdot m$. The aim is to identify the

range of the l_{sleeve}, and then calculate the length between the two ears, which should produce the acceptable length of the sleeve.
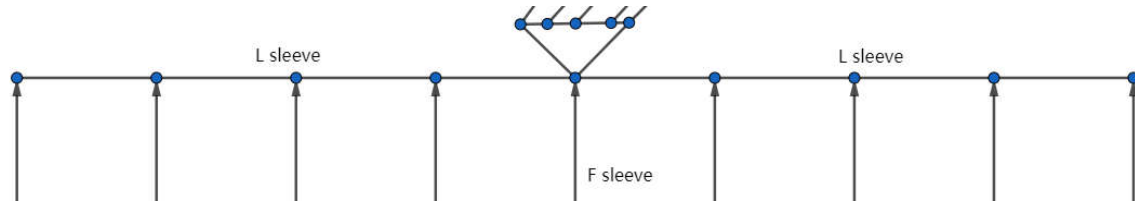
(a) Uniform load on sleeve
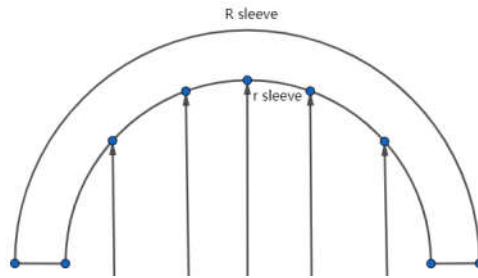
(b) Cross section of the sleeve applied with load

Figure 4-14 Force apply on rotary rod sleeve

Figure 4-14(b) shows the force application situation on the cross section of the sleeve. The bending stress for the sleeve is calculated using *Equation 13* (Budynas & Nisbett, 2011).

$$\sigma_{sleeve} = \frac{M_{sleeve} \cdot y_{sleeve}}{I_{sleeve}} \tag{13}$$

This equation is the same as *Equation 10* above; however, calculations of the parameters in *Equation 13* result in a huge difference due to the shape of the sleeve shown in *Figure 4-14(b)*. In the equation, the movement of the uniform load on the sleeve M_{sleeve} is $87.5 L_{sleeve}$ $N \cdot m$. The second-area movement of the sleeve I_{sleeve} is calculated using *Equation 14* (Budynas & Nisbett, 2011).

$$I_{sleeve} = \frac{\pi \cdot R_{sleeve}^4}{8} \cdot (1 - \alpha^4) \qquad \alpha = \frac{r_{sleeve}}{R_{sleeve}} \qquad (14)$$

Here, R_{sleeve} refers to the outer radius of the sleeve, and r_{sleeve} is the inner radius of the sleeve. The neutral axis y_{sleeve} is calculated using *Equation 15* (Budynas & Nisbett, 2011).

$$y_{sleeve} = \frac{4}{3\pi} \cdot \frac{R_{sleeve}^3 + r_{sleeve}^3}{R_{sleeve}^2 + r_{sleeve}^2} \qquad (15)$$

According to the equations shown above, the length of sleeve L_{sleeve} is closely related to the radius of the sleeve. As the inner radius of the sleeve r_{sleeve} is 3.25mm, due to the size of M6 bolt, the outer radius of the sleeve is assumed in following design. The assumption of the outer radius R_{sleeve}, in other words, the thickness of the sleeve, can be determined with the length L_{sleeve} at the same time. Thus, assume the thickness of the sleeve is 1mm, which means the outer radius of the sleeve $R_{sleeve} = 4.25mm$. The maximum bending stress is 172.339MPa. When adding these values to the equation, the data suggest that the length is the range L_{sleeve} and it should be shorter than 101mm. But L_{sleeve} is only half of length of the sleeve, which means the result of the total length of the sleeve should be controlled under 202mm.

Based on the above calculation, the height of the actuator cap and the length of the rotary rod sleeve are allowed a certain safety range for choosing. This helps the design of the base ring connection. The connection's dimension calculation, which will be in safety length range, is very complex because the dimension will directly affect the angle universal can rotate. The maximum angle of the universal joint could be bigger than the maximum calculated before because of the maximum tilt angle the spherical joint can provide was

determined and designed in a previous design. Moreover, the spherical joint is the direct force bearing point for the actuator, which means that the force is mainly applied through the spherical joint, so that the maximum tilt angle of the spherical joint could affect the maximum force applied on the actuator. The universal joint's function is to pass the force transferred from the actuator and apply it on the base ring of the Stewart platform so that the tilt angle of the universal joint does not impact too much on the actuator. Thus, it is important to bear in mind during the designing process that the rotation angle range of the universal could be bigger than the spherical joint.

(a) Front view of the joint   (b) Side view of the joint
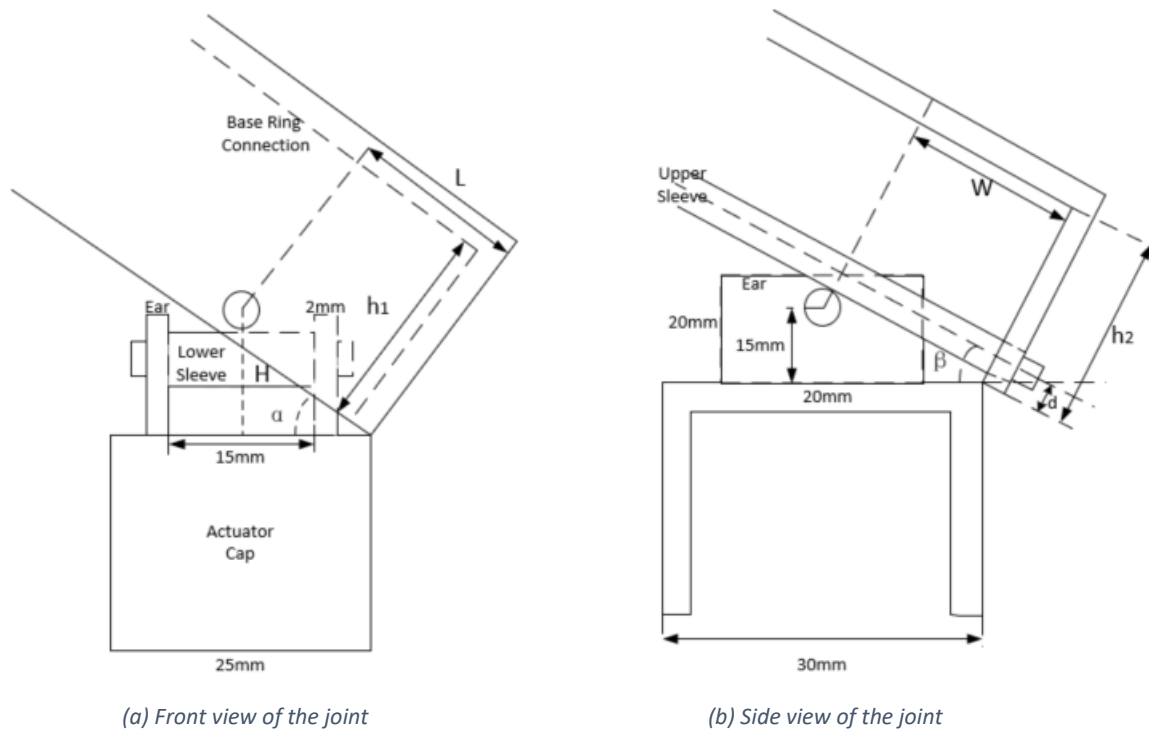
Figure 4-15 Universal joint dimension calculation

As shown in *Figure 4-15(a)* and *(b)*, the dimension of the universal joint is determined by the rotation angle of the joint. Previous calculations suggested that the height of the ear on actuator cap should be no more than 656.4mm. In the current design, the height of the ear is set to 20mm as shown in *Figure 4-*

15(b), and the height of the ear hole center to upper base of the actuator base is 15mm, while the width of the ear is 20mm. All the data provided above include a safety range that was previously calculated.

The next segment aims to calculate the length of the base ring connection L, and its inner width W. In *Figure 4-15(a)*, when the base ring connection has been rotated to its maximum angle α about the upper rotary rod, the length edge is just touching the width edge of the actuator cap's ear. The relationship between α and L is calculated using *Equation 16*.

$$L = H \cdot \sin(\alpha) - 12.5 \cdot \tan(\alpha) \cdot \sin(\alpha) + \frac{12.5}{\cos(\alpha)} \qquad (16)$$

Here, H refers to the height of the upper rotary rod to the upper surface of the actuator cap. In previous calculations it was assumed that the thickness of the sleeve is 1mm. The inner diameter of the rotary rod for M6 bolt is listed as 6.5mm and the outer diameter of the rod as 8.5mm. The height of the upper rotary rod H is 23.5mm. Assuming the maximum tilt angle α is 45 degrees, the calculation result of the base ring length is about 25.46mm. The following of the inner width W can be carried on. The result of W is was achieved by *Equation 17*.

$$W = \frac{15}{\cos(\beta)} + \frac{d - 4.25}{\sin(\beta) \cdot \cos(\beta)} - 4.25 \cdot \tan(\beta) - \frac{d - 4.25}{\tan(\beta)} \qquad (17)$$

Here, β refers to the maximum tilt angle the base ring connection can rotate about the lower rotary rod. For the calculation of the distance between the center of the lower rotary rod and the lower edge of the base ring connection d using t *Eq. 18* it is assumed that the inner width edge is just touching the length edge as shown in *Figure 4-15(b)*.

$$d = \frac{L}{\tan(\alpha)} - \frac{12.5}{\sin(\alpha)} \qquad (18)$$

According to the result of L and the assumed angle α from *Equation 16*, the calculated result for d is 7.778mm, round down to 7mm in the design. With the assumption that the maximum tilt angle β the base ring connection can rotate about the upper rotate rod is 45 degrees, the inner width W calculated from *Equation 17* is about 20.49mm, rounded up to 21mm in the design. As shown in *Figure 4-15(b)*, the result of the inner width W is longer than the half length of the actuator cap of 15mm. The length edge of the base ring connection and the upper surface of the actuator cap are not able to make contact with the rotation of the base ring connection about the upper rotary rod as shown in *Figure 4-15(a)*. Thus, the result of length of base ring connection according to *Equation 17* can be ignored since in for design the length L needs to be 20mm. However, the calculated results of length L and inner width W of the base ring connection represent only half of its total value, and including the thickness of the material, which is 2mm as mentioned before, the final results for the length is 40mm, and the width is 46mm. The sleeve length of the rotary rod will base on these results. This means that the length of lower sleeve shown in *Figure 4-15(a)* is 14mm, and the length of upper sleeve shown in *Figure 4-15(b)* is 41mm.

In addition to completing the dimension calculation above, one factor of the base ring connection still needs to be determined, namely the inner height of the base ring connection. The height is calculated for two conditions, both heights for rotation about the lower and upper rotary rod will be considered. The heights are calculated using *Equations 19* and *20*.

$$h_1 = \frac{20 - 3 \cdot \tan(\alpha)}{\cos(\alpha) + \sin(\alpha) \cdot \tan(\alpha)} \tag{19}$$

$$h_2 = \frac{20 - 5 \cdot \tan(\beta)}{\cos(\beta) + \sin(\beta) \cdot \tan(\beta)} \tag{20}$$

The results of the height from the equations are the minimum values to prevent any impact on the maximum angle. The final result will be the calculation result plus 5mm to ensure enough space for rotation. According to the conditions detailed above, the maximum angle α and β rotary rod can rotate is 45 degrees, and the design will use the bigger one of the two calculated heights. The calculated result for h_1 is about 12mm, and the result for h_2 is about 10mm. This means that the final result will use h_1 and add 5mm, resulting in an inner height of the base ring connection of 17mm.

With all the dimension calculated above, the design of the model of the universal joint can be finalised. The simulation of the joint under the maximum load are given below.
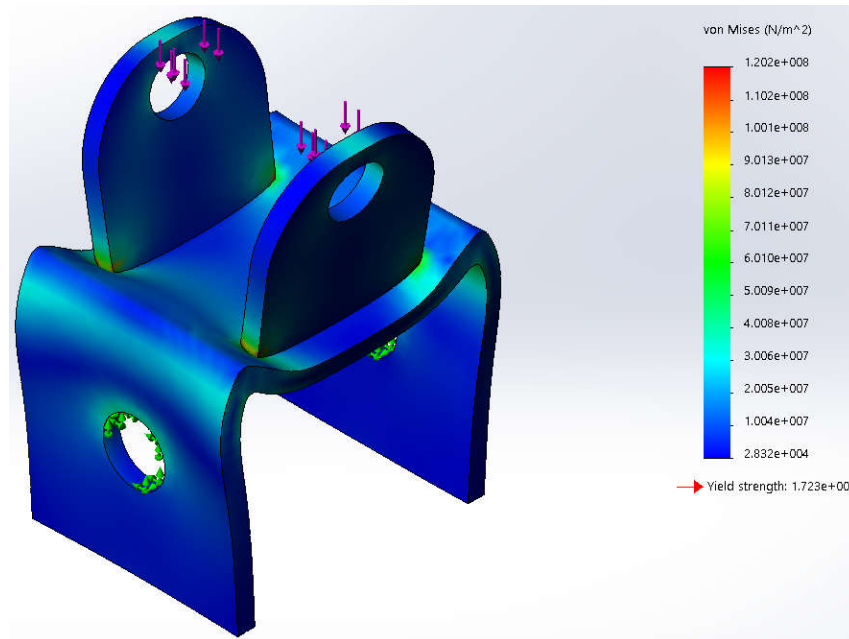

Figure 4-16 Simulation result of the actuator cap

Figure 4-16 shows the simulation result of the actuator cap, because the actuator cap is designed based the non-rod head of the selected actuator. The fixed points are the two holes on both sides of the cap which are going to be fixed on the actuator with a M6 bolt. The actuator can support a maximum load of 350N to absorb the reaction force from the lower bolt of the rotary rod that is applied on the cap is through the holes of the two ears has. As shown in *Figure 4-16*, the bending pressure all over the actuator cap is under the yield strength of the selected material, which makes the designed part safe to use.

(a) Lower sleeve load result
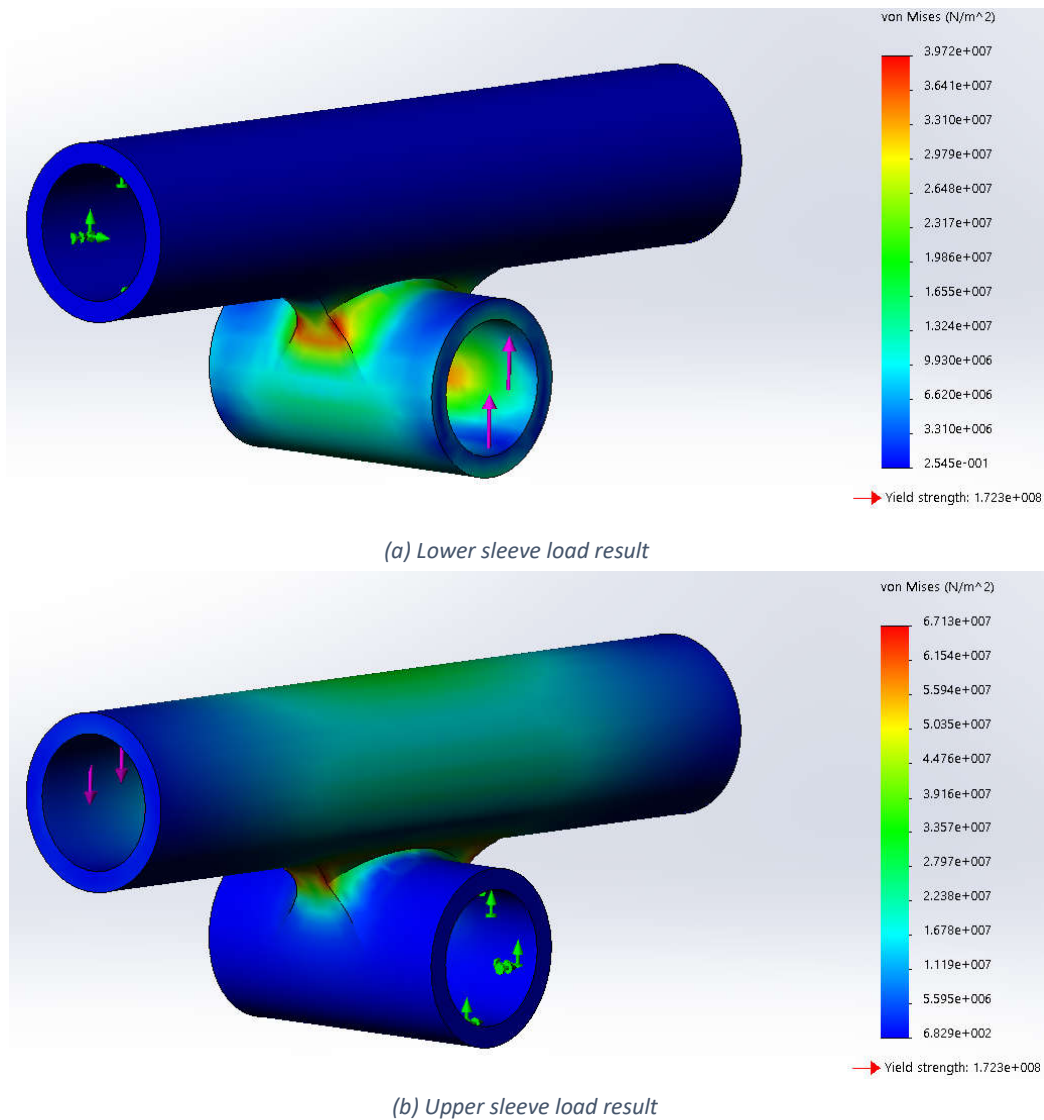

(b) Upper sleeve load result

Figure 4-17 Simulation results of the rotary rod sleeve

The rotary rod load simulation is conducted for two different conditions shown separately in *Figure 4-17*. In the first condition it is assumed that the upper sleeve is fixed inside by the bolt (*Figure 4-17(a)*), and the maximum load is applied in the inner surface upward. The result shows that the maximum bending press under the load of 350N happened in the welding section of the two sleeves, but because the pressure is under the yield strength of the material the design structure can be assumed to be safe for practical use. When the fixed point is in the inner surface of the lower sleeve and the load is applied downward to the inner surface of the upper sleeve (*Figure 4-17(b)*), the result is similar to the condition shown in *Figure 4-17(a)*. The maximum pressure occurred in welding section and was lower than the yield strength. Thus, the whole design for the rotary rod's sleeve is safe.
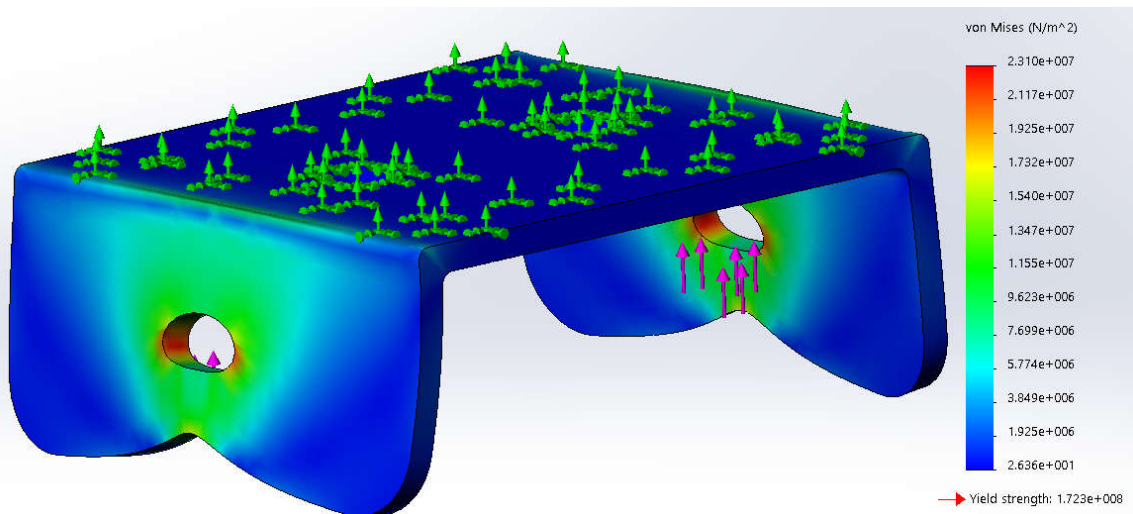
Figure 4-18 Simulation result of the base ring connection

Figure 4-18 shows the result of the base ring connection simulation. The fixed position is on the upper surface of the connection, which will be connected to the base ring around the crus with two M6 bolts. The force will be applied from the holes on both side of the connection through the bolt used to connect with the upper sleeve of the rotary rod. The result shows that the design is safe

for use as well. The picture of the assembly of the universal joint for the prototype is shown in *Figure 4-19*. As it was described above, the actuator cap is connected to the non-rod head of the actuator and the whole joint is connected by the rotary rod's sleeves, which are connected through the ear of the cap and side holes of the base ring connection. The base ring connection is connected to the base ring of the Stewart platform with two M6 bolts.

Figure 4-19 Universal joint in prototype

4.2.3 Base And Moving Platform Design

Now that the universal and spherical joints of the Stewart platform have been calculated and designed, the design process can now focus on the design of the moving platform and base of the structure. The base ring serves as a fixation device as it is attached around the crus of the lower limb, and the moving platform is placed under foot sole. For the force transferred from the moving platform needs to be applied to the knee joint through the knee brace structure and the fixation of the base ring around the crus is used for providing

a stable transfer station. Thus, the musculoskeletal system of the crus cannot be squeezed too much and cause unnecessary discomfort to the user.
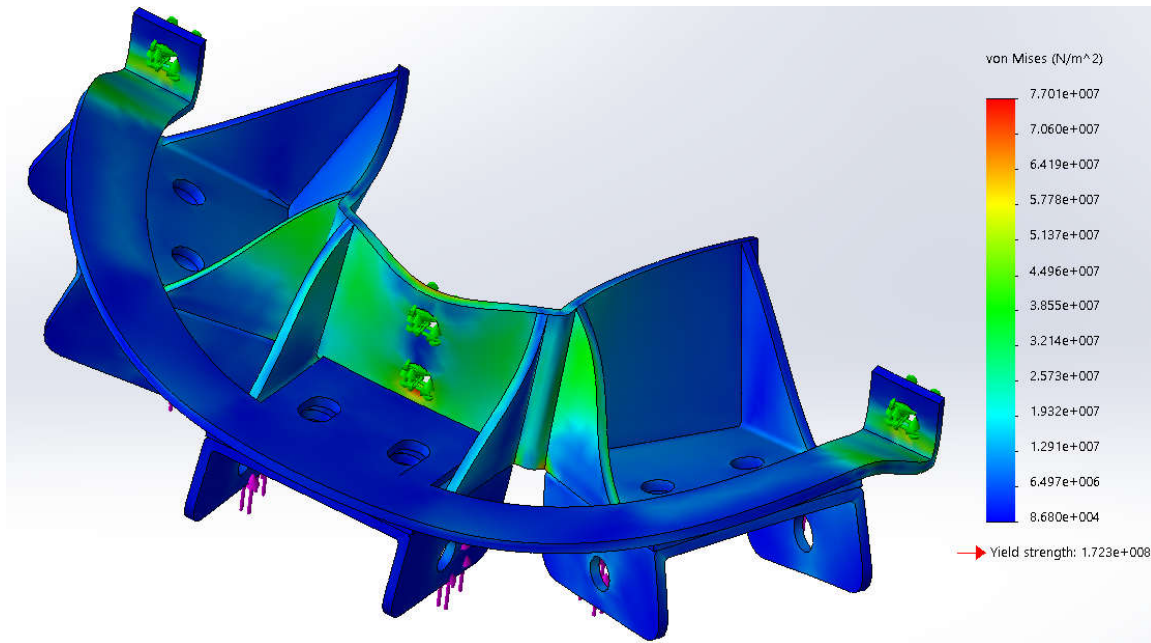

Figure 4-20 Simulation result of the base ring combination

The base ring, as the base platform of the Structure platform, is used to fix all six actuators through the universal joint. According to the design of the universal joint's base ring connection part, the edge of the universal joint is a straight line as shown in *Figure 4-19*. Due to the common shape of the crus (Platzer, 2008) and the number of the actuators, the base ring is designed as an equal hexagon with an edge length of 50mm, which means that the longest diagonal of the base ring when it is completely closed is 100mm. However, in order to make it easy for the user to put the device on and off and due to the different dimensions of the crus, the base ring is cut into two equal half hexagons. To connect the universal joints and the base ring together, a flange plate for the base ring has been designed. The flange plate can be welded to the base ring, three on each half of the ring. Moreover, each flange plate

connects to the universal joint with two M6 bolts. Thus, each flange plate receives the same maximum load of 350N from the universal joint. Since the base ring has been cut into two equal halves, to connect the two halves, a ring dimension adjuster is added. The ring dimension adjuster is not only used to fix the two halves together, but is able to adjust the distance between the two halves to fit different sized crura. Two plates are attached perpendicular to each ring dimension adjuster on both heads with a 6.5mm diameter hole on each plate. Those two holes are used to fit the M6 bolts, which act as a dimension adjuster with nuts. In this design, the device uses 100mm M6 bolts to adjust the dimensions of the base ring. This results in a base ring dimension range of 100mm to 200mm. The ring dimension adjuster is designed as a half circle because the base ring together with the flange plates have sharp edges and might cut the user. The half circle dimension adjuster covers all these sharp edges and decreases the injury rate for users' better experience with the developed device. *Figure 4-20* shows the simulation result of all the components in the base ring under the maximum load of 350N from each universal joint connected to the base ring. This feature is attached via the two M6 holes that are connected to the knee brace plate and the two M6 holes on the dimension adjuster. As the figure shows, the base ring combination was found to be safe under the maximum load.

The foot pad, as the moving platform of the device, is the last item that needs to be designed for the mechanical structure. The foot pad acts like the foot, and it is designed to contact the ground instead of the foot sole. Two slots are dug on the foot pad in order to connect the pad with the foot using Velcro so that the pad motion can be synchronised with the foot motion. The length of the foot pad is 400mm, which is longer than the largest human foot identified

by Curran et al. (Curran, Gillespie, Melville, Campbell, & Kagan, 2019). The maximum force applied on the foot pad is calculated as 1500N, as it directly receives the force from the human body. The fixation place is on the bottom surface of the pad which will contact the ground, and the force is applied straight down through six spherical joints' bases. The static simulation result is presented in *Figure 4-21*, and it shows that the design is safe with the selected material.
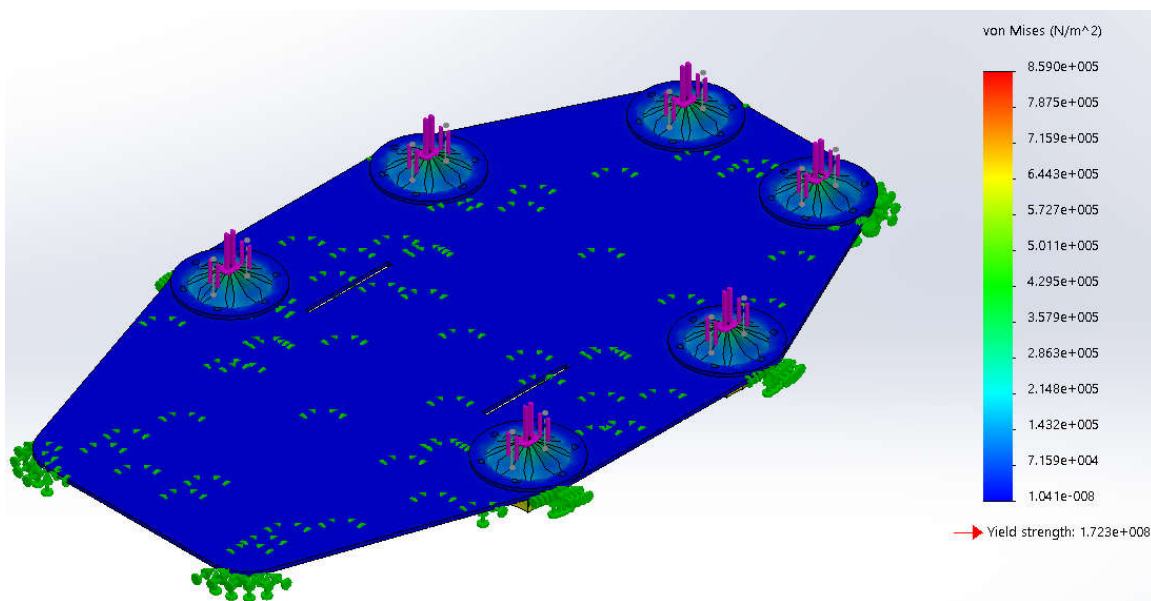
Figure 4-21 Simulation result of the footpad with spherical joint base

Since all the components in the Stewart platform have been completed it is now possible to combine all features to create a picture of the final design before approaches the next step of the design process. The final design rendering showing the whole device as it is attached to a human leg is presented in *Figure 4-22*.

Figure 4-22 Final rendering of the whole device on human leg

Chapter 5

Electronic System Design

The design of the main structure has been completed in the previous section. The main mechanical structure cannot work by itself but needs electronic components to function. In this section, the choice of the electronic components and the connections between all the components are discussed. The electronic control system includes the electronic hardware selection and the system programming.

5.1 Electronic Hardware Selection and Design

Different kinds of electronic parts are needed for the designed system. Each part is needed for a different purpose, and the purpose of this section is to consider and determine all the electronic parts required for the system. As mentioned above, the control chip of the system uses the Arduino development board, which means the components of the system need to be selected from Arduino related accessories. Once the number and type of the components have been identified, the specific type of Arduino board required can be chosen. Different types of Arduino boards have different numbers of ports for control and data reading connections. The number of ports the system needs to use can only be determined once the selection is complete.

The most important part of the system is the actuator that was selected before. The selected actuator needs to be powered by a 24V DC power supply. The working current of the actuator is about 1.5A when the actuator is working

probably. However, while controlling the actuators, it is possible for the actuator to jam, causing the current to increase 5 to 12 times higher compared to the normal working current. The power of the actuator will increase significantly. Therefore, for safety reasons, it is crucial to include a maximum working power in the design of the electronic system.

As mention in the previous chapter, the actuator needs to be extended as well as retracted while the system is working. An H-bridge circuit is introduced to use as a control method of the actuators. There are different kinds of H-bridge circuit boards available on the market, a certain type which can meet the needs of the device should be carefully chosen. Understanding the maximum power of the actuator, which is between 180W and 432W, the maximum power the H-bridge requires should be much higher than the power used during the actuator's locked rotor status. After researching the existing market, a dual DC motor driver DRI0041 (*Figure 5-1*) was chosen. This motor driver can supply a maximum continuous operating current of 7A, maximum peak current of 50A, with voltage supply of 24V. This is suitable for the selected actuator of the device. The circuit module has two output channels, which means one board can control two actuators at the same time. The input to the board needed are two PWM control signals for each actuator and the power supply. The board is fixed on the base ring by a 3D printing shell. Since there are six actuators in total, three of these driver board will be needed. The number of control pins require from the Arduino will be 12.
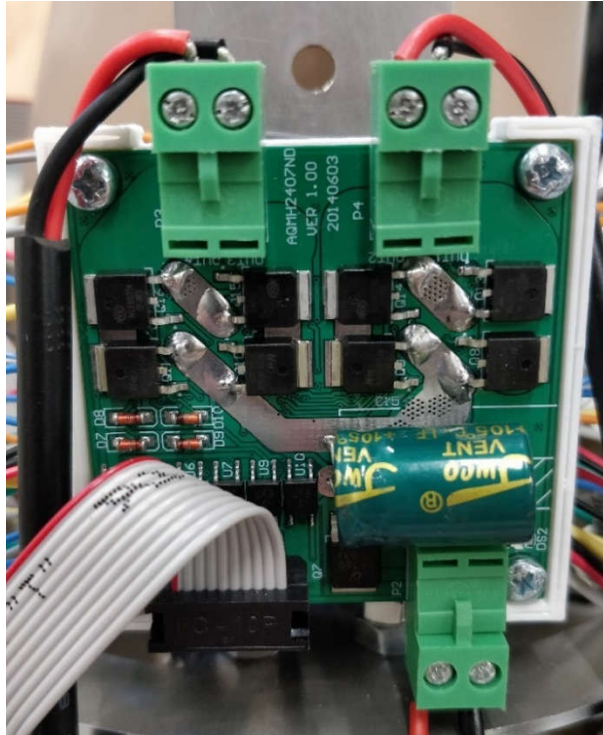
Figure 5-1 DC motor driver DRI0041

As mentioned previously, the method to test if the device is de-loading the ankle joint is by measuring the force on the foot sole (Dąbroś, Iwaniec, Patyk, & Wesół, 2018). Dąbroś, Iwaniec, Patyk, and Wesół (2018) suggest that three force sensors should be used to monitor the force applied on the foot sole. These force sensors may be exposed to a weight of up to150kg (approximately 1500N), which means that the measurement range of the force sensor needs to be up to 150kg. The force sensor's is basically working as a resistor that changes its resistive value (in ohms Ω) depending on the force applied. The selected force sensor (*Figure 5-2*) for this device is also called force sensor resistor (FSR). An FSR requires two connections, one to connect to the power of the Arduino board and the other to a pull-down resistor that is linked to the ground. The point between the fixed pulldown resistor and the variable FSR resistor is connected to the analog input of the Arduino board. The pin number

of the FSRs require from the Arduino board except the power and ground is 3 analog input pins.
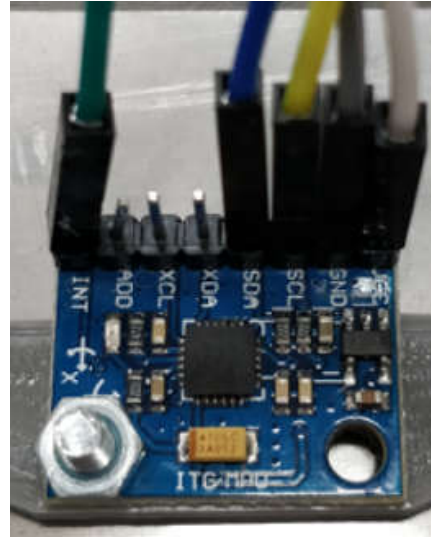

Figure 5-2 Selected FSR sensor

Figure 5-3 MPU6050 gyroscope

Another sensor used in the system is the gyroscope. As mentioned above, the gait cycle of humans can be detected by placing a gyroscope on the foot (Boutaayamou, et al., 2015). In the current design case, two MPU6050 gyroscopes are used (*Figure 5-3*). One of them is placed on the foot pad to detect the foot motion. This gyroscope is then combined with another one to allow the system to detect the relative position in 3D space of the base and the moving platform of the device. The double gyroscope approach will be used in future research for controlling the device with the foot motion, which will be discussed in greater detail in the recommendation section of the report.

The function of the gyroscopes in this study is to detect the gait cycle, relate the cycle to the force detected, and measure the ROM of the developed platform to test the if the device has sufficient ROM to fulfill the foot motion in gait cycle. The connection of the gyroscope to the Arduino board uses the

I^2C protocol for communication, which means that only two wires are needed to connect the Arduino board and two wires for powering. However, since two gyroscopes are used in the system, the address of the two gyroscopes should be different in the I^2C communication protocol. This problem can be solved by connecting the INT pin to Vcc to alter the register address (see in *Figure 5-3*). Thus, for two MPU6050 gyroscopes, only 2 pins from the board for I^2C connection are needed with the exception of a power and a ground connection.

During the testing stage, the device requires a large room to allow the test person to walk around. This poses the problem of how to collect data from a moving device. Obviously, collecting the data through a cable that is connected to a computer is very inconvenient as the cable may not be long enough and might affect the running of the device, which will cause tripping hazard. Therefore, it was decided to install an HC-05 Bluetooth module (*Figure 5-4*) to replacing the function of the physical cable for collecting the data when the device is moving around. The HC-05 module is a Bluetooth module, which means it communicates with the Arduino board via the serial communication, which will only require 2 pins from the Arduino board.

Figure 5-4 HC-05 Bluetooth module

All the electronic components have been chosen, and overall, 21 pins are required from the Arduino board, not include the power pin. This requires an Arduino board with a lot of pins, in case there will be more needs for pins at a later stage. The Arduino Mega 2560 (*Figure 5-5*) has been selected, for the board has 54 pins available, which means that all the components can be integrated into one control board.

The next problem is that there are quite a few components needed for connection onto the Arduino board. Some of the components will need extra resistors, which cannot directly be connected to the board. If using a bread board, the volume of the electronic system will be too big, and all the connection wire will be exposed so that they can easily become entangled. The solution of this problem is the development of a Printed Circuit Board (PCB) which will contain the resistors the components need. The size and plug pins of the PCB will exactly copy the size and pin position of the Arduino Mega 2560 board so that the PCB is able to cover and directly plug upon the Arduino board in order to protect it. The developed PCB board is shown in *Figure 5-6* and the schematic circuit of the PCB is included in Appendix I.
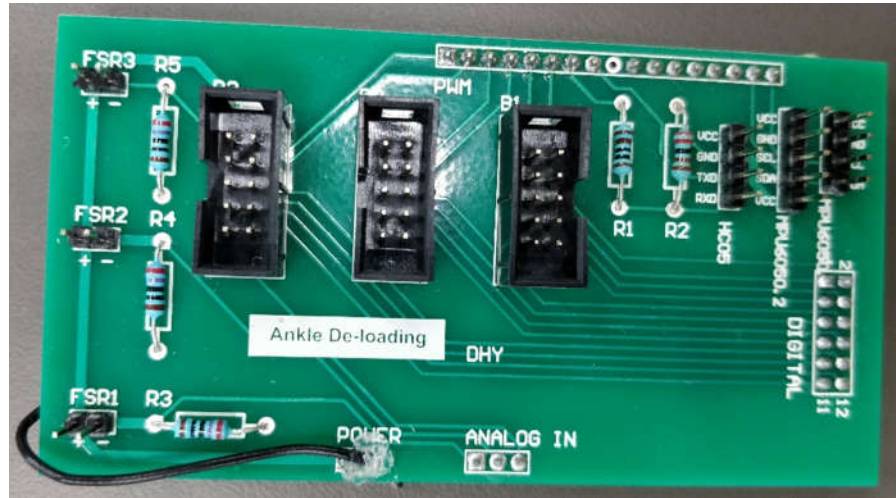

Figure 5-5 Arduino Mega 2560

Figure 5-6 PCB board

5.2 System Programming

The system will need a programmed code to activate the actuators and collect data from different sensors. This section introduces the program developed for the device. The function of the device is to de-load the human ankle joint and collect data from the device. When a user puts on the inactivated device, the foot will touch the foot pad, and as a result the ankle joint is not de-loaded yet. When the user is ready, the device can be activated, and all six actuators can be made to extend. The distance of the actuators' extension depends on the different dimensions of the user and is controlled by the researcher. According to the system program's flow chart shown in *Figure 5-7*, after the device is activated, the sensors will begin to collect data from the device.
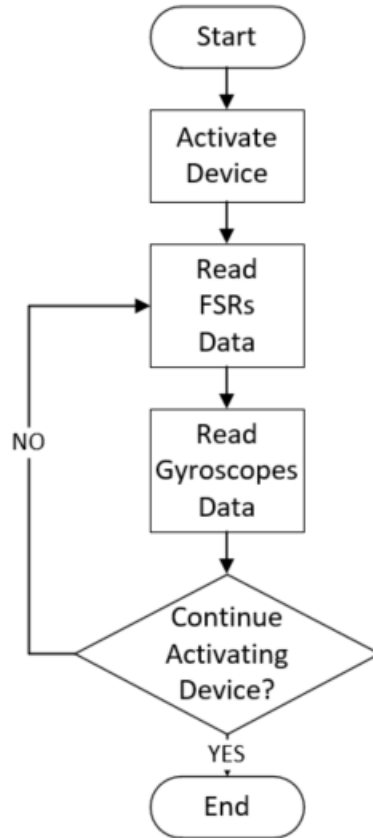
Figure 5-7 Flow chart of the control system

When using the selected sensors, the raw data always contains a lot of noise, which makes the data diagram hard to interpret. Certain control system filters are needed to filter out those noises and to make the diagram of the data easier to understand. There are two kinds of sensors in the system, FSR and gyroscope.

While the data from a FSR is usually quite easy to understand, from time to time the data is distorted by sudden jumps in data. The trends captured by the sensors are mostly easy to read, which means that the application of a simple LPF, also known as the first order filter, should suffice to filter the data of the FSR. The equation of LPF is given by *Eq. 21* (Sedra, 1991).

$$F_t = k \cdot F_{read} + (1 - k) \cdot F_{t-1} \qquad (21)$$

87

Here, F_t stands for the filtered force data at time t, k is the coefficient of the LPF, which is 0.9 in this case, F_{read} is the raw or unfiltered data directly from the FSR, and F_{t-1} is the previous filtered force data at time $t-1$. The data from the gyroscope are accelerations from accelerometer and angular velocities from the gyroscope's three axes. All these data cannot be directly used to determine the position of the foot. The position of the object with gyroscope's data is given by *Eq. 22* to *Eq. 26*.

$$\varphi_a = \arctan\left(\frac{ay}{\sqrt{ax^2 + az^2}}\right) \tag{22}$$

$$\theta_a = \arctan\left(\frac{-ax}{\sqrt{ay^2 + az^2}}\right) \tag{23}$$

$$\varphi_g = \varphi_{gpre} + gx \cdot dt \tag{24}$$

$$\theta_g = \theta_{gpre} + gy \cdot dt \tag{25}$$

$$\psi_g = \psi_{gpre} + gz \cdot dt \tag{26}$$

Here φ is roll angle rotates about x axis, θ is pitch angle rotates about y axis, ψ is yaw angle rotates about z axis. ax, and ay and az are the accelerations in three axes, while gx, gy, and gz are the angular velocities in three axes. The combination results of the data with the same rotation axis reveals the relative position of the object in 3D space.

Researchers suggest that using a Kalman filter can decrease the noise in the gyroscopes' data better (Ngo, Nguyen, Huynh, Le, & Nguyen, 2017), and help predict the tendency in the data. Therefore, a Kalman filter library has been applied in the program. The position data supplied by the gyroscopes can be interpreted easily.

After all the subsystems in the developed device have been designed, the next step is to test the developed prototype (*Figure 5-8*) and determine its status of validation. In the following chapter, the test method will be introduced and analyzed. The result of the test will be discussed and recommendations for further research on the prototype are presented.
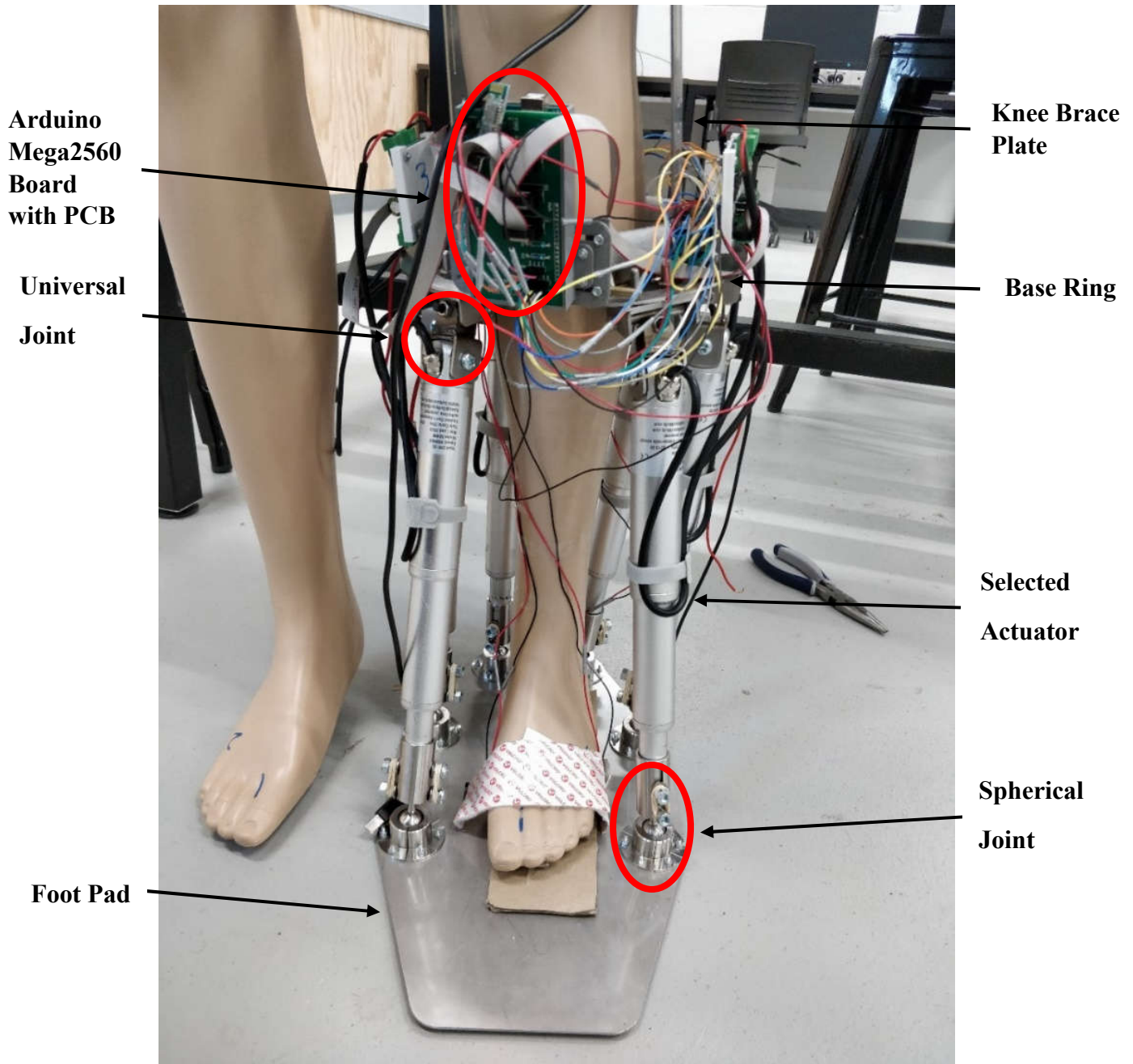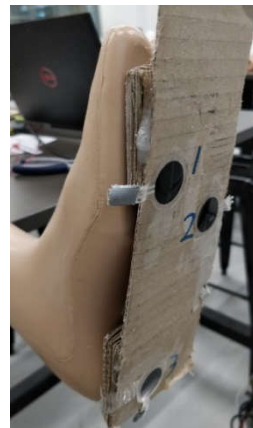

Figure 5-8 Final developed device

Chapter 6

Test and Validation

With the detailed design of the prototype complete, the study can now turn to the next step, which is to validate the prototype through different tests. As described previously, the main function of the developed device is to de-load the pressure applied on the ankle joint. The tests that are conducted to determine whether the device works will mainly focus on the differences between loading statuses in the ankle joint before and after the device has been activated. Researchers have suggested that ankle pressure can be related to the force applied in the foot sole (Amirudin, S.Parasuraman, Kadirvel, Khan, & I.Elamvazuthi, 2014), which means FSRs will be placed on the foot sole to measure the force the sole receives. Another research team suggests that three well positioned sensors on the foot sole are enough to detect the force. In accordance with Dąbroś et al. (2018), the sensors on the foot sole are placed at heel, 5th metatarsal bone and hallux (Dąbroś, Iwaniec, Patyk, & Wesół, 2018).


(a) Bottom view of dummy's foot   (b) Side view of dummy's foot

Figure 6-1 FSRs position in dummy test

Tests of the prototype are conducted on a dummy provided by school. Three FSRs are placed on the dummy's foot sole, in exactly the positions identified above (*Figure 6-1*). FSR1 is placed at hallux, FSR2 is placed at 5th metatarsal bone, and FSR3 is placed at heel. Cardboard is used to simulate the shoe bottom as well as make the dummy's foot sole flat, so that it will be easier to get the data from three FSRs. Several weight plates are borrowed from the school's gym and placed on the dummy to simulate the weight of a user. The total weight of the plates is 35kg. The loaded dummy is shown in *Figure 6-2*.
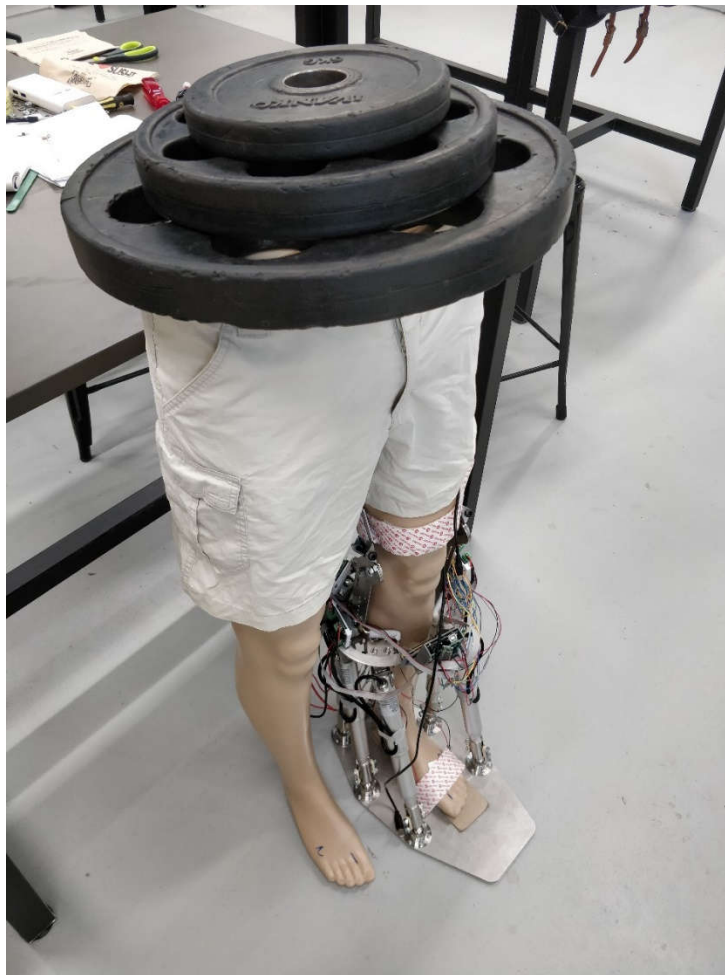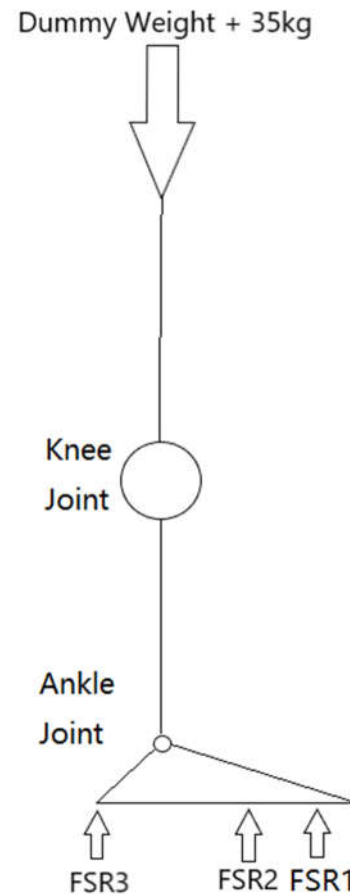
(a) Real test scene   (b) Free body diagram of the test

Figure 6-2 Loaded dummy with the developed prototype on its leg

The tests with the loaded dummy are conducted in two scenarios: a loading test without the developed device and a loading test with the activated device. The data collected from FSRs in two loading scenarios demonstrates if the developed device work by comparing the force response on the dummy's foot sole. If the foot heel section's force data in the loading test with the developed device is decreased remarkably by at least 50%, then the developed device is validated. The assembly of the device on the dummy's leg follows the same process described in the design section. Thus, the knee brace is attached around the dummy's knee joint with a Velcro bandage, while the base ring of the device is fixed around the crus of the dummy and connected to the knee brace. The dummy's foot is connected to the foot pad of the developed device, so that the device can follow the dummy's leg motion synchronously during the tests. For each test, the researcher moves the dummy leg with loads to simulate a gait cycle, starting from heel strike phase and ending with toe-off phase (see the human gait cycle shown in *Figure 2-3*). The experiment to validate the developed device follows the following steps:

1) Set up the sampling time and calibrate the FSRs.

2) Swing the dummy leg for a gait cycle (from heel strike to roe-off) without load and device, record the sample number, data, and elapsed time, find the FSRs' patterns in a gait cycle.

3) Set up a standard sampling number to represent a complete gait cycle for later tests.

4) Load the dummy leg with weight plates, and swing the leg for a gait cycle, record the data.

5) Unload the weight plates, put the dummy in the developed device.

6) Load the dummy leg again with the developed device and record data.

7) Analyze the data.

Since the actuators' working voltage is 24V DC, the power supply used in the experiment is a 24V 3A DC power supply provided by the school (*Figure 6-3(a)*). The Arduino Mega 2560 board with its accessories is powered by a 5V 2.1A DC power bank (*Figure 6-3(b)*).
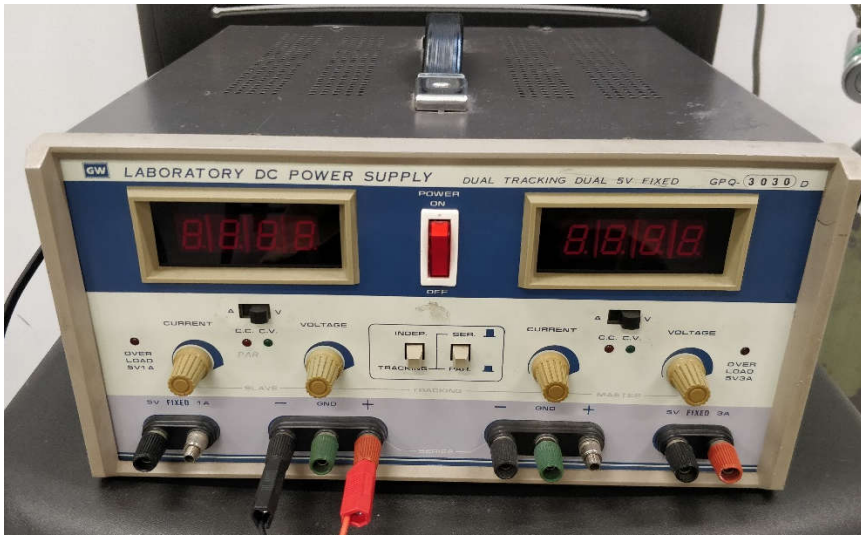
(a) 24V 3A DC power supply for actuators

(b) 5V 2.1A DC power bank for Arduino Mega 2560 board and its accessories

Figure 6-3 Power supplies of the device

All three FSRs' data collected during the gait cycle simulation are recorded through the Arduino board and uploaded to the computer. All the FSRs were able to maintain the same place throughout the whole test. Tests results are presented in following section, so that the validation of the developed ankle de-loading device can be verified.

Chapter 7

Results and Discussion

After the completion of the final prototype development, tests to confirm the validity of the device are conducted. In each test, the dummy leg is manually moved by the researcher to simulate a real-life gait cycle of a human. During the test, the data of three FSRs are collected and compared to assess the performance the developed device and verify its efficiency. The collected results are shown in *Figure 7-1*.

7.1 Test Results

As shown in *Figure 7-1*, in each test, 61 sample data are taken during a complete gait cycle of one leg from heel strike phase to toe-off phase, and each phase corresponds to the timeline shown in the results. The sampling time of the two tests is 50ms set by the researcher in the Arduino program, and the duration time of simulating a gait cycle in each test is the same as well. When collecting the data, the researcher set up a timeline for original data from FSRs, and compared that data with the FSRs' gait cycle pattern without load collected in the second step of the experiment, which enabled the researcher to locate the start time of the dummy leg gait cycle simulation. As can be seen from the sketch included on top of each graph of *Figure 7-1*, the dummy leg pattern is easy to identify. Starting with pressure in the heel and finishing with a pressure on the toes. The data of each FSR is taken separately from the first set of test results and is then compared to the data of the FSR at

the corresponding position in the second test. In each result diagram, the y axis represents the force magnitude measured by FSRs, and the x axis marks the sample number. The blue line represents the FSR's data when the object dummy with 35kg load was not wearing the device, and the red line stands for the data when the dummy was putting on the activated device in de-loading status. All the recorded data is under the load of 35kg on the dummy leg (*Figure 6-2*).
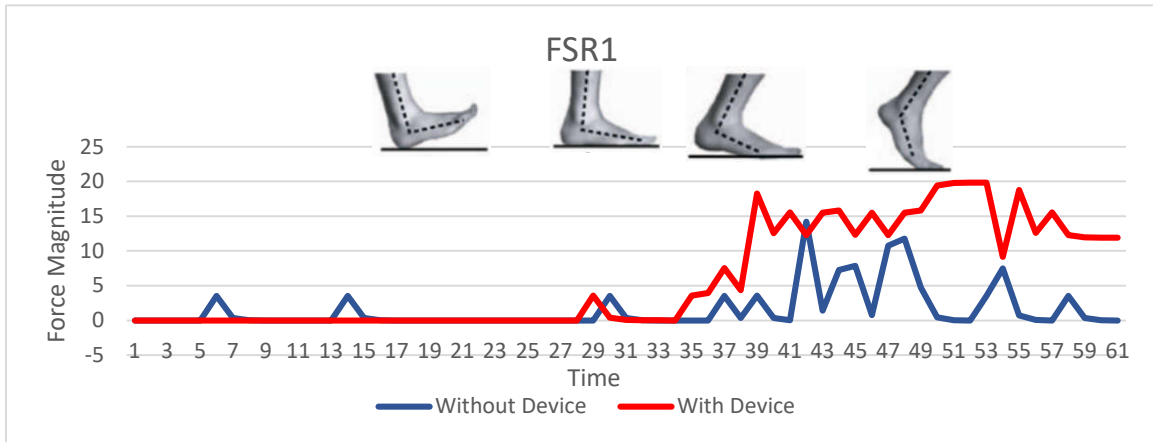
(a) FSR1 data
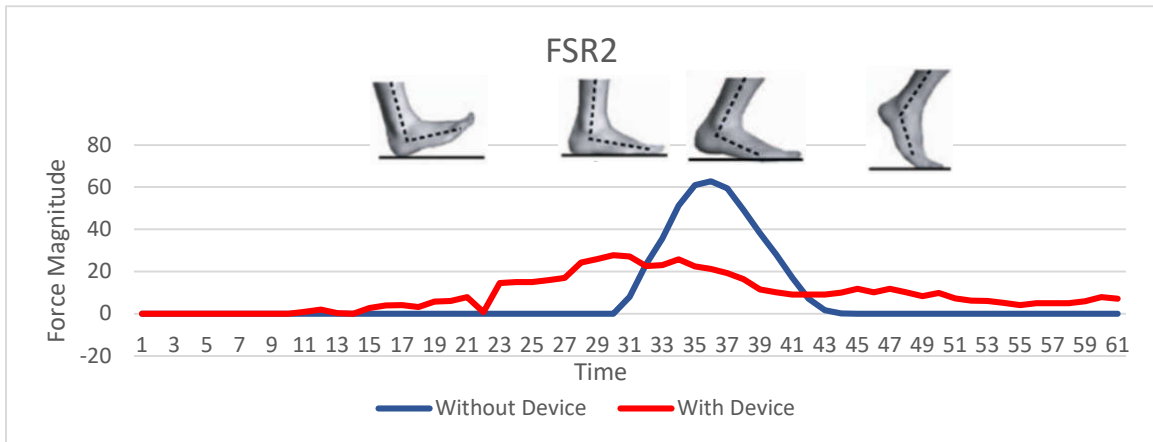
(b) FSR2 data
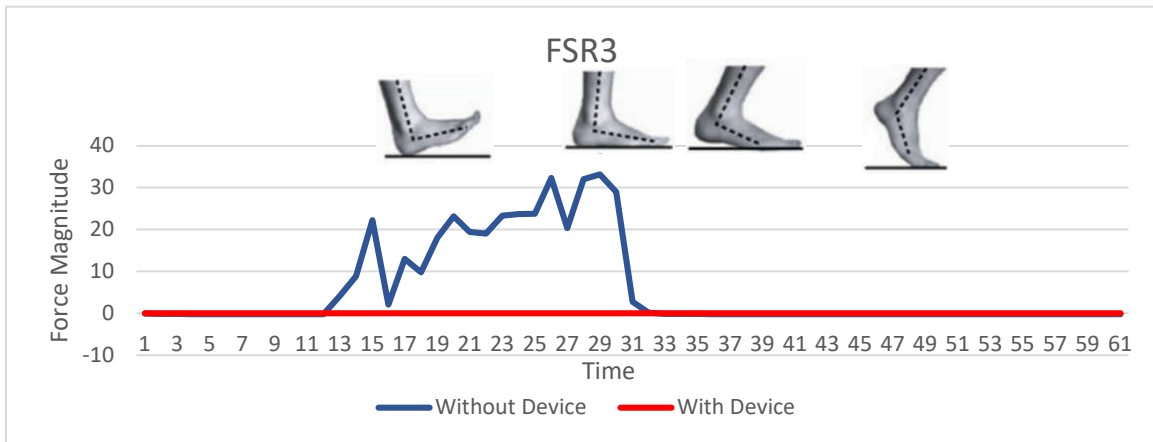
(c) FSR3 data

Figure 7-1 Collected data from three FSRs in a gait cycle

7.2 Results Discussion

Like it shown in *Figure 7-1(c)*, the blue line indicates that when the dummy is not wearing the developed device, the first phase in the gait cycle, heel strike, will cause a high stress at heel section of the foot. With the gait cycle continuing, the gait cycle is proceeding to the foot flat phase, in which the foot sole is completely contacting the ground and the force is concentrated on the heel section, which will slowly decrease and be distributed to the whole foot sole. As shown in *Figure 7-1(b)*, the force at the 5th metatarsal bone, also known as forefoot, is increasing rapidly right after the heel strike phase is over and heading to the foot flat phase without the device. And in the last phase of the stance phase of the gait cycle, the toe-off phase, like it shown in *Figure 7-1(a)*, the force at the hallux section is increasing without the device. At the same time, the heel section is off the ground and the data is 0 by then with a decrease in force at forefoot section. The blue lines in the three result shows a normal foot force pattern in a gait cycle without any de-loading device. However, the red lines in three results shows a different force reaction pattern when the tested dummy is wearing the developed device. The red line in *Figure 7-1(c)* keeps the value around 0 through the whole gait cycle, which means under the load of 35kg, the heel section of the dummy is lifted and receives no force from the ground. While in *Figure 7-1(b)*, the reaction force applied on the forefoot while the cycle moves from foot flat phase to heel off phase has a significant drawback, nearly only one third of the original reaction force without the developed device. The only increasing is in *Figure 7-1(a)*, the force at hallux was increasing to twice of the original force without the device. According to the results, the developed device is able to distract the

force from the ankle joint, the force data in two circumstances were different from each other.

The test results shown the possibility of the developed device in de-loading the ankle joint. However, the entire experiment was tested on a dummy's leg, the condition while the developed device is being wearing on a human's lower limb will be much more complicated. In the experiment, the device was attached tightly on dummy's leg. Since the dummy is made by plastic, while tightening the base ring around the crus with the help of dimension adjuster, the deformation of the object's leg is not similar with the real human's leg. Due to the softness of the muscle fiber, the human leg's deformation will be more significant comparing with the dummy's leg made by plastic. The performance of the developed device on human leg is still remained unknown. More clinic trials on the developed device while being putting on a human's leg should be conducted, to test the squeezing level and how the test object's feeling on the deformation.

While in testing, the developed device's actuators were extended fixed in a certain length. In the whole gait cycle, the author found that the fixed actuators might make it difficult for the user to synchronise the footpad with foot motion. Such limitation might cause sore in ankle joint, which will weaken the rehabilitation effect of the device. A more ideal improvement for the device is synchronising the device by using the two gyroscopes built in the electronic system. For the device's mechanical structure is based on a Stewart platform, the mathematics of platform's posture control is being discussed in mechanical engineering (Lopes, 2010; Petrescu, Petrescu, & Mirsayar, 2018; Wang, He, Shang, & Gu, 2009). The synchronisation of the footpad with the

user's foot motion will help the patient in ankle joint rehabilitation process by relieving the ankle joint from extra controlling force on foot pad.

The first prototype of developed device is able to de-loading the ankle joint by bypassing it with the device's structure. The author believes there are still many improvements could be used to perfect the device. Further clinic trials are required. The conclusion and recommendation for further research on the developed device will be discussed in following chapter.

Chapter 8

Conclusion and Recommendation

The aim of the developed device is to de-load the pressure applied on the ankle and relieve the pain problem caused by OA/RA or ankle fracture surgery. And the test results show the developed device is able to de-load the force in the ankle joint. The developed device has been tested in the previous section, and the test outcomes are presented in the diagrams in *Figure 7-1*. The test was conducted on a dummy with a load of 35kg, and the researcher manually swung the leg to simulate the human gait cycle so that force data from three FSRs located under the foot sole could be recorded. The result diagrams show the sampling number and time, which are linked to the foot pattern of the gait phases that was detected by the FSRs. The results in *Figure 7-1* show the same pattern duration time and the tendency of the two gait cycle simulations on a loaded dummy leg for easy comparison.

8.1 Research Conclusion

According to the results shown in *Figure 7-1*, the developed system manages to successfully lift the posterior section of the foot up and slightly leans the foot toward the toe section. As a result, the reaction force in heel and forefoot section is significantly decreased, while the force on the toe section is slightly increased. According to the research by Giacomozzi, Macellari, Leardini and Benedetti (2000), the ankle joint movement is mostly related to the force applied on the posterior section of the foot. And according to Malanga and

Delisa (2010), if the pain is in heel section, toe section of the foot could be more likely bearing the weight.

Based on these two findings, we hypothesise that decreasing the force applied on the ankle joint could relieve the ankle pain problem. In this project, we aimed to decrease the force by raising the heel section. However, the results of the test suggest that raising the heel results in an increased load in the toe section. This raises the question if this extra pressure in the toe section could overload and cause pain in a different part of the foot? Further research on the connection between pain and pressure in the toe section is needed to improve the design of our device. Based on the results show in *Figure 7-1*, the developed device could be able to relieve the ankle pain problem through distracting the reaction force from the posterior section of the foot. However, the experiment was only conducted on a dummy, meaning that the validation of the device on human leg remains unknown. Further clinical trials of the developed device using humans are needed to fully understand ankle the de-loading performance of the device and identify possible weaknesses and side-effects associated with the approach.

The result has shown that the developed device works as intended as it effectively de-loads the force applied on ankle joint by lifting the foot up and distracting the force to other parts of the body. Such de-loading function is rarely discussed in the existing research field, as most AFO devices are designed for ankle rehabilitation and limit the ankle's movement (Nomura, Yonezawa, Ogitsu, Mizoguchi, & Takemura, 2015; Yonezawa, et al., 2014). Controlling the motions of the ankle could prevent patients to sprain their foot further or even prevent trips; however, the force applied on the joint either from the reaction force of the ground or from the body weight can still further

aggravate the ankle pain problem by adding pressure on the damaged load bearing area in the joint.

The developed device was validated to de-load the ankle joint by lifting the foot up and thus the experiment results support the design purpose. Our de-loading device uses the same structure as devices developed by other teams, namely the Stewart platform, but unlike other devices it uses electromechanical actuators. Instead of electromechanical actuators, the other devices use pneumatic cylinders, which can only be used to assist the motions of the ankle. Our device has shown its potential in de-loading the ankle joint with electromechanical actuators, for its high torque which could support human weight.

8.2 Recommendations For Future Research

However, there is still some aspects of the design that need to be improved. The developed device is made up of stainless steel with six electromechanical actuators. This makes the system heavier than other AFO devices, which would make wearing the device more difficult. The motion control of the actuator requires a more accurate control strategy as the control system can control the activation time but without the displacement feedback of the actuators, the control system still needs to be improved in the future with a closed loop control strategy. Those problems require further research, followed by step by step modifications based on the findings. For instance, in order to facilitate a clinical trial and generally facilitate use for patients with ankle pain, it is suggested that a more wearable and most importantly lighter AFO device be developed. The developed prototype has a weight of around 7kg, which basically means it is unsuitable for use in a clinical trial as the

weight of the device would make it difficult for patients with ankle pain to walk with the added weight or to even put it on. The developed device is intended to be a wearable device, which means that the prototype needs to lose weight in further development. Since the weight of the actuators cannot be reduced, the only option would be to identify a different material of r the mechanical structure to replace the current stainless steel frame. The material used would need to be lighter yet maintain a high tension strength to meet the strength requirement of the device. One possible contender could be aluminum alloy.

In addition to the weight problem, the power system of the device is also non-negligible since the actuators used in the device require a power supply of 24V 3A as shown in *Figure 6-3(a)*. The weight and volume of the power supply are obviously not suitable for wear, which means that a specially designed power supply needs to be developed in the future to power the system and not affect the using of the device.

The system is based on a Stewart platform, right now the device is just using its high DOF in 3D space and ROM for providing the users' foot with the freedom to move unrestrictedly in order to improve the rehabilitation process. However, the Stewart platform can achieve more functions than simulating the foot motion and de-loading the foot ankle. The posture control of the Stewart platform can expand the range of the developed device's applications. The researchers suggest using the relative position of the base and moving platform to calculate the linkage length of the Stewart platform (Lopes, 2010; Petrescu, Petrescu, & Mirsayar, 2018; Wang, He, Shang, & Gu, 2009). With the right posture control system, the developed device could be able to do

more in the future, for instance precision control of Stewart platform in order to synchronise the developed device with foot motion.

Appendix I Schematic Circuit of PCB
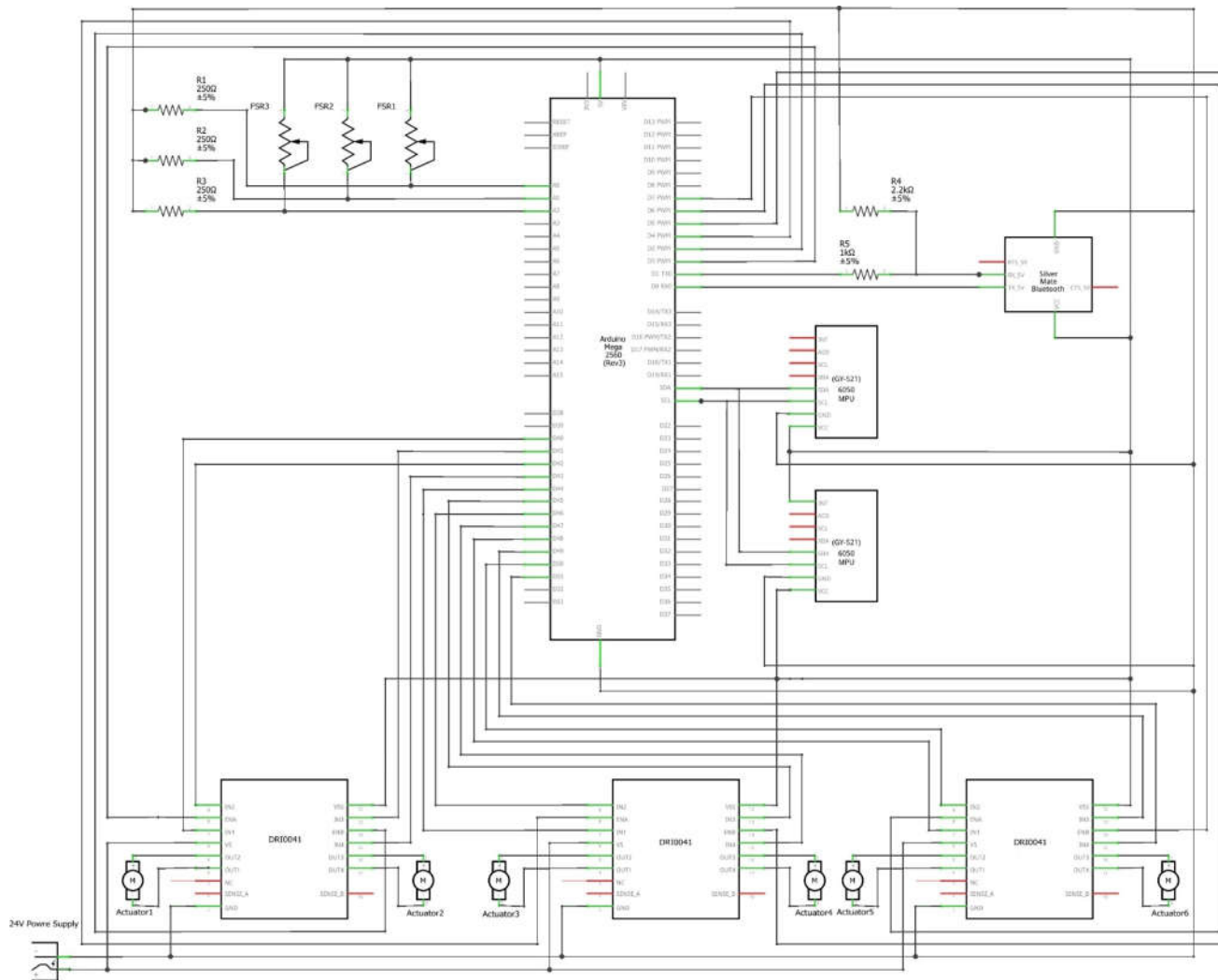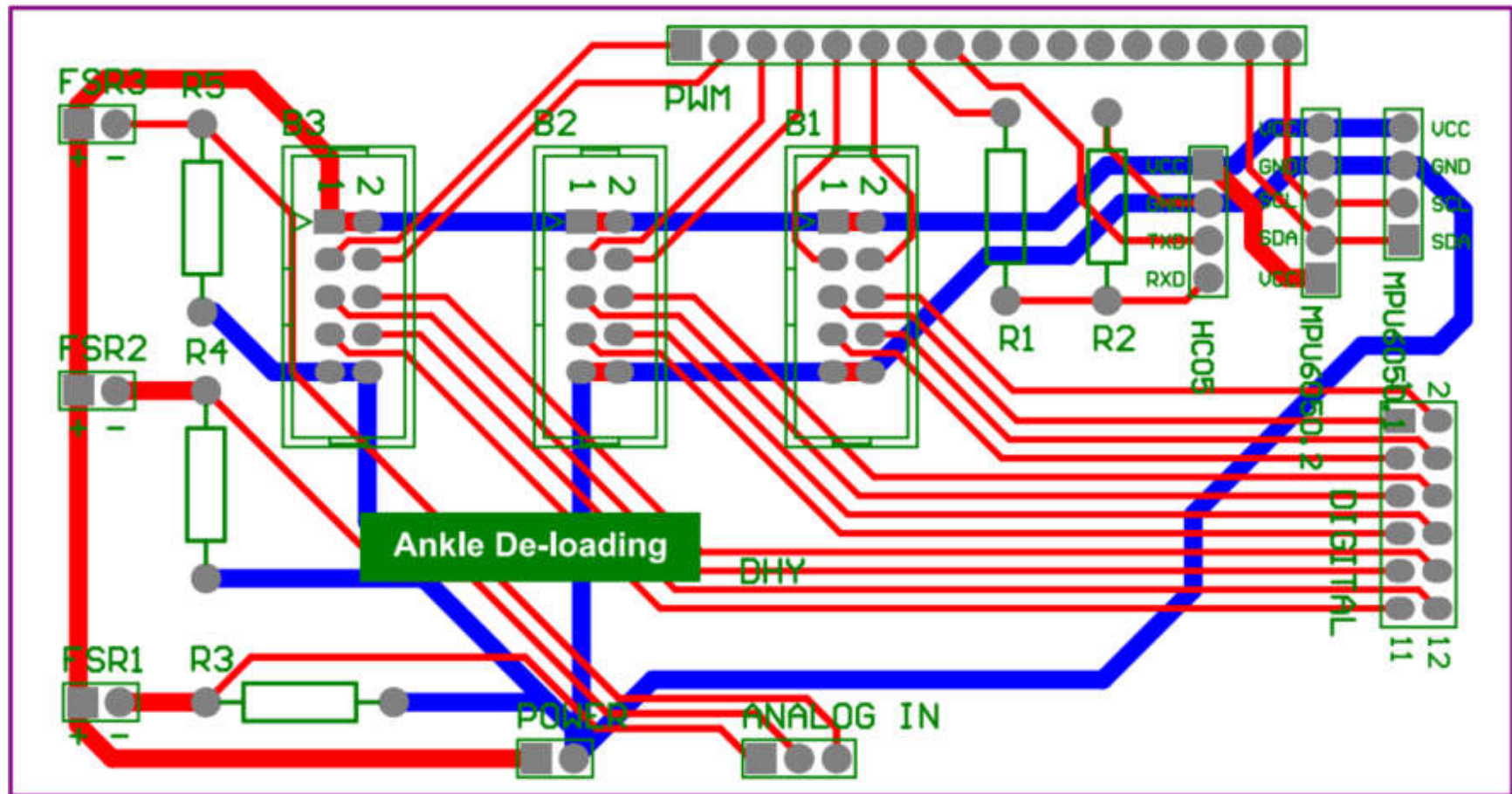
Appendix II Knee Brace Structure Assembly Diagram
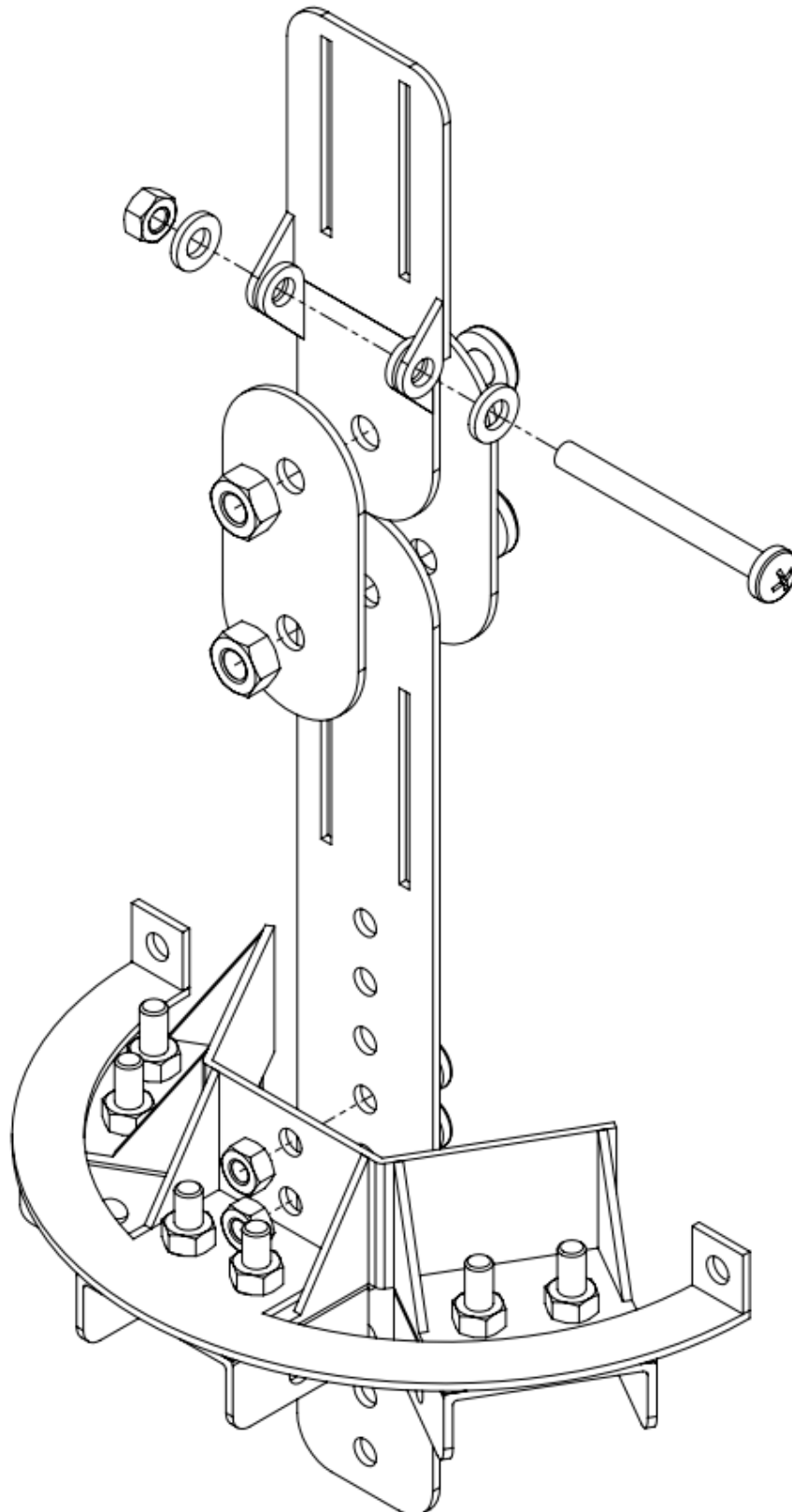
Appendix III Base Ring Assembly Diagram

Appendix IV Base Ring Connection Assembly Diagram

Appendix V Universal Joint Assembly Diagram (Dimetric)
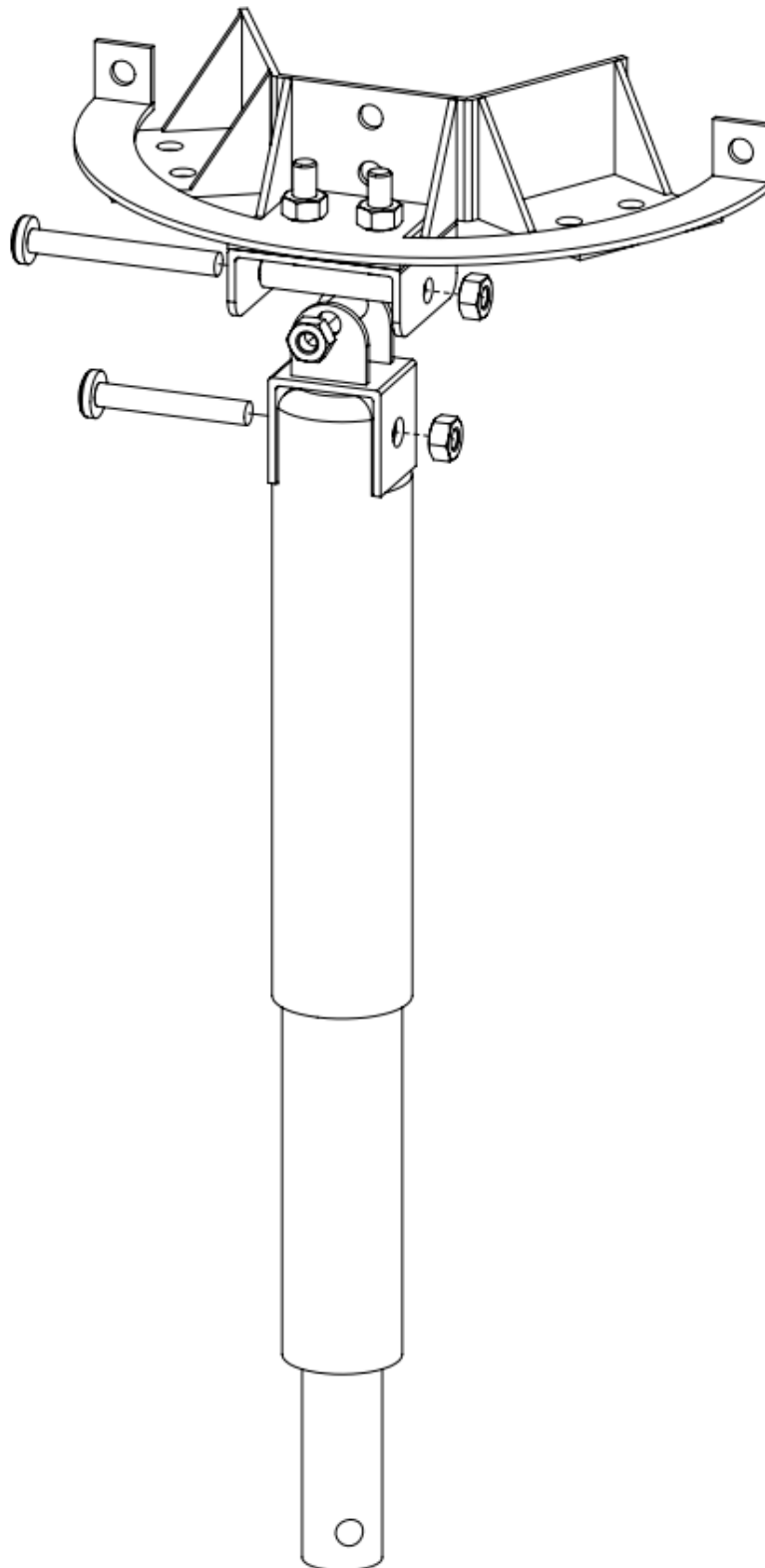
Appendix VI Universal Joint Assembly Diagram (Front)
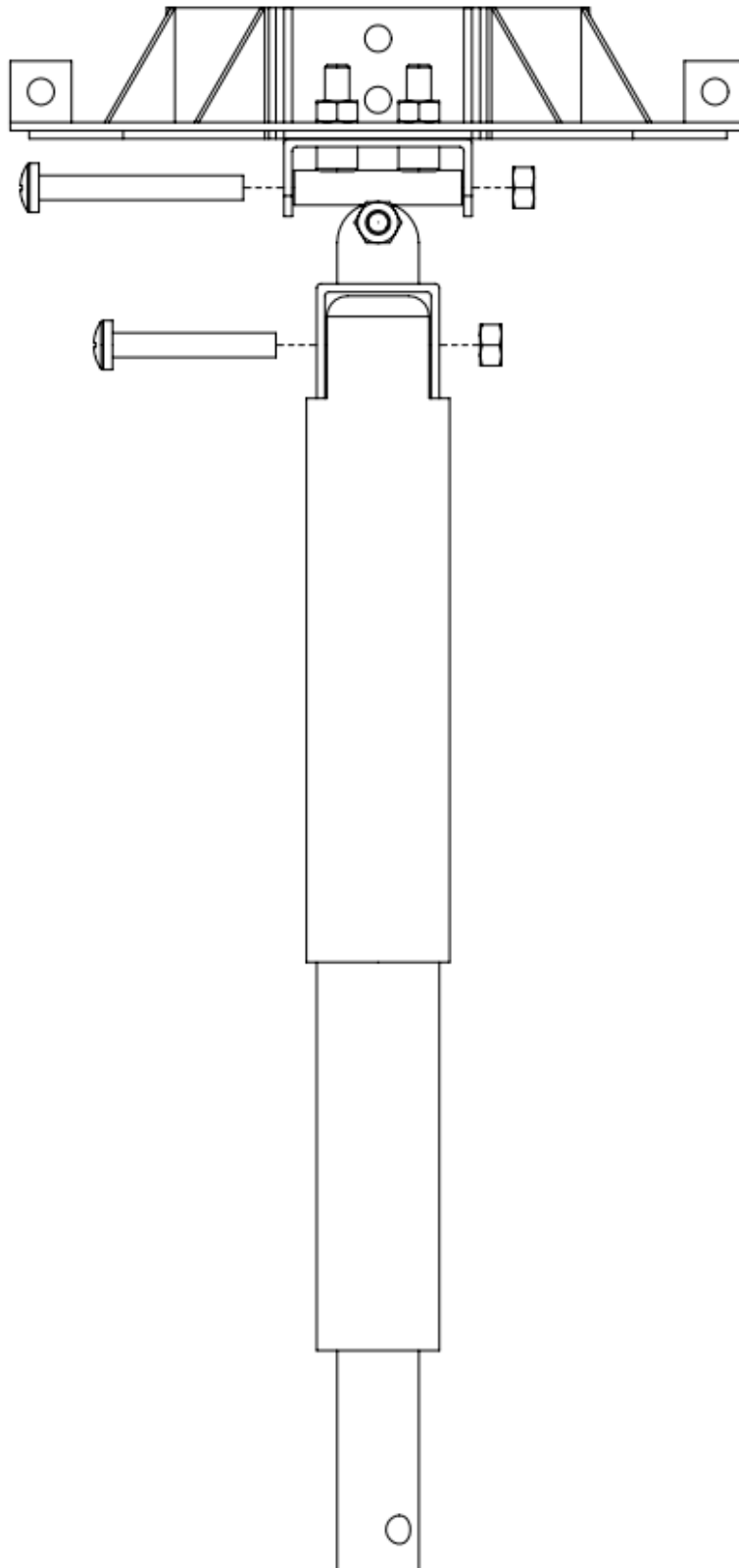
Appendix VII Universal Joint Assembly Diagram (Left)
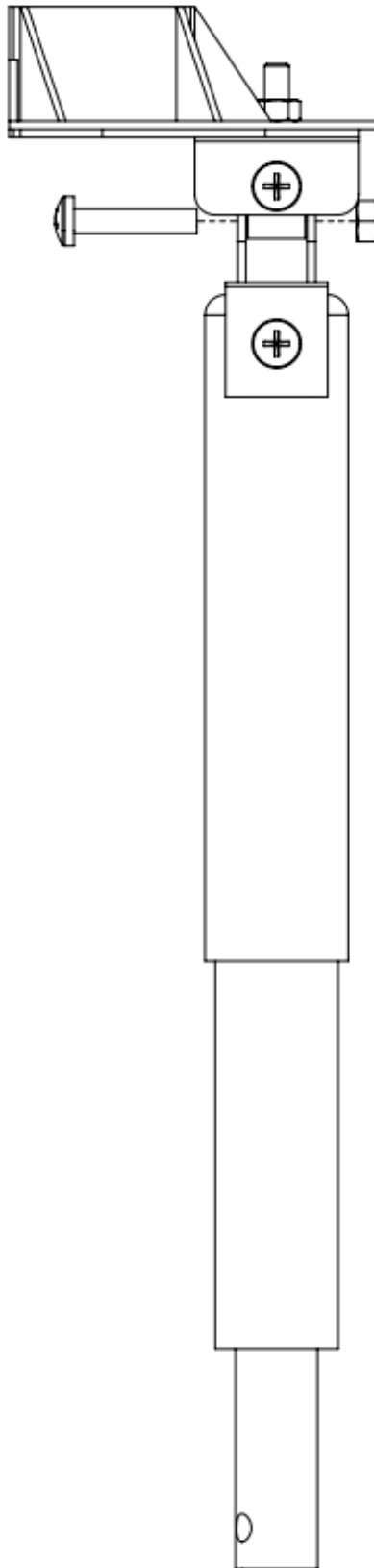
Appendix VIII Spherical Joint Assembly Diagram
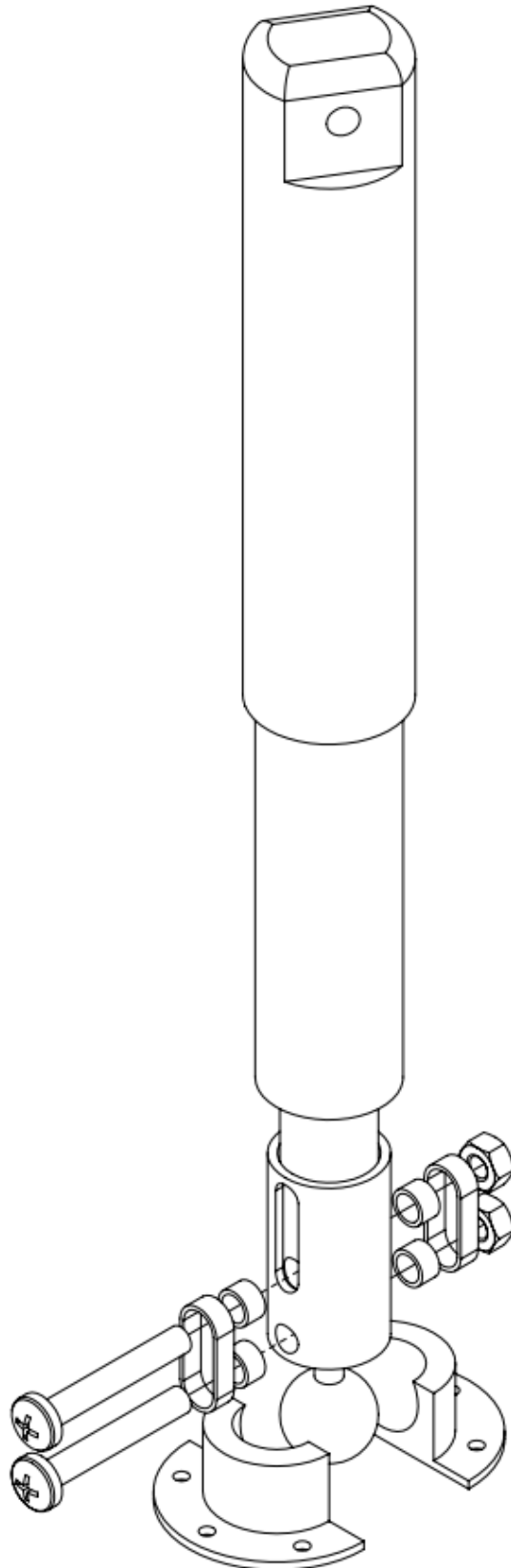
Appendix IX Foot Pad Assembly Diagram
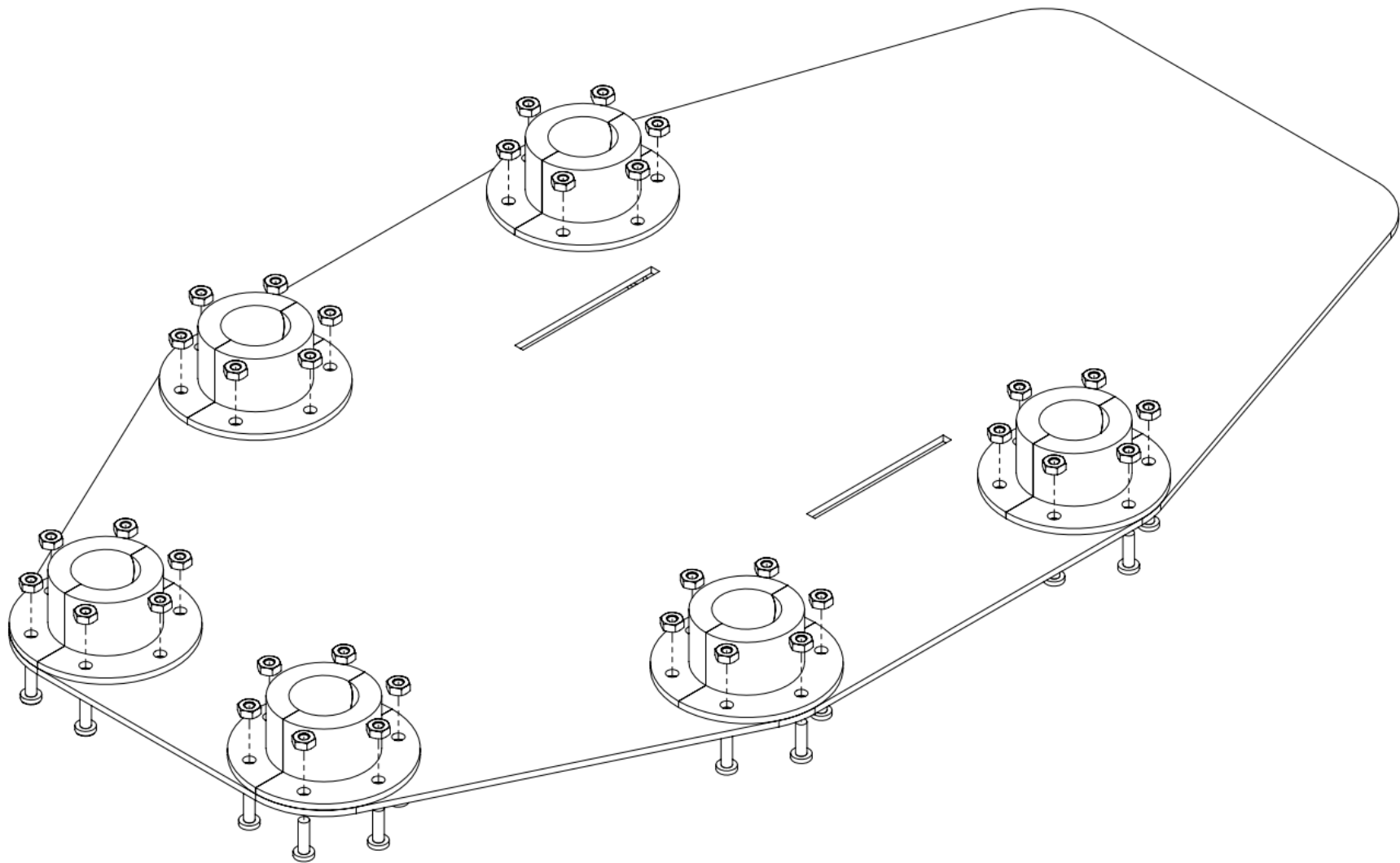
Appendix X Bill of Material

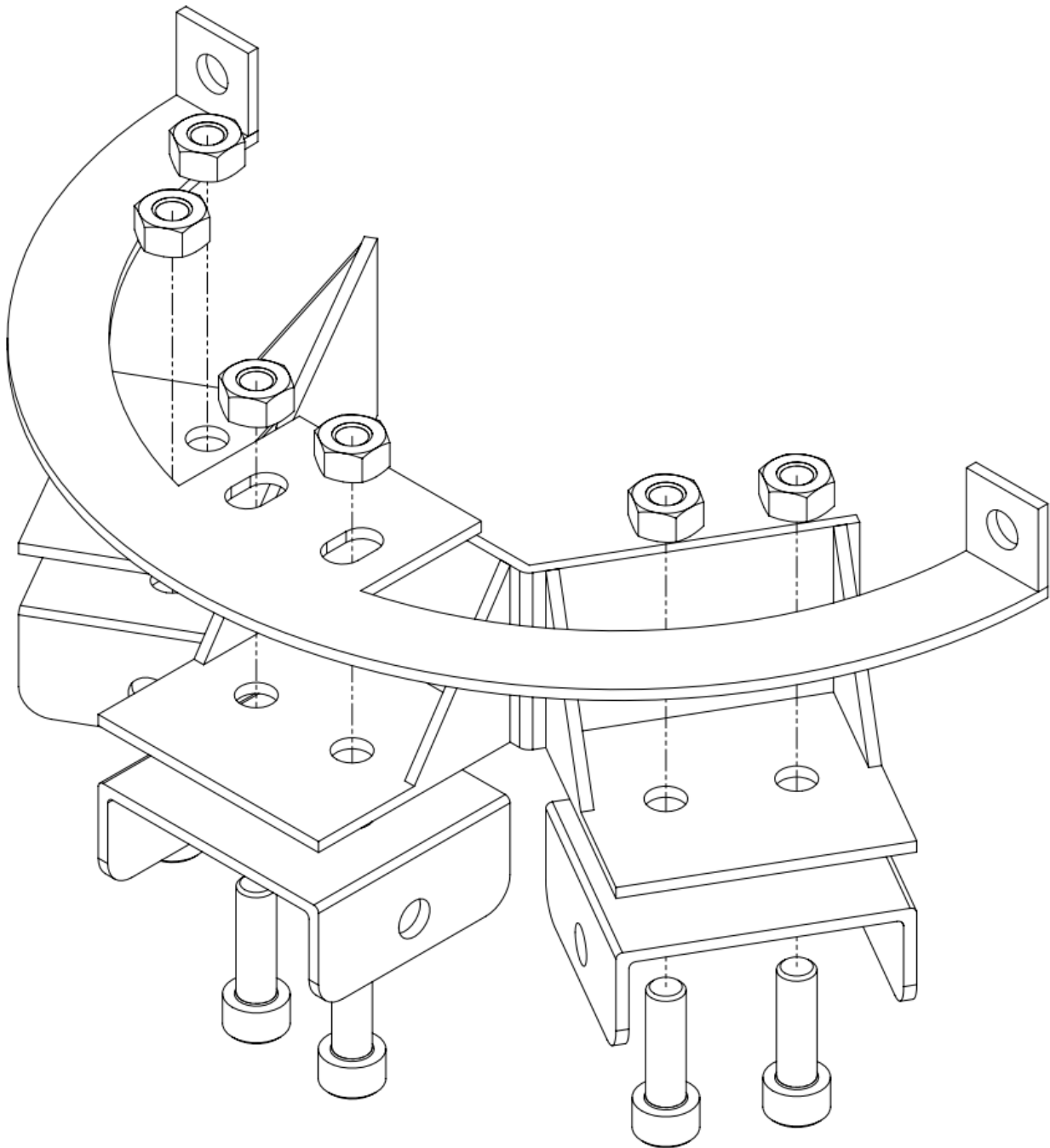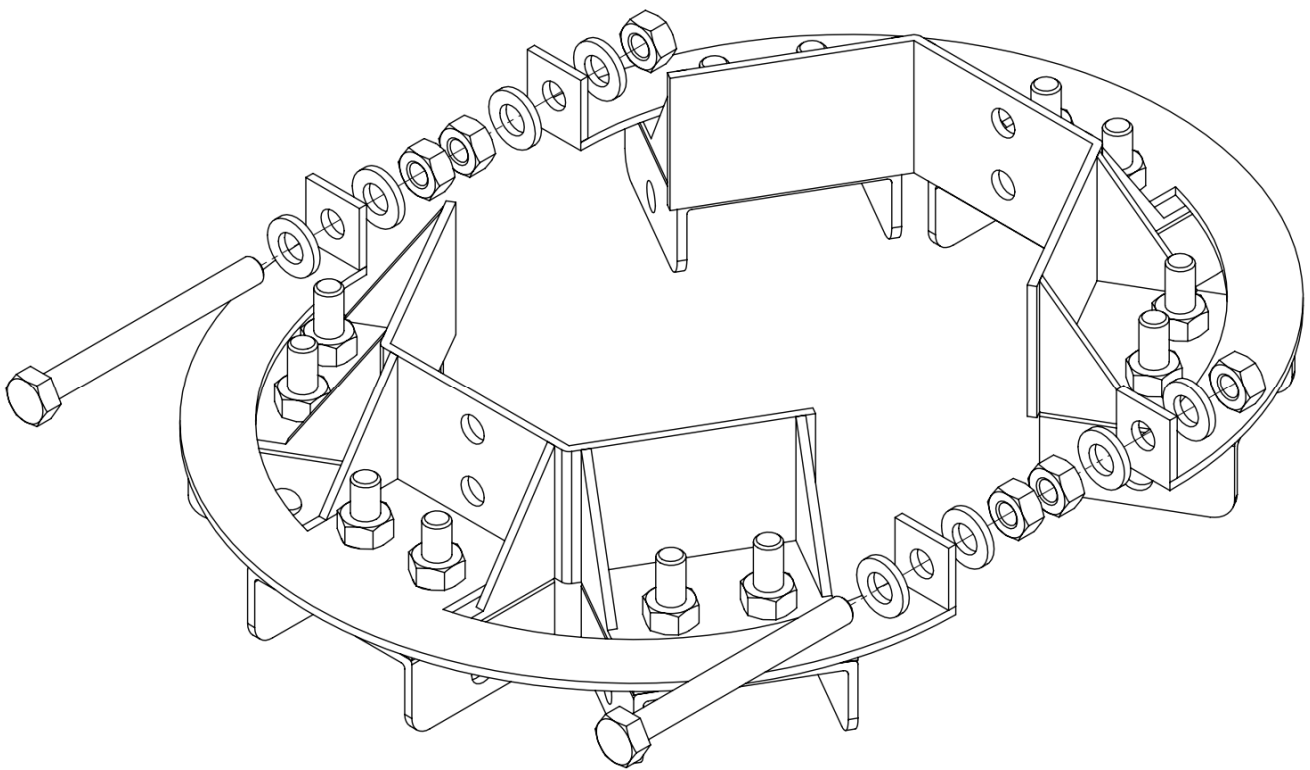|	Part List	Quantity	Type	Unit	Name	Supplier
1	Control Board	1	Control	Piece	Arduino Mega 2560 Rev3	Element 14
2	PCB Board	1	Control	Piece	PCB board	
3	Force Sensor	3	Sensor	Piece	FSR (Force Sensitive Resistor)	Aliexpress
4	Gyroscope	2	Sensor	Piece	MPU6050	Element 14
5	7A Dual DC Motor Driver	3	Control	Piece	DRI0041	DFROBOT
6	Bluetooth Module	1	Control	Piece	HC-05	Element 14
7	Actuator	6	Assembly	Piece	LA35T	Aliexpress
8	10mm M6 Bolt	4	Part	Piece	Grade 8.8 Zinc Pan Head 10mm M6 Bolt	Element 14

9	20mm M6 Bolt	12	Part	Piece	Grade 8.8 Zinc Socket Head 20mm M6 Bolt	Element 14
10	30mm M6 Bolt	18	Part	Piece	Grade 8.8 Zinc Pan Head 30mm M6 Bolt	Element 14
11	40mm M6 Bolt	6	Part	Piece	Grade 8.8 Zinc Pan Head 40mm M6 Bolt	Element 14
12	50mm M6 Bolt	6	Part	Piece	Grade 8.8 Zinc Pan Head 50mm M6 Bolt	Element 14
13	60mm M6 Bolt	2	Part	Piece	Grade 8.8 Zinc Pan Head 60mm M6 Bolt	Element 14
14	100mm M6 Bolt	2	Part	Piece	Grade 8.8 Zinc Hex Head 100mm M6 Bolt	Element 14
15	M6 Nut	66	Part	Piece	Grade 8.8 Zinc Hex M6 Nut	Element 14
16	M6 Washer	24	Part	Piece	M6 Zinc Flat Washer	Element 14
17	10mm M8 Bolt	4	Part	Piece	Grade 8.8 Zinc Pan Head 10mm M8 Bolt	Element 14

18	M8 Nut	4	Part	Piece	Grade 8.8 Zinc Hex M8 Nut	Element 14
19	12mm M3 Bolt	65	Part	Piece	Grade 8.8 Zinc Pan Head M3 Bolt	Element 14
20	M3 Nut	88	Part	Piece	Grade 8.8 Zinc Hex M3 Nut	Element 14
21	Ball Joint	6	Assembly	Piece	Ball Joint	
22	Ball Joint Base (Half)	12	Assembly	Piece	Ball Joint Base (Half)	
23	Actuator Cap	6	Assembly	Piece	Actuator Cap	
24	Rotroy Rod Sleeve	6	Assembly	Piece	Rotroy Rod Sleeve	
25	Ring Base Conncetion	6	Assembly	Piece	Ring Base Conncetion	
26	Base Ring	2	Assembly	Piece	Base Ring	

27	Ring Dimension Adjuster	2	Assembly	Piece	Ring Dimension Adjuster	
28	Crus Knee Brace Plate	2	Assembly	Piece	Crus Knee Brace Plate	
29	Knee Brace Joint Cover	4	Assembly	Piece	Knee Brace Joint Cover	
30	Thigh Knee Brace Joint Plate	2	Assembly	Piece	Thigh Knee Brace Joint Plate	
31	Thigh Knee Brace Plate	2	Assembly	Piece	Thigh Knee Brace Plate	
32	Foot Pad	1	Assembly	Piece	Foot Pad	
33	Rubber Band	6	Part	Piece	Rubber Band	
34	Velcro Bandage	5	Assembly	Meter	Velcro Bandage	Element 14

Appendix XI Program Code of Control System

```
// Libraries used in code
#include <Wire.h>
#include <Math.h>

// Parameter definition
#define PI 3.1415926
// Register address of gyroscopes definition
#define MPU1 0x68
#define MPU2 0x69

// Force sensors' pins used on Arduino board
int FSR1 = A0, FSR2 = A1, FSR3 = A2;
// Parameters of filtered data and reading data of force sensors
double f1, f2, f3,  r1, r2, r3;
// Confidence coefficient on reading data of force sensors
double a= 0.01;
// Parameters for calibration of force sensors
double biasr1, biasr2, biasr3;

// Calculated parameters of gyroscopes
double AccX[2], AccY[2], AccZ[2], Temp[2], GyrX[2], GyrY[2], GyrZ[2], n=0;
// Oringin reading data of gyroscopes
double ax[2],ay[2],az[2],gx[2],gy[2],gz[2],tax[2],tay[2],taz[2],tgx[2],tgy[2],tgz[2];
// Parameters for calibration of gyroscopes
double biasax[2],biasay[2],biasaz[2],biasgx[2],biasgy[2],biasgz[2];
// Differential time parameters
double PreTime, CurrentTime, dt;
// Angle calculation parameters
double AccPitch[2], AccRoll[2];
// Kalman filter covariance coefficient
double Q_angle = 0.001, Q_bias = 0.003, R_measure = 0.03;
// Kalman Yaw angle parameters
double ratez, anglez, biasz, Pz[2][2]={{0,0},{0,0}}, Sz, Kz[2], yz, Pz00, Pz01;
// Kalman Pitch angle parameters
double ratey, angley, biasy, Py[2][2]={{0,0},{0,0}}, Sy, Ky[2], yy, Py00, Py01;
// Kalman Roll angle parameters
double ratex, anglex, biasx, Px[2][2]={{0,0},{0,0}}, Sx, Kx[2], yx, Px00, Px01;
// Parameters of angles after Kalman filtering
double YawKalPre[2], YawKal[2], PitchKalPre[2], RollKalPre[2], PitchKal[2], RollKal[2];
// Angle differences between two gyroscopes
double dyaw, dpitch, droll;

// Actuators running time parameters (Set by researcher)
int at[3] ={0,0,0}, ate = 1, atr = 1;
```

```
void setup() {

  // Serial bond rate setup
  Serial.begin(9600);

  // Gyroscopes setup
  mpusetup(MPU1);
  mpusetup(MPU2);

  // Gyroscopes calibration
  mpucalibrate(MPU1, 0);
  mpucalibrate(MPU2, 1);


  // Force sensors setup
  for (int pin = 40; pin < 52; pin++)
 {pinMode(pin,OUTPUT);}

 // Force sensors calibration
 fsrcalibrate();

}

void loop() {

  deltatime();

  mpudata(MPU1, 0);
  mpudata(MPU2, 1);

  AccPitch[0] = atan((-ax[0])/sqrt(pow(ay[0],2)+pow(az[0],2)))*180/PI;
  AccRoll[0] = atan(ay[0]/sqrt(pow(ax[0],2)+pow(az[0],2)))*180/PI;

  AccPitch[1] = atan((-ax[1])/sqrt(pow(ay[1],2)+pow(az[1],2)))*180/PI;
  AccRoll[1] = atan(ay[1]/sqrt(pow(ax[1],2)+pow(az[1],2)))*180/PI;

  anglekalman(0);
  anglekalman(1);

  dyaw = YawKal[1] - YawKal[0];
  dyaw = (PI/180) * dyaw;
  dpitch = PitchKal[1] - PitchKal[0];
  dpitch = (PI/180) * dpitch;
  droll = RollKal[1] - RollKal[0];
  droll = (PI/180) * droll;

  // Reading data from force sensors
  r1 = analogRead(FSR1) - biasr1;
  r2 = analogRead(FSR2) - biasr2;
  r3 = analogRead(FSR3) - biasr3;
```

```
// Reading data from force sensors filtering
f1 = a * r1 + (1 - a) * f1;
f2 = a * r2 + (1 - a) * f2;
f3 = a * r3 + (1 - a) * f3;

// Actuators extension
if(ate == 0)
{
  controlone(1,0);
  controltwo(1,0);
  controlthree(1,0);
  ate = 1;
  }

// Actuators retractions
if(atr == 0)
{
  controlone(0,1);
  controltwo(0,1);
  controlthree(0,1);
  atr = 1;
  }

delay(1);

}

void mpusetup(int MPU)
{
  Wire.begin();
  Wire.beginTransmission(MPU);
  Wire.write(0x6B);
  Wire.write(0);
  Wire.endTransmission(true);

  Wire.begin();
  Wire.beginTransmission(MPU);
  Wire.write(0x1B);
  Wire.write(0);
  Wire.endTransmission(true);

  Wire.begin();
  Wire.beginTransmission(MPU);
  Wire.write(0x1C);
  Wire.write(0);
  Wire.endTransmission(true);
  }
```

```
void mpucalibrate(int mpu, int j)
{
  while(n<10)
  {
    Wire.beginTransmission(mpu);
    Wire.write(0x3B);
    Wire.requestFrom(mpu,14,true);
    Wire.endTransmission(true);
    AccX[j] = Wire.read() << 8 | Wire.read();
    AccY[j] = Wire.read() << 8 | Wire.read();
    AccZ[j] = Wire.read() << 8 | Wire.read();
    Temp[j] = Wire.read() << 8 | Wire.read();
    GyrX[j] = Wire.read() << 8 | Wire.read();
    GyrY[j] = Wire.read() << 8 | Wire.read();
    GyrZ[j] = Wire.read() << 8 | Wire.read();
    n++;

    delay(1);
  }

  n = 0;

  while(n<200)
  {
    Wire.beginTransmission(mpu);
    Wire.write(0x3B);
    Wire.requestFrom(mpu,14,true);
    Wire.endTransmission(true);
    AccX[j] = Wire.read() << 8 | Wire.read();
    AccY[j] = Wire.read() << 8 | Wire.read();
    AccZ[j] = Wire.read() << 8 | Wire.read();
    Temp[j] = Wire.read() << 8 | Wire.read();
    GyrX[j] = Wire.read() << 8 | Wire.read();
    GyrY[j] = Wire.read() << 8 | Wire.read();
    GyrZ[j] = Wire.read() << 8 | Wire.read();
    ax[j] = AccX[j] / 16384;
    ay[j] = AccY[j] / 16384;
    az[j] = AccZ[j] / 16384;
    gx[j] = GyrX[j] / 131;
    gy[j] = GyrY[j] / 131;
    gz[j] = GyrZ[j] / 131;
    tax[j] += ax[j];
    tay[j] += ay[j];
    taz[j] += az[j];
    tgx[j] += gx[j];
    tgy[j] += gy[j];
    tgz[j] += gz[j];
    n++;

    delay(1);
  }

  biasax[j] = tax[j] / 200;
  biasay[j] = tay[j] / 200;
  biasaz[j] = (taz[j] / 200) +1;
  biasgx[j] = tgx[j] / 200;
  biasgy[j] = tgy[j] / 200;
  biasgz[j] = tgz[j] / 200;
}
```

```cpp
void mpudata(int Mpu, int m)
{
  Wire.beginTransmission(Mpu);
  Wire.write(0x3B);
  Wire.requestFrom(Mpu,14,true);
  Wire.endTransmission(true);
  AccX[m] = Wire.read() << 8 | Wire.read();
  AccY[m] = Wire.read() << 8 | Wire.read();
  AccZ[m] = Wire.read() << 8 | Wire.read();
  Temp[m] = Wire.read() << 8 | Wire.read();
  GyrX[m] = Wire.read() << 8 | Wire.read();
  GyrY[m] = Wire.read() << 8 | Wire.read();
  GyrZ[m] = Wire.read() << 8 | Wire.read();
  AccX[m] = AccX[m] / 16384;
  AccY[m] = AccY[m] / 16384;
  AccZ[m] = AccZ[m] / 16384;
  Temp[m] = Temp[m] / 340 + 36.53;
  GyrX[m] = GyrX[m] / 131;
  GyrY[m] = GyrY[m] / 131;
  GyrZ[m] = GyrZ[m] / 131;
  ax[m] = AccX[m] - biasax[m];
  ay[m] = AccY[m] - biasay[m];
  az[m] = AccZ[m] - biasaz[m];
  gx[m] = GyrX[m] - biasgx[m];
  gy[m] = GyrY[m] - biasgy[m];
  gz[m] = GyrZ[m] - biasgz[m];
  }

void deltatime()
{
  PreTime = CurrentTime;
  CurrentTime = millis();
  dt = (CurrentTime - PreTime) / 1000;
  }

double kalmanfilterYaw(double newYaw,double newgz)
{
  ratez = newgz - biasz;
  anglez += ratez * dt;
  Pz[0][0] += dt * (dt*Pz[1][1]-Pz[0][1]-Pz[1][0]+Q_angle);
  Pz[0][1] -= dt * Pz[1][1];
  Pz[1][0] -= dt * Pz[1][1];
  Pz[1][1] += Q_bias * dt;
  Sz = Pz[0][0] + R_measure;
  Kz[0] = Pz[0][0] / Sz;
  Kz[1] = Pz[1][0] / Sz;
  yz = newYaw - anglez;
  anglez += Kz[0] * yz;
  biasz += Kz[1] * yz;
  Pz00 = Pz[0][0];
  Pz01 = Pz[0][1];
  Pz[0][0] -= Kz[0] * Pz00;
  Pz[0][1] -= Kz[0] * Pz01;
  Pz[1][0] -= Kz[1] * Pz00;
  Pz[1][1] -= Kz[1] * Pz01;

  return anglez;
  }
```

```
double kalmanfilterPitch(double newPitch, double newgy)
{
  ratey = newgy - biasy;
  angley += ratey * dt;
  Py[0][0] += dt * (dt*Py[1][1]-Py[0][1]-Py[1][0]+Q_angle);
  Py[0][1] -= dt * Py[1][1];
  Py[1][0] -= dt * Py[1][1];
  Py[1][1] += Q_bias * dt;
  Sy = Py[0][0] + R_measure;
  Ky[0] = Py[0][0] / Sy;
  Ky[1] = Py[1][0] / Sy;
  yy = newPitch - angley;
  angley += Ky[0] * yy;
  biasy += Ky[1] * yy;
  Py00 = Py[0][0];
  Py01 = Py[0][1];
  Py[0][0] -= Ky[0] * Py00;
  Py[0][1] -= Ky[0] * Py01;
  Py[1][0] -= Ky[1] * Py00;
  Py[1][1] -= Ky[1] * Py01;

  return angley;
  }

double kalmanfilterRoll(double newRoll,double newgx)
{
  ratex = newgx - biasx;
  anglex += ratex * dt;
  Px[0][0] += dt * (dt*Px[1][1]-Px[0][1]-Px[1][0]+Q_angle);
  Px[0][1] -= dt * Px[1][1];
  Px[1][0] -= dt * Px[1][1];
  Px[1][1] += Q_bias * dt;
  Sx = Px[0][0] + R_measure;
  Kx[0] = Px[0][0] / Sx;
  Kx[1] = Px[1][0] / Sx;
  yx = newRoll - anglex;
  anglex += Kx[0] * yx;
  biasx += Kx[1] * yx;
  Px00 = Px[0][0];
  Px01 = Px[0][1];
  Px[0][0] -= Kx[0] * Px00;
  Px[0][1] -= Kx[0] * Px01;
  Px[1][0] -= Kx[1] * Px00;
  Px[1][1] -= Kx[1] * Px01;

  return anglex;
  }
```

```
void anglekalman(int k)
{
  PitchKalPre[k] = AccPitch[k];
  RollKalPre[k] = AccRoll[k];
  PitchKal[k] = kalmanfilterPitch(PitchKalPre[k], gy[k]);
  RollKal[k] = kalmanfilterRoll(RollKalPre[k], gx[k]);

  YawKalPre[k] = YawKal[k] + dt * gz[k];
  YawKal[k] = kalmanfilterYaw(YawKalPre[k], gz[k]);
  }

void controlone(int cox, int coy) {
  digitalWrite(40,cox);
  digitalWrite(42,coy);
  digitalWrite(49,cox);
  digitalWrite(51,coy);
  delay(at[0]);
  digitalWrite(40,0);
  digitalWrite(42,0);
  digitalWrite(49,0);
  digitalWrite(51,0);
}

void controltwo(int ctx, int cty) {
  digitalWrite(41,ctx);
  digitalWrite(43,cty);
  digitalWrite(48,ctx);
  digitalWrite(50,cty);
  delay(at[1]);
  digitalWrite(41,0);
  digitalWrite(43,0);
  digitalWrite(48,0);
  digitalWrite(50,0);
}

void controlthree(int cttx, int ctty) {
  digitalWrite(44,cttx);
  digitalWrite(46,ctty);
  digitalWrite(45,cttx);
  digitalWrite(47,ctty);
  delay(at[2]);
  digitalWrite(44,0);
  digitalWrite(46,0);
  digitalWrite(45,0);
  digitalWrite(47,0);
}
void fsrcalibrate()
{
  int fci = 0;
  while (fci<200)
  {
    r1 += analogRead(FSR1);
    r2 += analogRead(FSR2);
    r3 += analogRead(FSR3);
    fci++;
    }
  biasr1 = r1 / 200;
  biasr2 = r2 / 200;
  biasr3 = r3 / 200;
  }
```

References

Adal, S. A., Pourkazemi, F., Mackey, M., & Hiller, C. E. (2019, Jun 1). The Prevalence of Pain in People With Chronic Ankle Instability: A Systematic Review. *Journal of Athletic Training, 54*(6), 662-670.

Alarcon, G. S. (1995, Aug 01). Epidemiology of rheumatoid arthritis. *Rheumatic Diseases Clinics of North America, 21*(3), 589-604.

Amirudin, A. N., S.Parasuraman, Kadirvel, A., Khan, M. A., & I.Elamvazuthi. (2014). Biomechanics of Hip, Knee and Ankle joint loading during ascent and descent walking. *International Conference on Robot PRIDE 2013-2014 - Medical and Rehabilitation Robotics and Instrumentation, ConfPRIDE 2013-2014 . 42*, pp. 336-344. Procedia Computer Science.

Arndt, A., Westblad, P., Winson, I., Hashimoto, T., & Lundberg, A. (2004, May). Ankle and Subtalar Kinematics Measured With Intracortical Pins During the Stance Phase of Walking. *Foot & Ankle International, 25*(5), 357-364.

Boutaayamou, M., Brüls, O., Denoël, V., Schwartz, C., Demonceau, M., Garraux, G., & Verly, J. G. (2015). Segmentation of gait cycles using foot-mounted 3D accelerometers. *2015 International Conference on 3D Imaging (IC3D).* Liege, Belgium: IEEE.

Brockett, C. L., & Chapman, G. J. (2016, Jun). Biomechanics of the Ankle. *Orthopaedics and Trauma, 30*, 232-238.

Broglio, S. P., Monk, A., Sopiarz, K., & Cooper, E. R. (2009, May). The influence of ankle support on postural control. *Journal of Science and Medicine in Sport, 12*(3), 388-392.

Budynas, R. G., & Nisbett, J. K. (2011). *Shigley's Mechanical Engineering Design 9th ed.* McGraw-Hill.

Burdett, R. G. (1982). Forces predicted at the ankle during running. *Medicine & Science in Sports & Exercise, 14*(4), 308-316.

Burgener, F. A., Meyers, S. P., Tan, R. K., & Zaunbauer, W. (2002). *Differential Diagnosis in Magnetic Resonance Imaging.* New York: Thieme.

Buschmann, J., & Bürgisser, G. M. (2017). *Biomechanics of Tendons and Ligaments.* Elsevier Science & Technology.

Cadick, J., Capelli-Schellpfeffer, M., & Neitzel, D. (2005). *Electrical Safety Handbook 3E 3rd Edition.* McGraw-Hill Professional.

Calhoun, J. H., Li, F., Ledbetter, B. R., & Viegas, S. F. (1994, Mar). A comprehensive study of pressure distribution in the ankle joint with inversion and eversion. *Foot & Ankle International, 15*(3), 125-133.

REFERENCE_____

Carberry, J., Hinchly, G., Buckerfield, J., Tayler, E., Burton, T., Madgwick, S., & Vaidyanathan, R. (2011). Parametric Design of an Active Ankle Foot Orthosis with Passive Compliance. *2011 24th International Symposium on Computer-Based Medical Systems (CBMS).* Bristol, United Kingdom: IEEE.

Chinh, N. D., Tan, P. N., Long, C. B., & Tien, N. T. (2017). Design of Force Support Device for Human Ankle Joint. *2017 14th International Conference on Ubiquitous Robots and Ambient Intelligence (URAI)* (pp. 274-279). Jeju, South Korea: IEEE.

Curran, M., Gillespie, L., Melville, S., Campbell, J., & Kagan, B. (2019, May). Estimating actual foot size from a static bare foot print in a White British Population. *Science & Justice, 59*(3), 317-321.

Dąbroś, J., Iwaniec, M., Patyk, M., & Wesół, J. (2018). User Movement Intention Detection Based on Gait Cycle Capturing Using Force Sensitive Resistors. *2018 XIV-th International Conference on Perspective Technologies and Methods in MEMS Design (MEMSTECH)* (pp. 219-222). Lviv, Ukraine: IEEE.

Dieppe, P. A., & Lohmander, L. S. (2005, Dec 3). Pathogenesis and management of pain in osteoarthritis. *Lancet, 365*(9463), 965-973.

Dieppe, P., Cushnaghan, J., Young, P., & Kirwan, J. (1993, Aug). Prediction of the progression of joint space narrowing in osteoarthritis of the knee by bone scintigraphy. *Annals of the Rheumatic Diseases, 52*(8), 557-563.

Duncan, J. A., Kowalk, D. L., & Vaughan, C. L. (1997, Jun). Six degree of freedom joint power in stair climbing. *Gait & Posture, 5*(3), 204-210.

Dunn, J., Link, C., Felson, D., Crincoli, M., Keysor, J., & McKinlay, J. (2004, Mar 1). Prevalence of Foot and Ankle Conditions in a Multiethnic Community Sample of. *American Journal of Epidemiology, 159*(5), 491-498.

Felson, D. T., & Schaible, H.-G. (2009). *Pain in Osteoarthritis.* Hoboken: John Wiley & Sons, Incorporated.

Ferran, N. A., & Maffulli, N. (2006, Sep). Epidemiology of sprains of the lateral ankle ligament complex. *Foot And Ankle Clinics, 11*(3), 659-662.

Feynman, R., Gottlieb, M., & Leighton, R. (2013). *Feynman's Tips on Physics, A Problem-Solving Supplement to the Feynman Lectures on Physics.* New York: Basic Books.

Fong, D. T.-P., Hong, Y., Chan, L.-K., Yung, P. S.-H., & Chan, K.-M. (2007). A Systematic Review on Ankle Injury and Ankle Sprain in Sports. *Sports Medicine , 37*(1), 73-94.

Frederick F. Buechel, S., Frederick F. Buechel, J., & Pappas, M. J. (2003, Jun 1). Ten-Year Evaluation of Cementless Buechel-Pappas Meniscal Bearing Total Ankle Replacement. *Foot & Ankle International, 24*(6), 462-472.

Gary, H. (2010). *Gray's anatomy: with original illustrations by Henry Carter.* London: Arcturus Publishing Limited.

Giacomozzi, C., Macellari, V., Leardini, A., & Benedetti, M. (2000, Mar). Integrated pressure–force–kinematics measuring system for the characterisation of plantar foot loading during locomotion. *Medical & Biological Engineering & Computing, 38*(2), 156-163.

Girone, M. J., Burdea, G. C., & Bouzit, M. (1999). 'Rutgers ankle' orthopedic rehabilitation interface. *Dynamic Systems and Control Division - 1999 (The ASME International Mechanical Engineering Congress and Exposition)* (pp. 305-312). Nashville, USA: ASME.

Glazebrook, M., Daniels, T., Younger, A., Foote, C., Penner, M., Wing, K., . . . Dunbar, M. (2008, Mar 1). Comparison of Health-Related Quality of Life Between Patients with End-Stage Ankle and Hip Arthrosis. *The Journal of Bone and Joint Surgery-American, 90-A*(3), 499-505.

Greenfield, J. R., Hwang, H. (., Davies, C., & McDaid, A. J. (2017). Soft-Stop Knee Brace for Rehabilitation from Ligament Injuries: Design and Pilot Trial. *2017 International Conference on Rehabilitation Robotics (ICORR)* (pp. 352-357). London, UK: IEEE.

Grimston, S. K., Nigg, B. M., Hanley, D. A., & Engsberg, J. R. (1993, May). Differences in Ankle Joint Complex Range of Motion as a Function of Age. *Foot & Ankle International, 14*(4), 215-222.

Hassan, M., Yagi, K., Kadone, H., Ueno, T., Mochiyama, H., & Suzuki, K. (2019). Optimized Design of a Variable Viscosity Link for Robotic AFO. *2019 41st Annual International Conference of the IEEE Engineering in Medicine and Biology Society (EMBC)* (pp. 6220-6223). Berlin, Germany: IEEE.

Huch, K., Kuettner, K. E., & Dieppe, P. (1997, Feb). Osteoarthritis in ankle and knee joints. *Seminars in Arthritis and Rheumatism, 26*(4), 667-674.

Irby, S. E., Kaufman, K. R., Mathewson, J. W., & Sutherland, D. H. (1999, Jun). Automatic Control Design for a Dynamic Knee-Brace System. *IEEE Transactions on Rehabilitation Engineering, 7*(2), pp. 135-139.

Jacobs, D. A., & Ferris, D. P. (2015, Oct 14). Estimation of ground reaction forces and ankle moment with multiple, low-cost sensors. *Journal of NeuroEngineering and Rehabilitation, 12*(1).

Jamwal, P. K., Hussain, S., & Xie, S. Q. (2015, Mar). Review on design and control aspects of ankle rehabilitation robots. *Disability & Rehabilitation: Assistive Technology, 10*(3), 93-101.

Kaminski, T. W. (1998, Jul). The History and Current Use of Ankle Brace Technology. *Athletic Therapy Today, 3*(4), 32-35.

Keegan, T. H., Kelsey, J. L., Sidney, S., & Quesenberry, C. J. (2002, May 15). Foot Problems as Risk Factors of Fractures. *American Journal of Epidemiology, 155*(10), 926-931.

Kennedy, J. G., Johnson, S. M., Collins, A. L., DalloVedova, P., McManus, W. F., Hynes, D. M., . . . Stephens, M. M. (1998, Oct). An evaluation of the Weber classification of ankle fractures. *Injury, 29*(8), 577-580.

Kulowski, J. (2007, Nov). Flexion contracture of the knee: The mechanics of the muscular contracture and the turnbuckle cast method of treatment; with a review of fifty-five cases. 1932. *Clinical Orthopaedics and Related Research, 464*, 4-10.

Lopes, A. M. (2010). Fast Dynamic Model of a Moving-base 6-DOF Parallel Manipulator. *Advances in Robot Manipulators*, 361-380.

Loudon, J. K., Swift, M., & Bell, S. (2008). *The clinical orthopedic assessment guide.* Kansas: Human Kinetics.

Malanga, G., & Delisa, J. A. (2010, February 6). *Section One: Clinical Observation.* Retrieved from Office of rehabilitation Research and Development: http://www.rehab.research.va.gov/mono/gait/malanga.pdf

Marx, R. C., & Mizel, M. S. (2015, May 20). What's New in Foot and Ankle Surgery. *Journal of Bone & Joint Surgery, American, 97*(10), 862-868.

Mazzuca, S. A., Brandt, K. D., Schauweckers, D. S., Buckwaltera, K. A., Katz, B. P., Meyer, J. M., . . . Carlson, K. A. (2004, Feb). Bone Scintigraphy Is Not a Better Predictor of Progression of Knee Osteoarthritis Than Kellgren and Lawrence Grade. *The Journal of Rheumatology, 31*(2), 329-332.

McCrae, F., Shouls, J., Dieppe, P., & Watt, I. (1992, Aug). Scintigraphic assessment of osteoarthritis of the knee joint. *Annals of the Rheumatic Diseases, 51*(8), 938-942.

Menz, H. B., & Lord, S. R. (2001, Dec 1). The Contribution of Foot Problems to Mobility Impairment and Falls in Community-Dwelling Older People. *Journal of the American Geriatrics Society, 49*(12), 1651-1656.

Michael, J. M., Golshani, A., Gargac, S., & Goswami, T. (2008, Oct). Biomechanics of the ankle joint and clinical outcomes of total ankle replacement. *Journal of the Mechanical Behaviour of Biomedical Materials, 1*(4), 276-294.

Miller, E. A., & Hergenroeder, A. C. (1990, Oct 1). Prophylactic ankle bracing. *Pediatric Clinics of North America, 37*(5), 1175-1185.

Moreland, J. R., Bassett, L. W., & Hanker, G. J. (1987, Jun 1). Radiographic Analysis of the Axial Alignment of the Lower Extremity. *The Journal of Bone and Join Surgery, 69*(5), 745-749.

Newman, A. P. (1998, Mar 1). Articular Cartilage Repair. *The American Journal of Sports Medicine, 26*(2), 309-324.

Ngo, H.-Q.-T., Nguyen, T.-P., Huynh, V.-N.-S., Le, T.-S., & Nguyen, C.-T. (2017). Experimental comparison of Complementary filter and Kalman filter design for low-cost sensor in quadcopter. *2017 International Conference on System Science and Engineering (ICSSE)* (pp. 488-493). Ho Chi Minh City, Vietnam: IEEE.

Nomura, K., Yonezawa, T., Ogitsu, T., Mizoguchi, H., & Takemura, H. (2015). Development of Stewart platform type ankle-foot device for trip prevention support. *2015 37th Annual*

International Conference of the IEEE Engineering in Medicine & Biology Society (EMBC) (pp. 4808-4811). Milan, Italy: IEEE.

Onodera, T., Ding, M., Takemura, H., & Mizoguchi, H. (2012). Posture Control Using New Ankle-Foot Assist Device with Stewart Platform Type Parallel Link Mechanisms. *2012 IEEE International Conference on Robotics and Biomimetics (ROBIO)* (pp. 1385-1390). Guangzhou, China: IEEE.

Onodera, T., Ding, M., Takemura, H., & Mizoguchi, H. (2014). Performance Evaluation of Novel Ankle-Foot Assist Device for Ankle-Foot Rehabilitation. *15th International Conference on Biomedical Engineering. 43*, pp. 492-495. Springer Verlag.

Ovaska, M. (2015, Feb). Complications in ankle fracture surgery. *Acta Orthopaedica, 358*(86), 1-32.

Petrescu, F. I., Petrescu, R. V., & Mirsayar, M. (2018). Inverse Kinematics of a Stewart Platform. *Journal of Materials and Engineering Structures, 5*(2), 111-122.

Platzer, W. (2008). *Color Atlas of Human Anatomy, Vol. 1: Locomotor System (th ed.).* New York: Thieme.

Pritzker, K. (2003). Pathology of osteoarthritis. In K. Brandt, M. Doherty, & L. S. Lohmander, *Osteoarthritis* (pp. 49-58). Oxford: Oxford University Press.

Pugely, A. J., Lu, X., Amendola, A., Callaghan, J. J., Martin, C. T., & Cram, P. (2014, Mar). Trends in the Use of Total Ankle Replacement and Ankle Arthrodesis in the United States Medicare Population. *Foot & Ankle International, 35*(3), 207-215.

Raikin, S. M., Kane, J., & Ciminiello, M. E. (2010, Sep 1). Risk Factors for Incision-Healing Complications Following Total Ankle Arthroplasty. *The Journal of Bone and Joint Surgery-American , 92-A*(12), 2150-2155.

Raikin, S. M., Rasouli, M. R., Espandar, R., & Maltenfort, M. G. (2014, Mar). Trends in Treatment of Advanced Ankle Arthropathy by Total Ankle Replacement or Ankle Fusion. *Foot & Ankle International, 35*(3), 216-224.

Ren'e, C. (1997). *Foot and ankle pain.* United State: F.A. Davis Company.

Reyes-Gibby, C. C., Aday, L., & Cleeland, C. (2002, Jan). Impact of pain on self-rated health in the community-dwelling older adults. *Pain, 95*(1-2), 75-82.

Roukis, T. S., Berlet, G. C., Bibbo, C., Hyer, ·. C., Penner, M. J., & Wünschel, M. (2016). *Primary and Revision Total Ankle Replacement.* New York: Springer.

Saglia, J. A., Tsagarakis, N. G., Dai, J. S., & Caldwell, D. G. (2009). A High Performance 2-dof Over-Actuated Parallel Mechanism for Ankle Rehabilitation. *2009 IEEE International Conference on Robotics and Automation Robotics and Automation* (pp. 2180-2186). Kobe, Japan: IEEE.

Sanchez-Guzman, F., Guerrero-Castellanos, J. F., Mino-Aguilar, G., Ambrosio-Lazaro, R. C., & Linares-Flores, J. (2017). Knee joint angle estimation during gait cycle using low-cost

inertial sensors. *2017 4th International Conference on Control, Decision and Information Technologies (CoDIT)* (pp. 161-166). Barcelona, Spain: IEEE.

Schepers, T., De Vries, M. R., Van Lieshout, E. M., & Van der Elst, M. (2013, Mar). The timing of ankle fracture surgery and the effect on infectious complications; a case series and systematic review of the literature. *International Orthopaedics, 37*(3), 489-494.

Schuenke, M., Schulte, E., & Schumacher, U. (2006). *Thieme Atlas of Anatomy: General Anatomy and Musculoskeletal System.* New York: Thieme.

Sedra, A. S. (1991). *Microelectronic Circuits, 3 ed.* Philadelphia: Saunders College Pub.

Self, B. P., Greenwald, R. M., & Pflaste, D. S. (2000). A Biomechanical Analysis of a Medial Unloading Brace for Osteoarthritis in the Knee. *Arthritis Care and Research, 13*(4), 191-197.

Shultz, S. J., Houglum, P. A., & Perrin, D. H. (2015). *Examination of Musculoskeletal Injuries.* North Carolina: Human Kinetics.

Simkin, P. A. (2004, Jan). Bone pain and pressure in osteoarthritic joints. *Novartis Foundation Symposium, 260*, 179-190.

Smith, K. W., Avis, N. E., & Assmann, S. F. (1999). Distinguishing between quality of life and health status in quality of life research: A meta-analysis. *Quality of Life Research, 8*(5), 447-459.

Soboroff, S. H., Pappius, E. M., & Komaroff, A. L. (1984). Benefits, risks, and costs of alternative approaches to the evaluation and treatment of severe ankle sprain. *Clinical Orthopaedics and Related Research, 183*, 160-168.

Stauffer, R. N., Chao, E. Y., & Brewstec, R. C. (1977). Force and Motion Analysis of the Normal, Diseased, and Prosthetic Ankle Joint. *Clinical Orthopaedics and Related Research, 127*, 189-196.

Stewart, D. (1965, Jun 1). A Platform with Six Degrees of Freedom. *Proceedings of the Institution of Mechanical Engineers, 180*(1), 371-386.

Su, E. P., Kahn, B., & Figgie, M. P. (2004, Jul). Total Ankle Replacement in Patients with Rheumatoid Arthritis. *Clinical Orthopaedics and Related Research, 424*, 32-38.

Taiar, R., Adel, C., Belassian, G., Lamare, D., Dumont, J., Chené, A., . . . Boyer, F. C. (2019, Nov 2). Can a new ergonomical ankle–foot orthosis (AFO) device improve patients' daily life? A preliminary study. *Theoretical Issues in Ergonomics Science, 20*(6), 763-772.

Tejwani, N. C. (2017). *Fractures of the Foot and Ankle : A Clinical Casebook.* New York: Springer.

Thomas, E., Peat, G., Harris, L., Ross, W., & Peter, R. C. (2004, Jul). The prevalence of pain and pain interference in a general populationof older adults: cross-sectional findings from the North StaffordshireOsteoarthritis Project (NorStOP). *Pain, 110*(1-2), 361-368.

REFERENCE

Tinetti, M. E., Speechley, M., & Ginter, S. F. (1988, Dec 29). Risk factors for falls among elderly persons living in the community. *New England Journal of Medicine, 319*(26), 1701-1707.

United Nations. (2019). *World Population Prospects 2019.* Online Edition: Department of Economic and Social Affairs, Population Division (2019).

University of Washington. (2015, February 5). *Pathologic Gait: Musculoskeletal.* Retrieved from University of Washington: http://courses.washington.edu/anatomy/KinesiologySyllabus/PathGait1Ortho.pdf

Unstal, H., & Baerga, E. (2004). *Gait Analysis.* New York: Demos Medical Publishing.

Wang, Z., He, J., Shang, H., & Gu, H. (2009). Forward kinematics analysis of a six-DOF Stewart platform using PCA and NM algorithm. *Industrial Robot: An International Journal, 36*(5), 448-460.

Watt, I., & Doherty, M. (2003). lain radiographic features of osteoarthritis. In K. Brandt, M. Doherty, & L. S. Lohmander, *Osteoarthritis* (pp. 211-225). Oxford: Oxford University Press.

Wervey, R. A., Harris, G. F., & Wertsch, J. J. (1997). Plantar pressure characteristics during stair climbing and descent. *19th Annual International Conference of the IEEE Engineering in Medicine and Biology Society. 4*, pp. 1746-1748. Chicago, IL: IEEE.

Wheeler, J. W., Krebs, H. I., & Hogan, N. (2004). An Ankle Robot for a Modular Gait Rehabilitation System. *2004 IEEE/RSJ International Conference on Intelligent Robots and Systems (IROS). 2*, pp. 1680-1684. Sendai, Japan: IEEE.

Williams, A. (2002). *Microcontroller projects using the Basic Stamp.* Taylor & Francis.

Wolfe, M. W. (2001, Jan 1). Management of Ankle Sprains. *American family physician, 63*(1), 93-104.

Yonezawa, T., Nomura, K., Onodera, T., Ding, M., Mizoguchi, H., & Takemura, H. (2014). Development and Performance Evaluation of Parallel Link Type Human Ankle Rehabilitation Assistive Device. *2014 IEEE International Conference on Robotics & Biomimetics (ROBIO 2014)* (pp. 802-807). Bali, Indonesia: IEEE.

Yoshizawa, N. (2010). Prototype Active AFO with Ankle Joint Brake for Achilles Tendon Ruptures. *2010 3rd International Conference on Biomedical Engineering and Informatics (BMEI 2010). 4*, pp. 1775-1778. Yantai, China: IEEE.